Distribution Agreement

In presenting this thesis or dissertation as a partial fulfillment of the requirements for an advanced degree from Emory University, I hereby grant to Emory University and its agents the non-exclusive license to archive, make accessible, and display my thesis or dissertation in whole or in part in all forms of media, now or hereafter known, including display on the world wide web. I understand that I may select some access restrictions as part of the online submission of this thesis or dissertation. I retain all ownership rights to the copyright of the thesis or dissertation. I also retain the right to use in future works (such as articles or books) all or part of this thesis or dissertation.

Signature:

_____ _____

Lei Shi Date

I. Self-Assembly of Thioether-Modified Cationic Surfactants

II. Electrostatic Binding among Equilibrating 2-D and 3-D Self-Assemblies

By

Lei Shi
Doctor of Philosophy

Chemistry

Fredric M. Menger, Ph.D.
Advisor

Lanny S. Liebeskind, Ph.D.
Committee Member

Vince Conticello, Ph.D.
Committee Member

Accepted:

Lisa A. Tedesco, Ph.D.
Dean of the Graduate School

Date

I. Self-Assembly of Thioether-Modified Cationic Surfactants

II. Electrostatic Binding among Equilibrating 2-D and 3-D Self-Assemblies

By

Lei Shi

M.S., Fudan University, Shanghai, China, 2002
B.S., Fudan University, Shanghai, China, 1999

Advisor: Fredric M. Menger, Ph.D.

An Abstract of
A dissertation submitted to the Faculty of the Graduate School of Emory University
in partial fulfillment of the requirements for the degree of
Doctor of Philosophy
in Chemistry

2009

Abstract

I. Self-Assembly of Thioether-Modified Cationic Surfactants

II. Electrostatic Binding among Equilibrating 2-D and 3-D Self-Assemblies

By Lei Shi

Cationic surfactants with one or two sulfur atoms inserted at various locations along their alkyl chains, were synthesized. Their colloidal properties were thoroughly explored by surface tension, fluorescence, and NMR. Furthermore, the thio-surfactants were adsorbed into sodium dodecyl sulfate micelles. An oxidant, periodate, was added to the system, and the subsequent rate of thioether oxidation to sulfoxide, determined by in-situ NMR, was found to be diminished (more or less equally for all sulfur loci) by two orders of magnitude. In contrast, rates of hydrogen peroxide oxidation were hardly perturbed by micellization. Once again, however, there was no rate dependence on sulfur location within the chains. These results are interpreted in terms of a disordered micelle in which all chain positions have roughly equivalent access to the micelle surface. The kinetic method for assessing exposure to the external medium is applicable to self-assemblies and polymer systems wherever the NMR resolution so permits.

Six organic additives bearing a different number of anionic charges, were added to a large excess of cationic surfactant (dodecyltrimethylammonium bromide, DTAB). The surface-tension vs. log [DTAB] plot for solutions containing DTAB/trianion = 15:1 showed an abrupt break (routinely taken as the critical micelle concentration, CMC) at 2.9

mM. This constitutes a 5-fold decrease compared with a CMC of 15 mM for pure aqueous DTAB. There is a 10-fold decrease in the break-point concentration caused by a mere 3.3 mol-% of hexanion. Corresponding CMC values from DTAB/trianion mixtures, measured by both conductivity and diffusion-NMR, gave normal values of 14 mM. The unusual discrepancy between the CMC based on surface tension and on the two "bulk" methods was attributed to saturation of the air/water interface by a DTAB/trianion complex far below the concentration at which the micelles form. Thus, the sharp break seen in surface-tension "CMC plots" need not in fact attest to actual micelle formation as is almost universally assumed in colloid chemistry.

I. Self-Assembly of Thioether-Modified Cationic Surfactants

II. Electrostatic Binding among Equilibrating 2-D and 3-D Self-Assemblies

By

Lei Shi

M.S., Fudan University, Shanghai, China, 2002
B.S., Fudan University, Shanghai, China, 1999

Advisor: Fredric M. Menger, Ph.D.

A dissertation submitted to the Faculty of the Graduate School of Emory University
in partial fulfillment of the requirements for the degree of
Doctor of Philosophy
in Chemistry

2009

Acknowledgments

First of all, I would like to thank Dr. Menger. As my advisor, he always encourages independent thought and keeps his door open to any science discussions and questions even when they look unrealistic or naive sometimes. Among the many things I learned from Dr. Menger, two most important ones are (1) How to generate novel research ideas. In Dr.Menger's words, it would be like a dog trying to "mark trees" (*Pure Appl. Chem.* 2005, *77*, 1873.). and (2) Good and correct writing can dramatically transform a normal (or boring) result into a pleasant and significant story. I often enjoy reading his unique writing such as the citation of "One Hundred Years of Solitude" as the ending of a *JACS* paper (2000, *122*, 11679). I also thank Lib Menger for her fresh organic vegetables and southern-style cooking.

My committee members, Dr. Liebeskind and Dr. Conticello, have been extremely open and willing to help. It is never difficult for Dr. Liebeskind's to re-attract attention from students by telling a joke in a sleepy afternoon class or seminar. And nobody will forget his own characteristic laughing. Dr. Conticello provides indispensable advices for both my yearly report and proposal. I still remember how proud I was when I learned that he told Dr. Menger that I performed like a faculty in my second year qualify exam. Additionally, I want to thank Dr. Liotta for his valuable suggestions on my research proposal and Dr. McDonald for his intensest and most useful organic synthesis course at Emory.

I am very grateful to the department staff especially the directors of NMR center, Dr. Wu and Dr. Wang. Under their patient directions, I have learned a lot of advanced NMR techniques. Otherwise, I couldn't finish my first project within my second year.

Our lab is a happy and productive group. I have been lucky to work and being friends with everyone of my lab mates. Ashley Galloway was the sweat heart of the lab. She helped me a lot on preparing my second year report. Hailing Zhang is a wonderful mentor and cook. I frequently benefited from resolving spectra with her help. Hao Lu, who is also my alumnus at Fudan University, sat beside me and we often worked together to solve experimental problems. Mary Chlebowski is an independent girl from whom straightforward opinions can be obtained. She is now a successful patent lawyer in Washington, DC. Meanwhile, I enjoyed working with our post-docs, Fabrizio Pertusati and Dan Lundberg. Ciao! I would also like to thank Syed Rizvi for teaching me how to do fluorescence and film balance experiments. At present, he is the only one working with me.

I truly appreciate my classmates at Emory. Hao Li and Zhihui Zhang, working next to our lab, have been great friends throughout the past five years. Hongjun Zhang was an excellent roommate and driving teacher when I first came to Atlanta.

Finally, I wish to thank my entire family for everything that they have done for me. Most importantly, I would like to express my deepest gratitude to my wife, Liqiong Cai. She has always been there for all the ups and downs. Talking with her everyday is my greatest relax and joy. All of this work would never have been accomplished without her love, sacrifice, and support.

Dedicated to My Family

Table of Contents

List of Figures

List of Schemes

List of Tables

I. Self-Assembly of Thioether-Modified Cationic Surfactants

Introduction

Surfactant and Self-Assembly

Surfactant is a surface-active agent characterized by its tendency to adsorb at interfaces. The first synthetic surfactant (alkyl naphthalene sulfonates) was developed in Germany during World War I while the oldest form of surfactant - soap dates back well over 2000 years.[1] At present, surfactants are among the most versatile products of the chemical industry and have been widely applied in oil exploration,[2] detergents and cosmetics,[3] paints and coatings,[4] textiles and fibres,[5] organic synthesis,[6] drug delivery,[7] chromatography,[8] and nano materials.[9] All surfactant molecules consist of two distinctly different portions: one soluble in a specific fluid (lyophilic) and one insoluble (lyophobic).[10] If the fluid in which the surfactant is to be used is water, then the terms "hydrophilic" and "hydrophobic" are used, respectively (Figure 1.1).

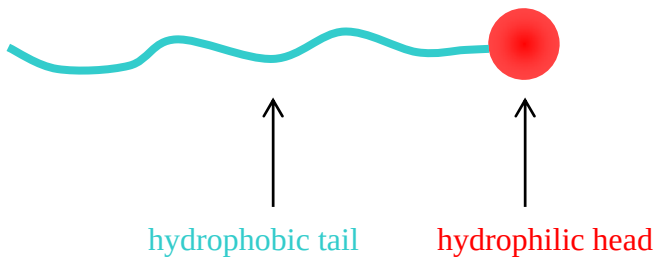

Figure 1.1. Illustration of a surfactant molecule

That amphiphilic characteristic provides surfactants two unique properties. First, surfactant can adsorb at an interface of two immiscible phases (vapor/solid, solid/liquid, solid/solid, liquid/liquid, and vapor/liquid. See Figure 1.2). Traditionally, vapor/liquid interfaces are referred to "surfaces" among which air/water interface is the most

commonly encountered type. The driving force of surfactant adsorption at an interface is to lower the interfacial free energy, which is the minimum amount of work required to expand the phase boundary. Instead of interfacial free energy, surface tension (γ), is often used for vapor/liquid interface. The unit of surface tension is millinewtons per meter (mN/m) or dynes per centimeter (dyn/cm) in non-SI units. For example, the surface tension of pure water at 20 ℃ is 72.8 mN/m.[11] When surfactants are added to water, they preferentially adsorb at the surface replacing the high-energy water molecules. The hydrophilic head groups immerse in water and the hydrophobic tail groups align in air (Figure 1.2a). As a result, the free energy of the system as a whole is dramatically lowered. Usually, hydrocarbon surfactants can reduce the surface tension to 30-40 mN/m, and lower values (20 mN/m) may be achieved using fluorocarbon surfactants.[12]

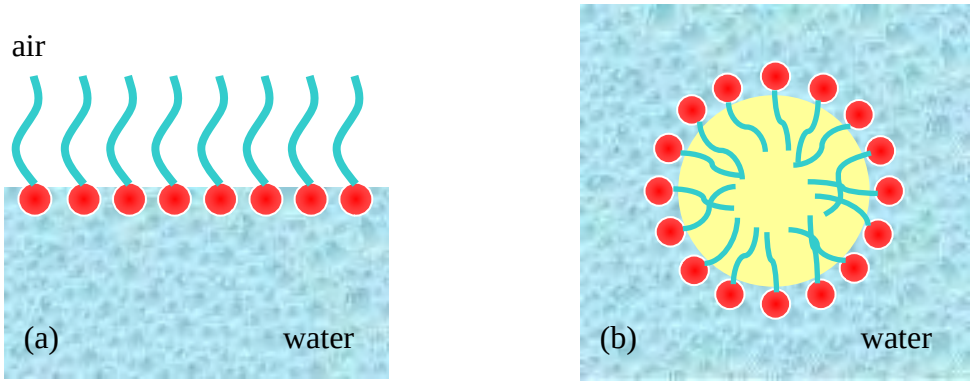

Figure 1.2. Surfactants adsorbed at an interface of (a) water/air and (b) water/oil

Second, at some high concentrations, surfactants can self assemble to form aggregates in a bulk solution. It has been observed that, depending on their structures and conditions (solvent, concentration, temperature, etc), surfactants can form a variety

of aggregation patterns such as spherical micelles, cylindrical micelle, reverse micelle, vesicle, and lamella (Figure 1.3). All of the self-assemblies are in dynamic equilibrium and surfactant molecules constantly join and leave these aggregates on a timescale of microseconds.

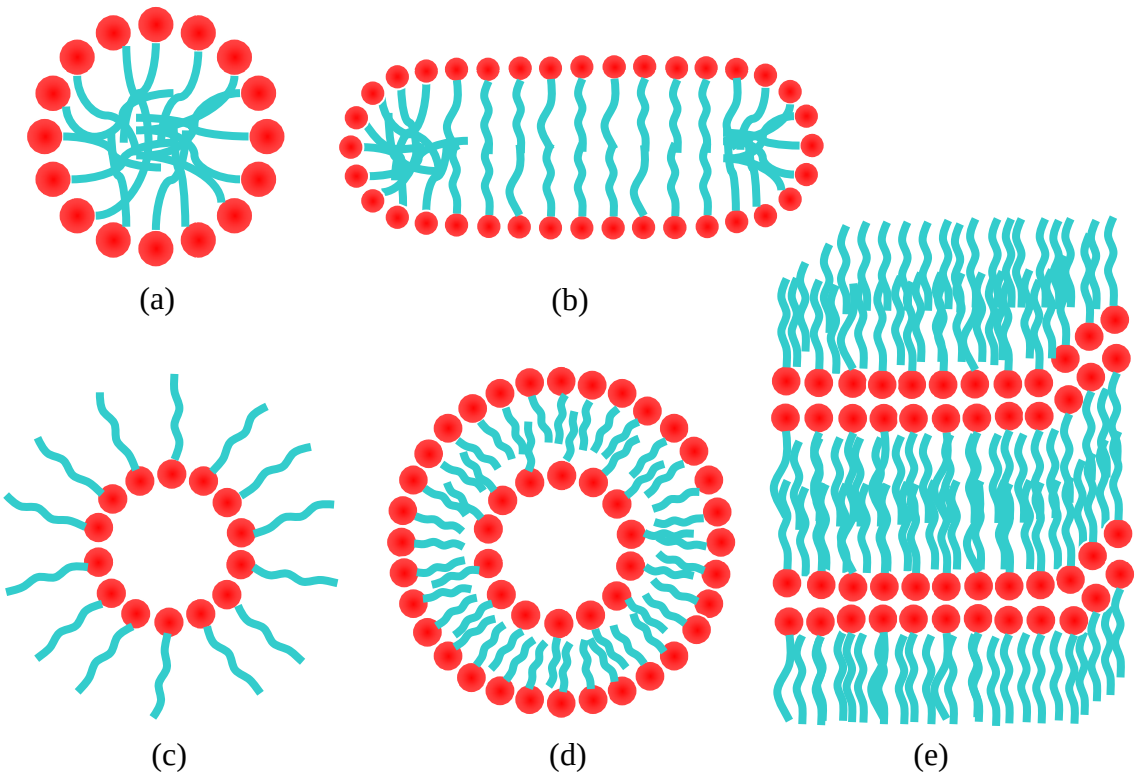

Figure 1.3. Various self-assembly patterns of surfactants. (a) spherical micelle. (b) cylindrical micelle. (c) reversed micelle. (d) vesicle. (e) lamella.

In aqueous solutions, the tendency of self-assembling mainly originates from water/water intermolecular interactions being stronger than those between water/hydrophobic chain (namely hydrophobic effect).[13] As shown in Figure 1.3a, the first-formed aggregates in water are generally spherical micelles. The hydrophobic tails

are directed towards the interior of the micelle and the hydrophilic heads are orientated towards the solvent. Thus, exposure of the hydrophobic parts to the surrounding water molecules is minimized, so is the free energy. As illustrated in Figure 4,[14] for an ionic surfactant, the properties at low concentrations in water are similar to those of simple electrolytes except the surface tension. However, these properties (interfacial and bulk) all show a sharp break at a particular concentration. This peculiar phenomenon indicates and is consistent with the formation of self-associated units - micelles. The concentration at which micelles start to form (micellization) is called the critical micelle concentration (CMC). Each surfactant has a characteristic CMC value at a given temperature. Above the CMC, the concentration of surfactant unimers remains constant while the concentration and structure of micelles vary with increased surfactant concentration.

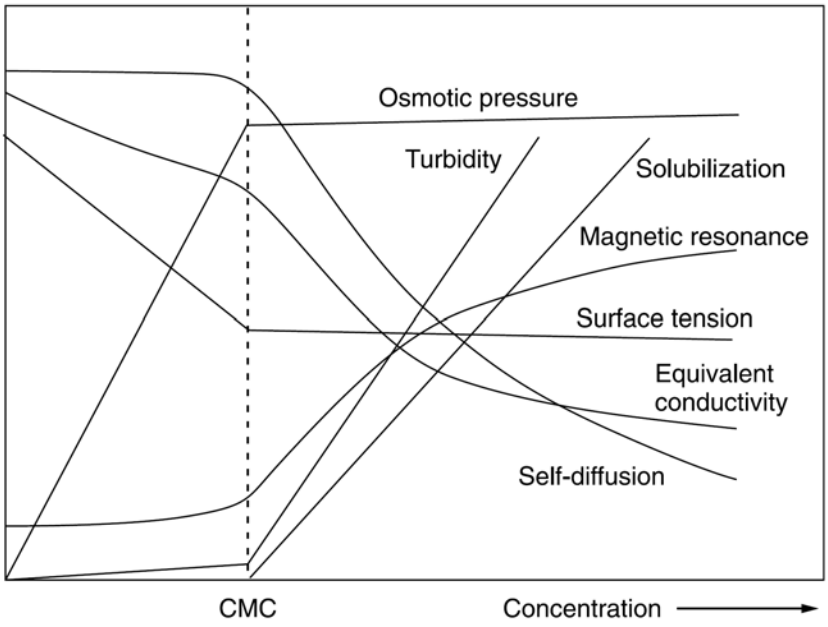

Figure 1.4.[14] The concentration dependence of physico-chemical properties for solutions of an ionic surfactant

Surfactant Modification

The physico-chemical properties of surfactants are governed by a number of structural factors: the ionic type of the hydrophilic head groups, the relative sizes and shapes of the hydrophilic and hydrophobic moieties of the molecule (the hydrophilic-lipophilic balance (HLB) and the critical packing parameter (CPP)), the degree of repulsive or attractive interactions between the building blocks (hydrophobic effect, steric effect, mechanic interlocking, etc). Therefore, the structure-performance relationship is of great importance in fundamental research, as well as in the practical applications of surfactants.[15,16]

Surfactants of various structures have been synthesized and extensively studied. Based on the nature of the hydrophilic group, there are four types of surfactants: anionic, cationic, zwitterionic (or amphoteric), and nonionic. A general formula may be ascribed to major anionic surfactants as follows:

Carboxylates: $C_nH_{2n+1}COO^-M^+$

Sulfates: $C_nH_{2n+1}OSO_3^-M^+$

Sulfonates: $C_nH_{2n+1}SO_3^-M^+$

Phosphates: $C_nH_{2n+1}OPO(OH)O^-M^+$

with n = 8–16 atoms and the counter ion M^+ is usually Na^+.[12,17] The most common cationic surfactants are the quaternary ammonium compounds (e.g. $C_{12}H_{25}N^+(CH_3)_3Br^-$). N-alkyl betaines ($C_nH_{2n+1}N^+(CH_3)_2CH_2COO^-$) and their derivatives are the main type of zwitterionic surfactants. They behave like cationic surfactants in acid solutions or anionic surfactants in alkaline solutions. The most important nonionic surfactants are based on ethylene oxide in the formula of $C_nH_{2n+1}X(CH_2CH_2O)_nH$ where X is O, N, or

another linking functionality. The other types of nonionic surfactants include derivatives of polyglucosides, polyols, and polyamides.[18,19] Figure 1.5 illustrates some typical surfactants with different hydrophilic head groups. Approximately, the CMC decreases by a factor of 2 for ionic surfactants and by a factor of 3 for nonionic surfactants on adding one methylene group to the alkyl chain. With nonionic surfactants, increasing the length of the hydrophilic group, poly (ethylene oxide), causes an increase in CMC.

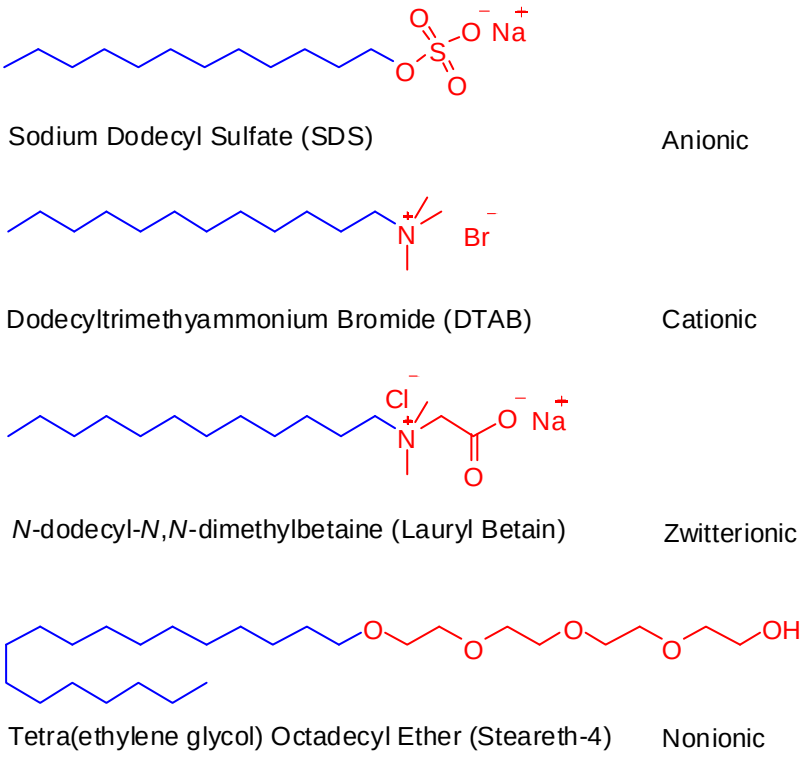

Figure 1.5. Typical surfactants with different hydrophilic head groups

When the skeleton feature is considered, surfactants can also be classified as the following types: single-tailed, bolaform, gemini (or dimeric) and oligomeric, and polymeric (Figure 1.6). Bolaamphiphiles contain one hydrophobic moiety and two

water-soluble groups on both ends.[20,21] They can form unusual aggregates such as monolayer vesicle membranes (MLM Vesicles) in solutions.[22,23] A gemini surfactant has two amphiphilic parts (identical or unsymmetrical) connected by a spacer.[24-26] CMCs of gemini surfactants are one to two orders of magnitude lower than for the corresponding conventional (monomeric) surfactants. Polymeric surfactants have gained enormous popularity in the past twenty years.[27-29] They are more complicated than monomeric surfactants in terms of structure and three principal types of surface active polymers are block copolymer, graft copolymer and homopolymer.

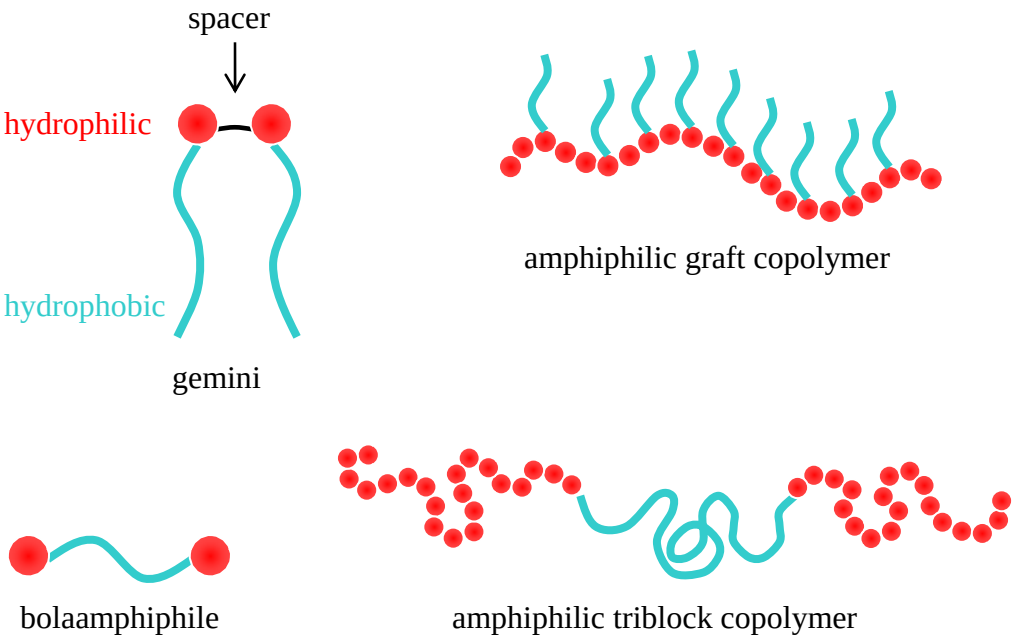

Figure 1.6. Schematic representations of surfactants with various backbone structures

The hydrophobic tail groups are also upon modification. Increase in the length of the tail decrease its solubility in water and increase its solubility in organic solvent. And the building blocks can be straight or branched alkyl chains, alkyl aromatics,

fluorocarbons, and silicones.[30-32] The introduction of branching or unsaturation (such as double bond and aromatic ring) into the hydrophobic part of a surfactant (while keeping the total number of carbons constant) generally has the effect of increasing the CMC. This tendency can, at least in part, be attributed to steric constraints, since the presence of bulky groups in the hydrophobic tails impedes an effective packing in the micellar core.[33] Replacing the hydrocarbon with a perfluoroalkyl or polysiloxane group results in a dramatic lowering of the CMC.[11]

Another, less common, type of surfactant tail alteration is the incorporation of non-hydrocarbon substituents along the hydrocarbon chain. It has been shown that, depending on the type and position of the inserted atom(s) or group(s), the consequences of such a modification can vary over wide ranges.[34-38] If an insert is too polar, it can inhibit micelle formation even if the amphiphile carries a tail of significant size. For instance, if a surfactant tail is modified with an ester or ether group,[35,36] both of which can act as hydrogen bond acceptors and show significant interactions with water, the compound must have an uninterrupted terminal hydrocarbon chain of at least 8-10 carbons to form conventional micelles. In a recent study it was shown that an amphiphile carrying two ester groups along its tail (Figure 1.7a) forms only loose clusters in aqueous solutions all the way up a concentration of approximately 75 wt%, above which the solution coexists with a solid.[38] One potential application of such alterations is to improve the solubilizing capacity of surfactants for modestly polar organics. In the same way that ethyl acetate is a better solvent than hexane, the presence of non-hydrocarbon functionalities in a surfactant might enhance the partitioning of organic guests from the bulk water phase into the micelles.

All those research has greatly enhanced the knowledge of structure-performance relationship of surfactants and contributed to achieve desired colloidal properties of surfactants for particular purposes. In recent years, environmental aspects have gained growing interests in designing new surfactants. "Natural" or "green" surfactant is becoming an important trend for surfactant development.[39,40] Modifications by interrupting the tail group of a surfactant with non-hydrocarbon functionality would promote the biodegradability and reduce the toxicity in the environment.

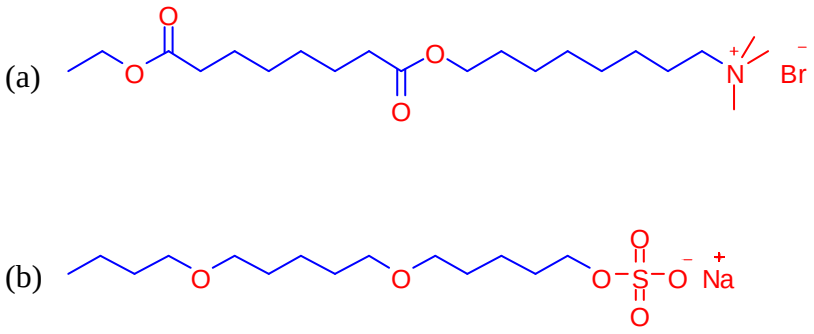

Figure 1.7. (a) An ester-modified surfactant and (b) an ether-modified surfactant

Thioether

Thioethers, also called thiol ethers or sulfides, are simple ether derivatives where the oxygen is replaced by sulfur. The decision to choose sulfur incorporated into the alkyl chain of surfactants is justified by the following reasons.

Sulfur is larger (more polarizable) and much less electronegative than oxygen. In fact, it is similar to carbon in electronegativity (2.55 for C, 2.58 for S, and 3.55 for O, respectively).[41] Thus, thioethers behave very differently from ethers[42,43] and have been extensively utilized in the application of self assembled monolayer (SAM),[44] molecule-

based magnet,[45] organic cofactors,[46] lubricant[47] and especially surfactants and polymer modification.[48-50] Since the 1960s, studies exploring the basic physico-chemical properties of thioethers including hydrogen bonding, polarity, solvation and solubility have been developed.[51-53] Researchers have found that thioether has a weak hydrogen-bond accepting ability.[54-57] For example, the Hansch partition constant between octanol and water for $-SCH_3$ favors octanol (π = 0.45), whereas the constant for $-OCH_3$ favors water (π = -0.47).[58] Also, ethylene oxide ($-OCH_2CH_2-$) is often used as a hydrophilic group, but thioethylene ($-SCH_2CH_2-$) is generally considered hydrophobic.[59-61] However, the relationship between the structure of thioethers as a hydrophobic tail of surfactants and their overall physical properties has not been studied on a systematic basis.

Furthermore, the properties of the amino acid, methionine, also reveal particularity of the sulfur atom. Methionine has a very low occurrence and merely one codon,[62] but it performs important physiological functions: signal recognition and oxidant scavenger.

In 1989, Bernstein studied the binding of proteins to a target peptide chain and suggested that methionine residues play a key role in a nonpolar peptide recognition process.[39] O'Neil and DeGrado also reported that eight exposed methionine side chains of calmodulin bind diverse nonpolar surfaces on associative partners.[63] According to Gellman, two crucial properties of the thioether group, flexibility and polarizability, play a major role in the sequence-independent recognition of nonpolar protein surfaces.[64] From one hand, the flexibility promotes the structural "plasticity" of the methionine residues, and finally, makes it more adaptable to nonpolar surfaces of different shapes.

From the other hand, as also pointed out by Gellman,[64] protein-protein association is dominated by dispersion forces. The dispersion attraction between two molecular surfaces is proportional to each surface's polarizability, so due to the large polarizability of the side-chain sulfur atom, methionine residues are extremely "sticky".

Except for signal recognition, methionine residues in proteins are readily oxidized to the sulfoxide derivative (Met(O)) by various oxidizing reagents such as hydrogen peroxide (H_2O_2), periodate (IO_4^-), hydroxyl radicals, iodine, dimethyl sulfoxide, a dye-sensitized photooxidation, chloramines-T, and *N*-chlorosuccinamide.[65,66] Levine et al. explored the antioxidant defense mechanism of methionine.[67-69] They found that naked methionine residues create a high concentration of reactant, efficiently scavenging oxidants without affecting the activity of the protein, so the buried methionine residues remain intact (Figure 1.8).[69] Thereby, it was proposed that the exposed methionine residues are "physically arranged in an array that guarded the entrance to the active sites". Once the gate is open under continued oxidation, the activity would dramatically decrease in that other essential residue such as tryptophan may be oxidized. The oxidation rate of methionine residues in calmodulin by hydrogen peroxide has also been reported.[70]

Based on those results, new surfactants with sulfur inserted into the hydrophobic region may show some unusual properties. Of potential practical importance, thioether groups within the micelle interior might enhance the solubilization in water of proteins or other "sticky" compounds that are normally not prone to enter hydrocarbon regions. Therefore, we synthesized a series of thioether-modified cationic surfactants. How the sulfur atom affect the self-assembling behavior relative to surfactants without the sulfur

unit is studied. We also examined the oxidation of thioether-modified surfactants in water by a kinetic method, which can be used to assess chain exposure to the external medium in solutions.

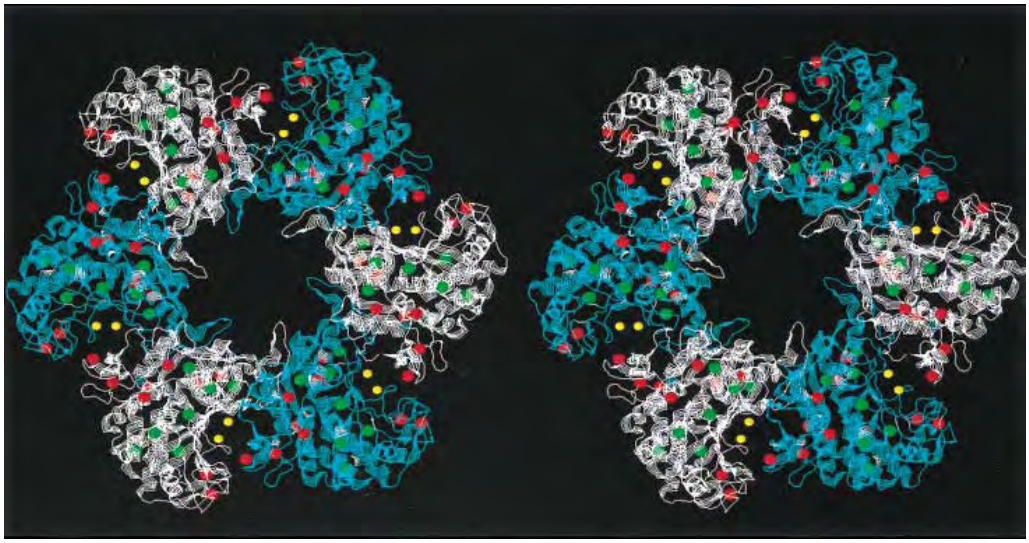

Figure 1.8. Locations of oxidized and intact methionine residues in glutamine synthetase. Sulfur of methionine residues are shown as balls, with intact residues in green and the oxidized residues in red.

Synthesis

Each proposed thioether trimethylammonium bromide (except for **G**) possesses one sulfur atom within its hydrocarbon chain. Surfactant **G** contains two sulfurs to manifest if the perturbation is additive while minimizing the risk of non-micellization. The total chain length is altered: C12 for **B** and **C**, C14 for **D** and **E**, C16 for **F**, and C18 for **G**. The alkyl chain of amphiphile **A** contains only seven carbons, which is below minimum requirement of chain length (C8) for a self-assembling surfactant. Hence, **A** always exists in the unimer form in solutions. In the oxidation study, **A** can serve as an unmicellized thioether to compare with the micelle-protected (under hydrophobic environment) ones (**B**-**G**).

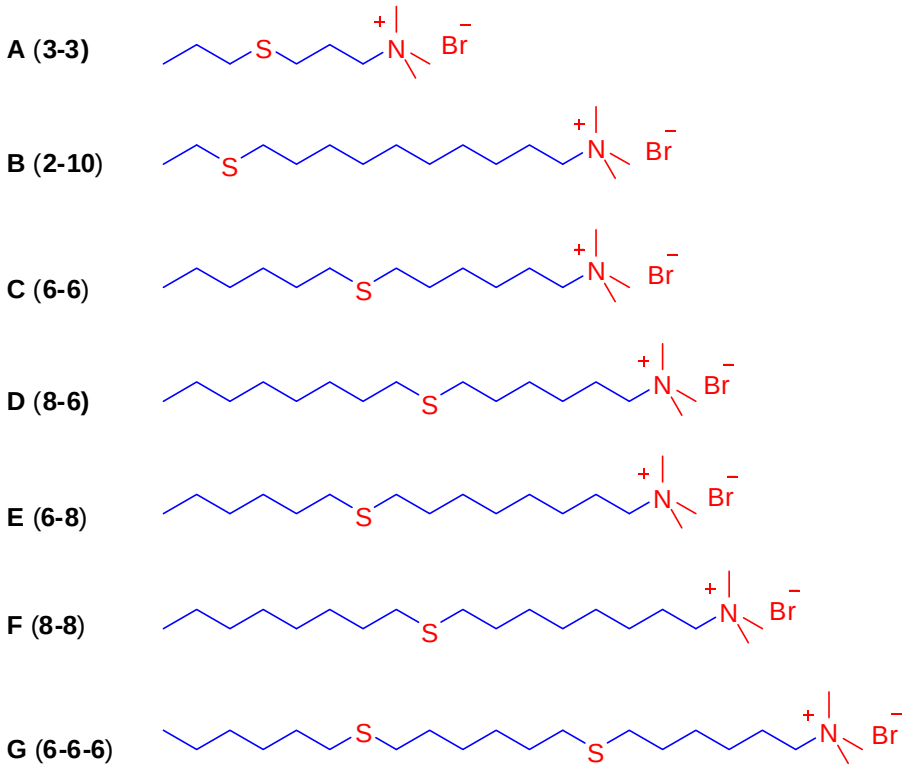

Figure 1.9. Proposed thioether trimethylammonium bromides

To examine the segment length dependence, sulfur is inserted along the alkyl chain from different positions characterized by n, m and p values (Table 1). For convenience, numbers such as **3-3** and **6-6-6** will also be used for the thioether-modified salts in the discussion part.

Table 1.1. Tail segment lengths of the thioether trimethylammonium bromides

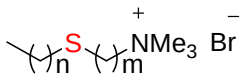

A-F

G

compound	**A**	**B**	**C**	**D**	**E**	**F**	**G**
n	2	1	5	7	5	7	5
m	3	10	6	6	8	8	6
p	/	/	/	/	/	/	6

The thioether trimethylammonium bromides **A-F** investigated in this work were synthesized via the two-step procedure shown in Scheme 1.1. The first step starts from a S_N2 reaction[71] between an alkanethiol and a dibromoalkane with the assistance of sodium ethoxide in ethanol.[72,73] The intermediate product - thioether bromide was purified by a flash column chromatography (The yield varied from 32-72 % depending on the specific alkanethiol and dibromoalkane). Then, the intermediate was treated with excess

trimethylamine to achieve the final product -thioether trimethylammonium bromides with a 90-95 % yield.[74]

Scheme 1.1. Synthesis of thioether trimethylammonium bromides

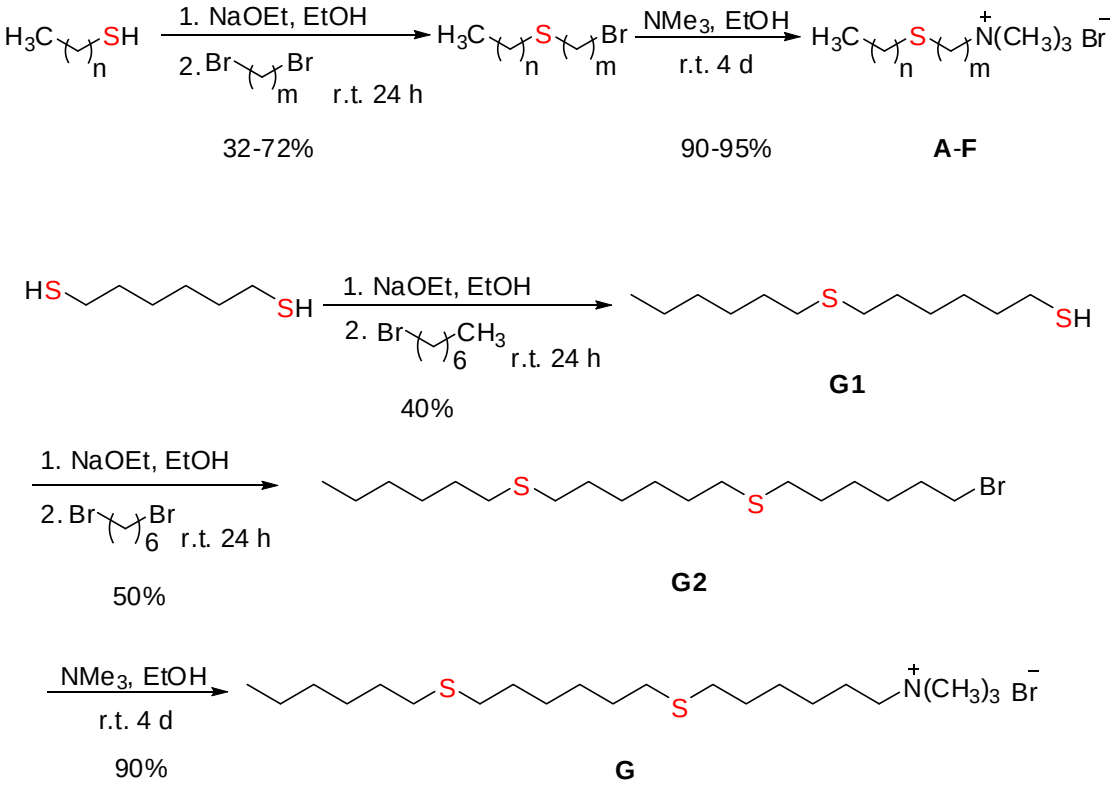

Synthesis of the amphiphile **G** was somewhat more difficult than **A**-**F**. First, 1-bromohexane reacted with excess 1,6-hexanedithiol to give 6-(Hexylthio)-1-hexanethiol. Due to the very close polarities of the starting material and the product, purification of 6-(hexylthio)-1-hexanethiol by means of flash column chromatography requires a large amount of nonpolar solvent as eluent (more than 30 liters of hexane for 0.8 gram of **G1**. Yield: 40 %). Meanwhile, purification of the intermediate by distillation is unlikely

owing to high boiling point and viscosity of 1,6-hexanedithiol. In the second step, 6-(hexylthio)-1-hexanethiol was reacted with excess 1,6-dibromohexane to form 1-bromo-6-[6-(hexylthio)hexylthio]hexane. Again, the current way to purify the intermediate is flash column chromatography using a large volume of hexane (30 liters of hexane for 1 gram of **G2**. Yield: 50 %). Finally, **G** was achieved with the same procedure as for compounds **A**-**F** using **G2** with excess trimethylamine (yield: 90 %). All the final products (**A**-**G**) are white powder, and **A** and **E** are hygroscopic. In fact, **A** becomes fluid within minutes when exposed to open air. All compounds are dried prior to tests and stored in a desiccator. The structures and purities of **A-G** were proved by traditional means of characterization including ^{1}H and ^{13}C NMR, high-resolution FAB-MS, and elemental analysis.

Results and Discussions

Surface Tension

As mentioned in the beginning, one essential property of surfactant is the formation of colloidal-sized aggregates in solutions when the concentration is above the critical micelle concentration (CMC). The CMC value is an important parameter in characterizing the colloidal behavior of a surfactant because it represents the minimum concentration to achieve the greatest performance in applications involving emulsification, dispersion, solubilization, foaming, or simply surface tension lowering. Experimentally, it is determined by observing the break in the plot of a physico-chemical property of solutions versus the surfactant concentration (or the logarithm of concentration). Surface tension, the minimum amount of work required to create unit area of the interface, is such a physico-chemical property that can be used for measuring CMC. Besides the CMC, surface tension measurements also provide many other parameters of a surfactant including efficiency, effectiveness, and surface area per molecule. Measuring the CMC by surface tension is based on the Gibbs adsorption equation (or Gibbs equation).[1,10-12,32] The basic form of the Gibbs equation is:

$$d\gamma = -\sum_i \Gamma_i d\mu_i \tag{1.1}$$

where $d\gamma$ = the change in surface tension of the solution (mN/m), Γ_i = the surface excess concentration of the component per unit area of surface (mmol/m^2), and $d\mu_i$ = the change in chemical potential of the component in the solution. For an air/two-component solution system (such as air/aqueous surfactant solution), the surface excess concentration of the solvent is zero. Hence, eq 1.1 is reduced to:

$$d\gamma = -\Gamma_2 d\mu_2 \tag{1.2}$$

in which 2 designates the solute (surfactant) dissolved in the bulk phase (water). At equilibrium, the chemical potential of the solute is equal in all phases, so μ_2 at the surface can be taken as the value in the bulk phase. The chemical potential of the solute can be related to its concentration in the bulk phase by:

$$d\mu_2 = RTd\ln a \tag{1.3}$$

where R is the gas constant (8.314 J/mol·K), T is the absolute temperature, and a is the solute activity in the solvent. The solute activity, at low concentration, can be replaced by the molar concentration (c) and eq 1.3 is written as:

$$d\mu_2 = RTd\ln c \tag{1.4}$$

Then, substituting eq 1.4 into eq 1.2 gives:

$$\Gamma_2 = -\frac{1}{RT}\frac{d\gamma}{d\ln c} \tag{1.5}$$

or

$$\Gamma_2 = -\frac{1}{2.303RT}\frac{d\gamma}{d\log c} \tag{1.6}$$

Since surfactant is surface-active ($\Gamma_2 > 0$), the surface tension decreases with the addition of surfactants when c is below the CMC. Above the CMC, additional surfactant molecules self assemble to form micelles in the bulk phase and so the surface tension remains constant. This abrupt change of surface tension in the plot of surface tension versus log c represents the CMC (Figure 1.10).[12] The equilibrium surface tension can be measured by several techniques such as Du Nouy ring, Wilhelmy plate, pendent drop, and drop weight (volume).[12,33] Here, the Du Nouy ring method[75-77] is used to determine the CMCs of thioether-modified surfactants.

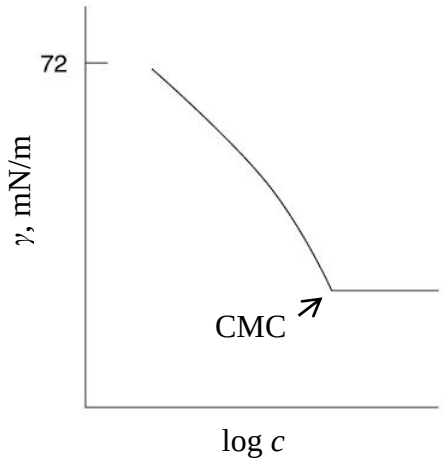

Figure 1.10. Plot of surface tension versus log of the bulk phase concentration for an aqueous solution of a surfactant

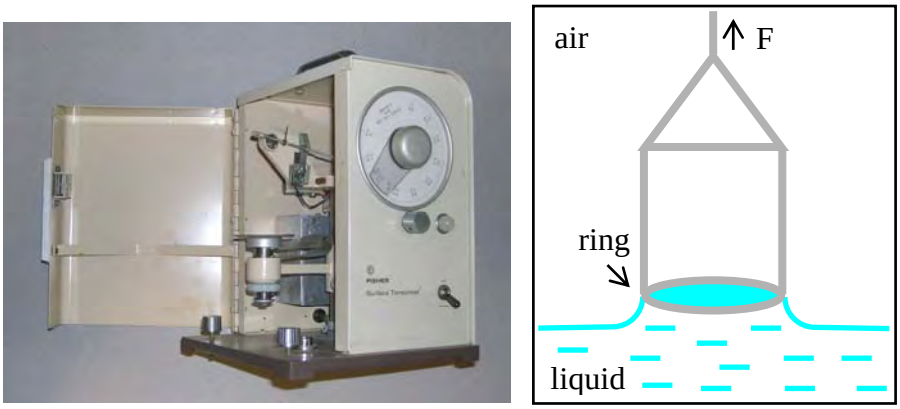

Figure 1.11. Fisher surface tensiometer and close-up of the Pt/Ir ring

As shown in Figure 1.11, the tensiometer employs a Pt/Ir ring which is horizontally placed on the surface of a solution. The ring is slowly pulled up. The

minimum force (F) required to detach the ring from the surface gives the surface tension (γ) of a solution with the approximation:

$$F = W + 4\pi R\gamma \tag{1.7}$$

where W is the ring weight and R is the ring radius. The factor 4 is used here because surface tension acts on both the inside and the outside edge of the ring.

Tensiometry measurements were completed for all surface active thioether trimethylammonium bromides (**3-3** is not included due to its too short tail group). First, as shown in Figure 1.12, all plots display typical changes of surface tension versus concentration: surface tension decreases with increased concentration and starts to level off at a certain concentration. This sharp transition proves the formation of micelles as a result of cooperative assembling behavior. Hence, the CMCs were deduced and listed in Table 1.2. From the CMC values, we can see that the general trend (**6-6** > **2-10** > **8-6** ≈ **6-8** > **8-8** > **6-6-6**) is in agreement with the theory: the longer the tail, the lower the CMC.[78]

As a rule of thumb, CMC values are lowered by a factor of 4 as the ionic surfactant chain increases by two carbons. In this sight, according to literatures,[79-81] the CMC values for conventional cationic surfactants DTAB, TTAB, CTAB, and OTAB (refers to dodecyl-, tetradecyl-, cetyl-, and octadecyltrimethylammonium bromide) are 15, 3.3, 0.82, and 0.29 mM, respectively (Table 1.2).

The CMC values for **2-10** and DTAB are very similar (14 and 15 mM, respectively). Since both **2-10** and DTAB have 12 carbons in the tail group, it suggests that a single sulfur atom has little effect of on the self-assembling tendency of a surfactant. Unfortunately, things are not so straightforward. The CMCs of **6-8** and **8-6**

are 2-fold of TTAB and **8-8** is 3-fold of CTAB. Therefore, the rule of thumb mentioned above does not hold true for thioether cationic surfactants owing to the disturbing of sulfur insertion. The lower-CMC effect caused by elongation of the alkyl chain is reduced for thioether-modified surfactants. Furthermore, **6-6-6,** with two sulfurs, has a CMC 6 fold of OTAB (1.9 and 0.29 mM for **6-6-6** and OTAB, respectively). This significant difference can be explained by the following reasons: (1) the intramolecular S/S interactions cause additive effect of sulfur; (2) Sulfur disruption is accentuated for longer alkyl chain which promotes self-assembly and favors a drier, more compact environment.

Table 1.2. The CMC values for thioether-modified surfactants and conventional surfactants at room temperature

surfactant	CMC, mM	total carbon number of the tail group
2-10	14	12
6-6	22	12
8-6	6.6	14
6-8	6.5	14
8-8	2.7	16
6-6-6	1.9	18
DTAB	15	12
TTAB	3.8	14
CTAB	0.96	16
OTAB	0.29	18

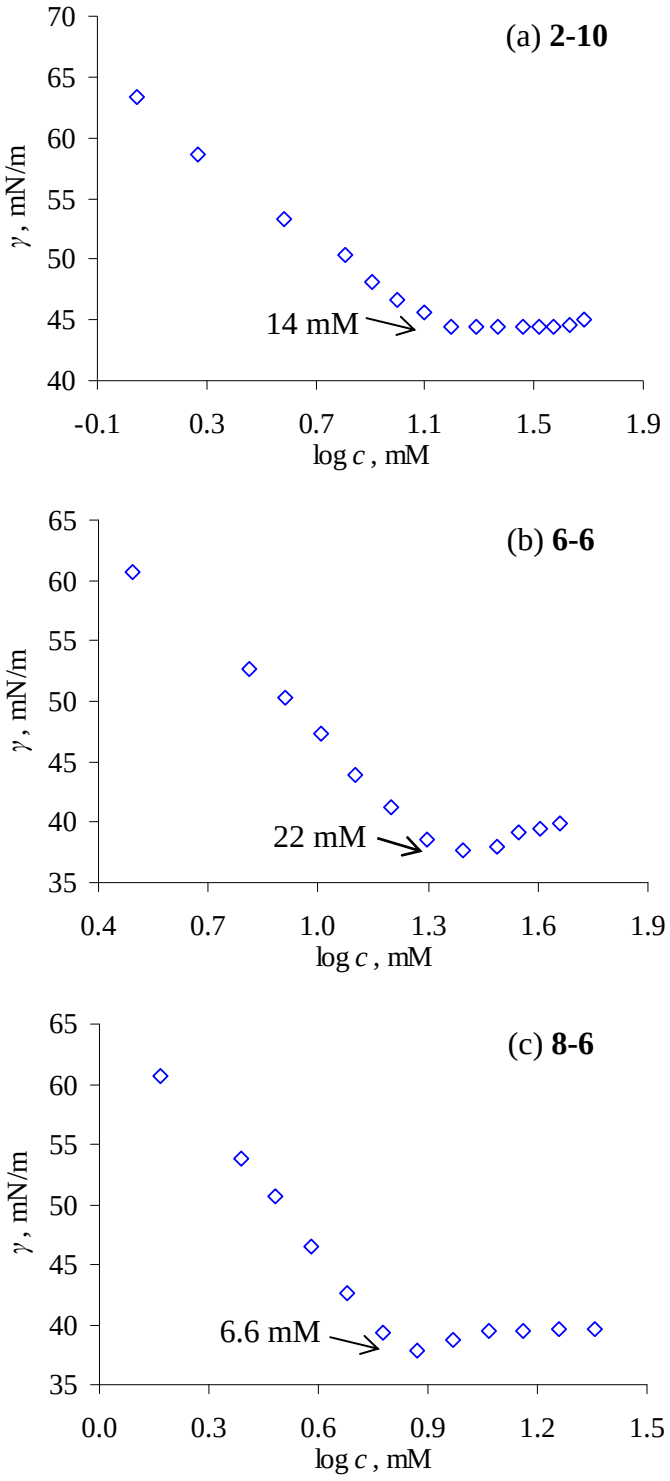

Figure 1.12. Surface tension versus log *c* of thioether-modified surfactants using Du Nouy ring method

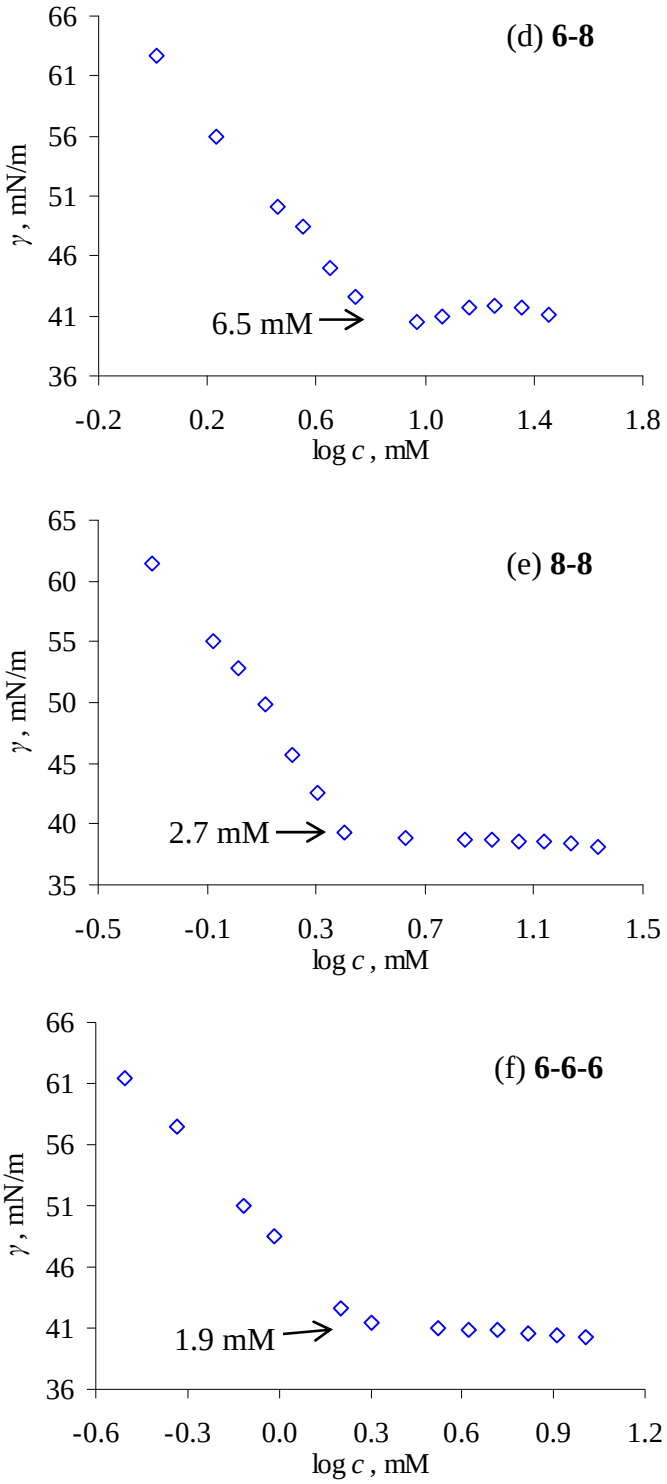

Figure 1.12. Surface tension versus log *c* of thioether-modified surfactants using Du Nouy ring method

CMC values also show some interesting effect of the sulfur position in the chain. For **6-8** and **8-6** (both have a 14-carbon tail group, but sulfur in **8-6** is 2-carbon closer toward the head group than that in **6-8**), the difference in CMC is ignorable (6.6 and 6.5 mM for **8-6** and **6-8**, respectively). In comparison, the CMC of **2-10** is 14 mM but **6-6** has a CMC of 22 mM. It is an interesting question that why sulfur in the center of hydrophobic chain causes more unfavorable interaction between hydrocarbon chains than sulfur close to the hydrophobic chain terminal. To answer this question, the structure of DTAB, **2-10**, **6-6** should be carefully reanalyzed. The major driving force of micellization is the hydrophobic effect, so a longer alkyl chain of surfactant can better induce self-assembling than a short one. The longest hydrocarbon part of **2-10** contains 10 carbons, which is 2-carbon shorter than DTAB. The reduced hydrophobicity can be compensated by the separate 2-carbon part of **2-10**. However, **6-6** has only two equally long hydrocarbons of which the much more impaired hydrophobicity (6-carbon shorter than DTAB) can not be sufficiently compensated by each other. Therefore, the CMC differences among DTAB, **2-10**, and **6-6** originate from the degree of segmentation of the hydrocarbon and in particular, upon the longest segment. This also explains that **6-8** and **8-6** have almost equal CMC values (the longest segment is the same – 8 carbons). It seems reasonable to predict that a hypothesized thioether-modified surfactant **12-2** should have a more similar CMC to TTAB than **6-8** or **8-6**.

Perturbations of micellization from other non-hydrocarbon functionalities such as ester and ether have been reported.[35,36] For ester-modified cationic surfactants, when two ester groups are inserted and the longest hydrocarbon portion is less than 8 carbons (see Figure 1.13a), the surface tension does not level off at higher concentrations. Instead of

the abrupt transition, it displays a steady post-CMC decline of surface tension. An ether-surfactant containing two oxygens shows a similar plot of surface tension versus concentration (Figure 1.13b).

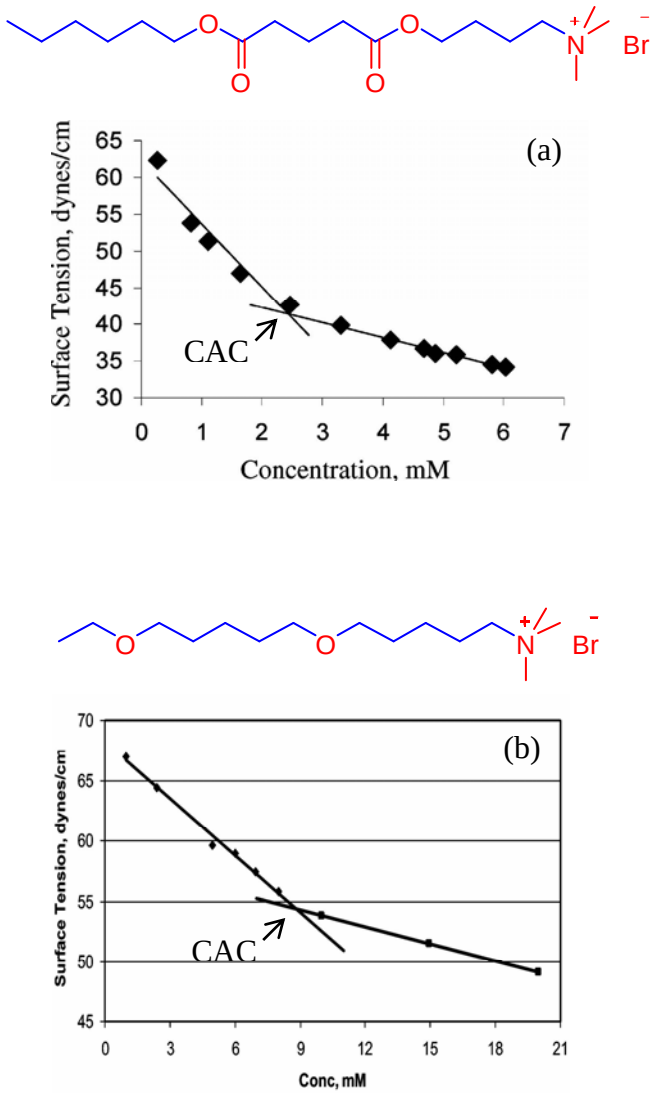

Figure 1.13. Surface tension versus concentration of (a) an ester-modified surfactant and (b) an ether-modified surfactant

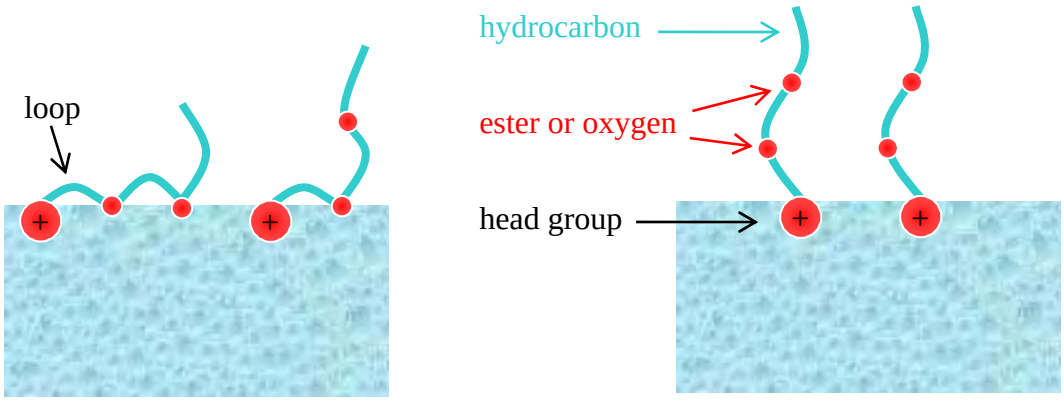

Figure 1.14. Conformational changes of ester- or ether-modified surfactants at the air/water interface

Other researchers have also observed the gradual decline of surface tension but provided no explanation.[82-84] Menger et al.[35-37] proposed two possible rationales for this abnormal phenomenon. First, instead of forming micelles, the ester- or ether-modified surfactants may self-assemble into small, loosely packed aggregates in a stepwise process starting from a specific concentration referred to as the critical aggregation concentration, or CAC. The small aggregates (composed of 5 to 10 molecules) are not as efficient as micelles in consuming additional surfactant molecules. When the concentration is higher than CAC, only a portion of the added unimers forms small aggregates and the rest is still available for the air/water interface. Thereby, the decrease of surface tension with increased concentration is continued but the slope is reduced. Second, both the ester and ether group have a propensity of hydrogen-bonding with water molecules. At low concentrations, the hydratable portion of surfactant molecules could lie flat to form loops at the interface with one or both esters/ethers residing at the interface (Figure 2.14).

Above CAC, the added surfactants not only begin to form small aggregates, but also force the interfacial surfactants rearrange into a more upright conformation. The percentage of additional surfactants entering the air/water interface is lower than that below CAC. That is why a smaller slope was observed from CAC in the plot of surface tension versus concentration.

In contrast, all the thio-surfactants, especially **6-6-6** with two sulfurs, show no such a gradual decline in surface tension, confirming that real micelles are formed. It reveals that sulfur, when inserted into the alkyl tail groups, has a minor disturbing effect on the self-assembly of surfactants compared to the much polar functionalities such as ester and ethers.

Surface tension measurements provide other parameters characterizing colloidal properties of surfactants. The surface tension at the CMC (γ_{cmc}) and area per molecule (A) are useful in discussing the adsorption effectiveness of a surfactant. Values of these parameters for thioether-modified surfactants and their all carbon analogs[11,85-88] are given in Table 1.3. γ_{cmc} is directly obtained from the surface tension plot, ranging from 44 to 38 mN/m for thioether-modified surfactants. No substantial change in γ_{cmc} was found with increase in the length of the hydrophobic groups. Moreover, the γ_{cmc} values (except **2-10**) of thioether-modified surfactants are similar to those of conventional cationic surfactants (41-38 mN/m, see Table 1.3), indicating comparable surface activities. The surface tensions at the CAC (γ_{cac}) of ester- or ether-modified surfactants (up to 60 mN/m) are generally higher than the γ_{cmc} values of thioether-modified surfactants.

The A value is an intricate issue and some debate remains about if the interface is saturated with surfactant molecules for concentrations below the CMC.[37] According to

the traditional theory,[11] the interface reaches saturation at a very low concentration. Below this saturation concentration (C_{sat}), the surface tension changes only slightly with concentration. In the range of concentration between the C_{sat} and CMC, the precipitous drop in the surface tension is due mainly to the increased activity of surfactants in the bulk phase. For the purpose of comparison, this traditional method is used to calculate the area per molecule of thioether-modified surfactants. *A* is derived from the surface excess concentration of the surfactant per unit area of surface (Γ_2, mmol/m^2) which is defined by the Gibbs equation:

$$\Gamma_2 = -\frac{1}{2.303RT}\frac{d\gamma}{d\log c} \tag{1.6}$$

where *R* is the gas constant (8.314 J/mol·K), *T* is the absolute temperature, $d\gamma$ is the change in surface tension of the solution (mN/m), and *c* is the molar concentration of a surfactant. For ionic surfactants, the adsorption of counterions must be considered, so the number of electrolytes at the air/water interface is 2 and eq 1.6 becomes:

$$\Gamma_2 = -\frac{1}{2\times 2.303RT}\frac{d\gamma}{d\log c} \tag{1.8}$$

For concentrations below but near the CMC, the slope of the curve (= $d\gamma/d\log c$) is essentially constant, so a constant surface excess concentration (Γ_2) is achieved. With Γ_2, the area per molecule (*A*) is calculated from the relation:

$$A = \frac{10^3}{N\times\Gamma_2} \tag{1.9}$$

where *N* is Avogadro's number (6.022×10^{23} molecule/mol). For example, **8-8** has a slope of –31.6. At room temperature (T = 298.15 K), the surface excess concentration $\Gamma_2 = -(-31.6)/(2\times2.303\times8.314\times298.15) = 2.77\times10^{-3}$ mmol/m^2 and

$A = 10^3/(2.77\times10^{-3}\times6.022\times10^{23}) = 0.060\times10^{-17}$ m^2/molecule = 60 $Å^2$/molecule.

The *A* vaules of thio-surfactants (except **2-10**) range from 53 to 74 $Å^2$/molecule which are somewhat larger than those of normal cationic surfactants. The only exception is the area per molecule of **2-10** (114 $Å^2$/molecule) which is twice of DTAB. It is consistent with the larger γ_{cmc} of **2-10** because denser surfactant packing at the air/water interface causes lower surface tension. The *A* values, together with results of CMC and γ_{cmc}, support the notion that the interference of the thioether entity is of little important on the colloidal properties of surfactants.

Table 1.3. The surface tension at the CMC (γ_{cmc}) and the area per molecule (*A*) for thioether-modified surfactants and conventional surfactants at room temperature

surfactant	γ_{cmc}, mM/m	*A*, $Å^2$/molecule
2-10	44	114
6-6	37	69
8-6	38	53
6-8	40	70
8-8	38	60
6-6-6	40	74
DTAB	39	57
TTAB	38	61
CTAB	40	52
OTAB	41	64

Fluorescence Spectroscopy

Surface tension experiments provide important data of surfactants such as CMC but not the size and morphology of micelles. The aggregation number (N_{agg}) is one of the most important structural parameters of micelles. Many physical/chemical methods have been developed to measure the N_{agg}.[89] Compared to other means (NMR and thermodynamics), fluorescence quenching (FQ) shows unique advantages such as wider applicable range of N_{agg} and being less costly. Hence, FQ has been widely used in determining N_{agg} of various systems including surfactants,[90-94] mixed surfactants,[95] surfactants/polymers,[96-98] surfactants/additives,[99-101] and peptides.[102]

Measuring the N_{agg} by FQ still relies on the specific techniques and experimental conditions. To achieve reliable results of aggregation numbers, the following factors must be taken into consideration.

1. Which technique to choose: Steady-State Fluorescence Quenching (SSFQ) or Time-Resolved Fluorescence Quenching (TRFQ)?

The basic theory of FQ is detailedly described in the literature.[92,94,103,104] Suppose a homogeneous solution contains a probe, P, and a quencher, Q, so the process of excitation, dynamic quenching and fluorescence decaying can be represented by the following reactions:

$$P + h\gamma \longrightarrow P^* \qquad \text{Excitation (1.10)}$$

$$P^* + Q \xrightarrow{k_Q} P + Q \qquad \text{Quenching (1.11)}$$

$$P^* \xrightarrow{k} P \qquad \text{Fluorescence decaying (1.12)}$$

where k_Q is the second-order quenching rate constant and k is the probe decay rate constant. In the absence of the quencher Q, the probe fluorescence lifetime $\tau_0 = 1/k$, and in the presence of Q, the probe lifetime τ is given by:

$$\frac{1}{\tau} = \frac{1}{\tau_0} + k_Q[Q] \tag{1.13}$$

Eq 1.13 can be transformed into the Stern-Volmer equation:

$$\frac{\tau_0}{\tau} = 1 + K_{SV}[Q] \tag{1.14}$$

where $K_{SV} = \tau_0 k_Q$ is the Stern-Volmer constant. For pure dynamic quenching, the ratio τ_0/τ is equal to the ratio of I_0/I_Q (I_0 and I_Q are the fluorescence intensities measured in the absence and in the presence of the quencher, respectively).

If static quenching (eq 1.15) and dynamic quenching take place simultaneously, the Stern-Volmer equation (eq 1.14) becomes eq 1.16:

$$P + Q \rightleftharpoons^{K_{eq}} PQ \qquad \text{Static quenching} \tag{1.15}$$

$$\frac{I_0}{I_Q} = (1 + K_{eq}[Q])(1 + K_{SV}[Q]) \tag{1.16}$$

The equilibrium constant, K_{eq}, for the formation of the complex PQ depends on the nature of the probe/quencher pair and its microenvironment.

In SSFQ experiments, it is assumed that (1) quenching is purely dynamic, (2) there is no intermicellar migration of the probe and quencher on the time scale of the experiment (residence time of the probe and quencher in a micelle >> probe fluorescence lifetime, τ), (3) $k_Q/k >> 1$ and (4) the distribution of probes and quenchers among micelles obey Poisson's statistics. Therefore, the variation of the fluorescence emission intensity is reduced to:

$$\frac{I_0}{I_Q} = exp(\frac{[Q]}{[micelle]}) \quad (1.17)$$

Usually, eq 1.17 is transformed to:

$$Ln(\frac{I_0}{I_Q}) = \frac{[Q]}{[micelle]} \quad (1.18)$$

By recording the fluorescence emission intensity at increasing quencher concentration and plotting Ln (I_0/I_Q) against [Q], the concentration of micelle can be determined (1/[micelle] = the slope). Then N_{agg} can be calculated by:

$$N_{agg} = \frac{C_{surf} - CMC}{[micelle]} \quad (1.19)$$

where C_{surf} and CMC are the total concentration and the critical micelle concentration of the surfactant, respectively.

In TRFQ experiments, after exciting the probe by a very short pulse of light, a single photon counting apparatus is used to record the probe fluorescence decay (variation of I(t) with time, t). In the absence of quencher, the excited probe decays with a rate constant $k = 1/\tau_0$ (τ_0: the probe lifetime in its micellar environment) and the decay curves are single exponential. In the presence of quencher, the decay curves are multiexponential and obey:

$$I(t) = A_1 \exp\{-A_2 t - A_3[1 - \exp(-A_4 t)]\} \quad (1.20)$$

I(t) and A_1 (= I(0)) are the fluorescence intensities at time t and zero, respectively. Due to the complication of mathematical descriptions (related to quenching rate constants (k_Q), intermolecular quencher exchange rate constants (k_e), quencher adsorption and desorption rate constants (k^+ and k^-), quencher concentration ([Q]), and micelle concentration ([micelle])), coefficients A_2, A_3 and A_4 are not explained in details here. If the quencher

molecules do not exchange via the water phase within the time scale of the excited state of the probe, eq 1.20 is reduced to:

$$I(t) = I(0)\exp\{-\frac{t}{\tau_0} - R[1-\exp(-k_Q t)]\} \quad (1.21)$$

By fitting recorded fluorescence decay curves to eq 1.21 using a nonlinear weighted least squares procedure, R = [Q]/[micelle] is achieved. N_{agg} is obtained from:

$$N_{agg} = R\frac{C_{surf} - CMC}{[Q]} \quad (1.22)$$

Other kinetic factors including k, k_Q, k_e, k^+ and k^- can also be obtained with various mathematical techniques.

Based on the above description, for the TRFQ technique, the ratio k_Q/k does not necessarily be $>>$ 1, which is a major assumption for SSFQ. Zana et al.[103] found a good agreement between the two techniques when $k_Q/k > 5$ in the presence of air. For lower values of this ratio, the discrepancy between the two techniques increases very rapidly. It can be concluded that theoretically, TRFQ is more accurate and realistic than SSFQ but requires precise/expensive instruments and involves complicated data processing. Compared to TRFQ, SSFQ is convenient to perform and easy for data analysis. Limited by the availability of TRFQ instruments, SSFQ is used to determine N_{agg} for all thio-surfactants. Some results from the literature and our calibrations are listed in Table 1.4.

2. Concentration of surfactants

Aggregation numbers are concentration dependent in most surfactant systems especially when the concentration of surfactant is much higher than its CMC. For instance, the aggregation number of CTAB increases from 40 to 93 when the CTAB concentration rises from 3 to 8 mM.[105] A similar trend was found for the anionic

surfactant SDS.[106] However, Schryver et al.[107] stated that the aggregation numbers of DTAC (dodecyltrimethylammonium chloride) and TTAC (tetradecyltrimethylammonium chloride) remain constant within experimental error, while the N_{agg} of CTAC (cetyltrimethylammonium chloride) increases only at higher concentrations. Consequently, due to the complexity of the solution system (head group type, counterion, chain length, etc), the concentration dependence has not been defined clearly and quantitatively. It seems arbitrary to use one concentration for all thio-surfactants investigated.

3. Probe/Quencher pair and their concentrations

Currently, pyrene/CPyCl (Cetyl pyridinium chloride) is one of the most popular probe/quencher pairs in that both pyrene and CPyCl reside exclusively in the micellar phase. The pyrene concentration should be kept at a very low level (1×10^{-6} M) to prevent the formation of excimers. This means that no more than one pyrene molecule exists in one micelle. In addition, too many quenchers in a solution may interfere with the micelles studied, so the [Q]/[micelle] ratio is kept around 0–1.5 to ensure all quenchers are completely solubilized in the micelles while minimizing the interference.

4. Other factors

Some other factors may also affect the self-assembling behavior of surfactants. According to Malliaris and Zana,[108,109] for example, N_{agg} decreases upon increasing the temperature for ionic and zwitterionic surfactants but increases for nonionic ones. The change of N_{agg} within the room temperature range (23–25 ℃) is neglected. Another potential factor is the equilibration time after each addition of quencher solution. Calibrations using solutions of SDS or CTAB show no obvious changes of N_{agg} with

equilibration time. In the study of thioether-modified surfactants, quenched solutions were equilibrated for 3 minutes prior to measurements.

Table 1.4. Aggregation numbers and polarities of SDS and CTAB micelles at 23-25 ℃

surfactant	technique[a]	probe/quencher	*c*, mM	N_{agg}	polarity,[b] I_1/I_3
SDS	TRFQ[103]	Pyrene/CPyCl	97	76.1	/
(CMC: 8.2 mM)	SSFQ[94]	$Ru(bipy)_3^{2+}$/ 9-methlanthracene	45	60	/
	SSFQ[106]	1-methylpyrene/mDCB	70	63	/
	SSFQ[110]	pyrene/CPyBr	20.8	55	/
	SSFQ[111]	pyrene/CPyCl	50	62	1.26
	SSFQ[103]	pyrene/CPyCl	97	75.2	/
	SSFQ	pyrene/CPyCl	39.9	54	1.18
	SSFQ	pyrene/CPyCl	79.7	60	1.10

Table 1.4. Aggregation numbers and polarities of SDS and CTAB micelles at 23-25 ℃

surfactant	technique[a]	probe/quencher	*c*, mM	N_{agg}	polarity,[b] I_1/I_3
CTAB	TRFQ[99]	pyrene/DMBP	30	146	/
(CMC: 0.96 mM)	TRFQ[107]	1-pethylpyrene/ TPyCl	31	104	/
	SSFQ[112]	pyrene/CPyCl	35	41	/
	SSFQ[105]	pyrene/CPyCl	3	40	1.34
	SSFQ[105]	pyrene/CPyCl	5	45	1.34
	SSFQ	pyrene/CPyCl	6.02	43	1.32
	SSFQ	pyrene/CPyCl	36.0	56	1.30

[a] The numbers in superscript represent references. Those without superscripts are from our work. [b] The Polarity of micelles is calculated by the ratio of the first and the third vibronic peak intensities (I_1/I_3).

In summary, measurements of micelle aggregation number by the fluorescence quenching method depend on the technique and conditions used (Table 1.4). Even for the TRFQ technique under very critical conditions, the error margin on the aggregation number may go up to ±10 %.[106] Therefore, conventional surfactants such as SDS and CTAB were tested repeatedly to explore the optimized experimental conditions. For instance, the pyrene fluorescence spectra in solutions of [CTAB] = 6.02 mM but with different quencher concentrations ([CPyCl]) were recorded (Figure 1.15a). The intensity decay ($\ln (I_0/I_Q)$) at the fifth vibronic peak (λ = 395 nm) was plotted against [CPyCl].

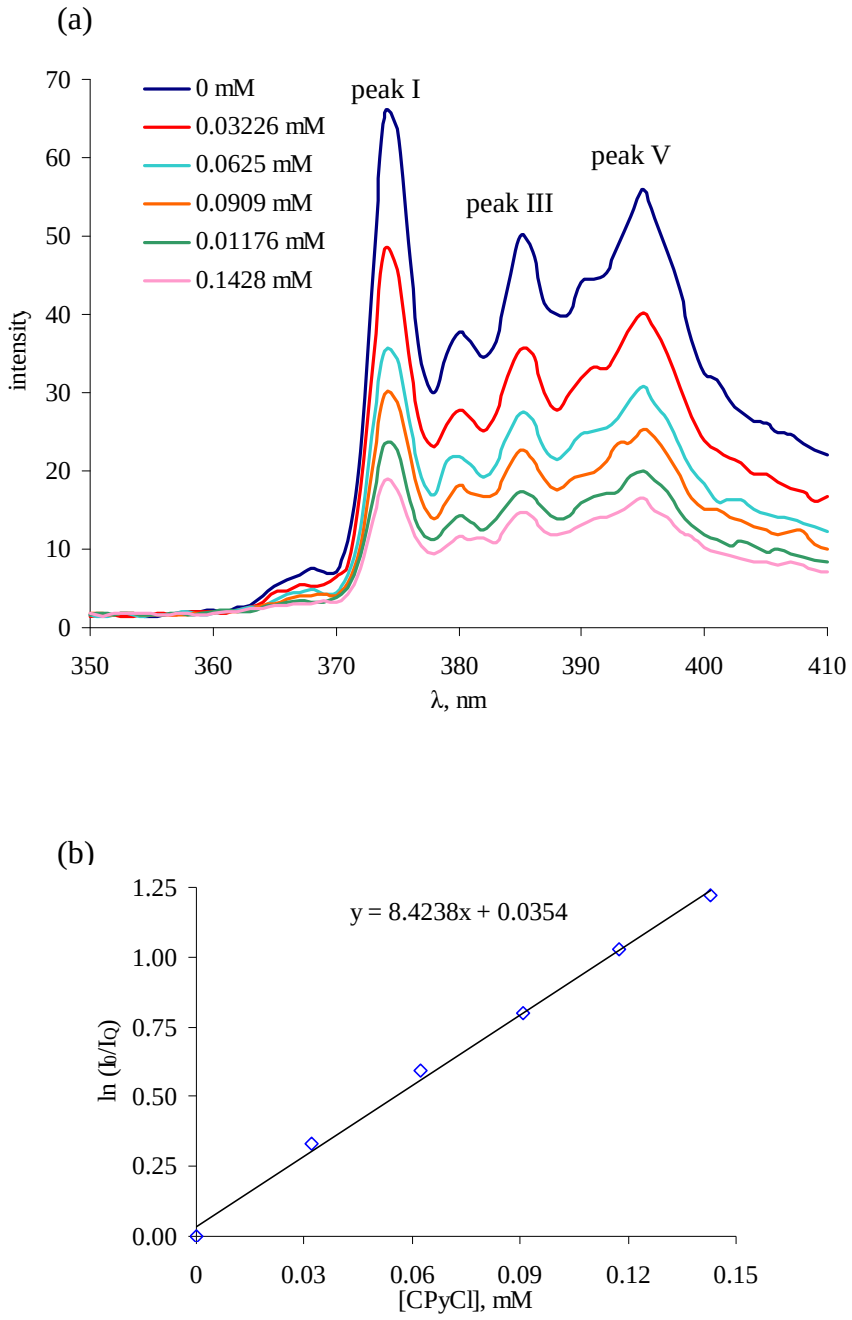

Figure 1.15. (a) Steady-state emission spectra of pyrene in CTAB micelles ([CTAB] = 6.02 mM) quenched at different quencher concentrations ([CPyCl], see inserted legends). (b) Plot of ln (I_0/I_Q) versus [CPyCl] at the fifth vibronic peak (λ = 395 nm).

The slop (= 1/[micelle], Figure 1.15b) was applied in eq 1.18 to give the aggregation number, N_{agg} = ([CTAB]–CMC)/[Micelle]= (6.02–0.96)×8.4328 ≈ 43. This number matches the literature very well (Table 1.4), and so does the polarity of micelles (I_1/I_3). By contrast, the higher concentration (36 mM) of CTAB causes a large deviation in N_{agg} from the reference value (N_{agg} >100) due to the limitation of SSFQ or the shape change (from spherical to rod-like) of CTAB micelles. Measuring N_{agg} of SDS micelles by SSFQ has a broader applicable concentration range. For thio-surfactants, results by SSFQ at the concentration of 5 to 8 fold of the CMC are listed in Table 1.5. The corresponding plots of the intensity decay are shown in Figure 1.16.

Table 1.5. Aggregation numbers and polarities of micelles of thioether-modified surfactants at 23–25 ℃ by the SSFQ technique with pyrene/CPyCl as the probe/quencher pair

surfactant	CMC, mM	*c*, mM	N_{agg}	polarity, I_1/I_3
2-10	14	112	78	1.43
6-6	22	110	60	1.43
6-8	6.5	39	54	1.43
8-6	6.6	41	51	1.51
8-8	2.7	17	46	1.45
6-6-6	1.9	13	29	1.41

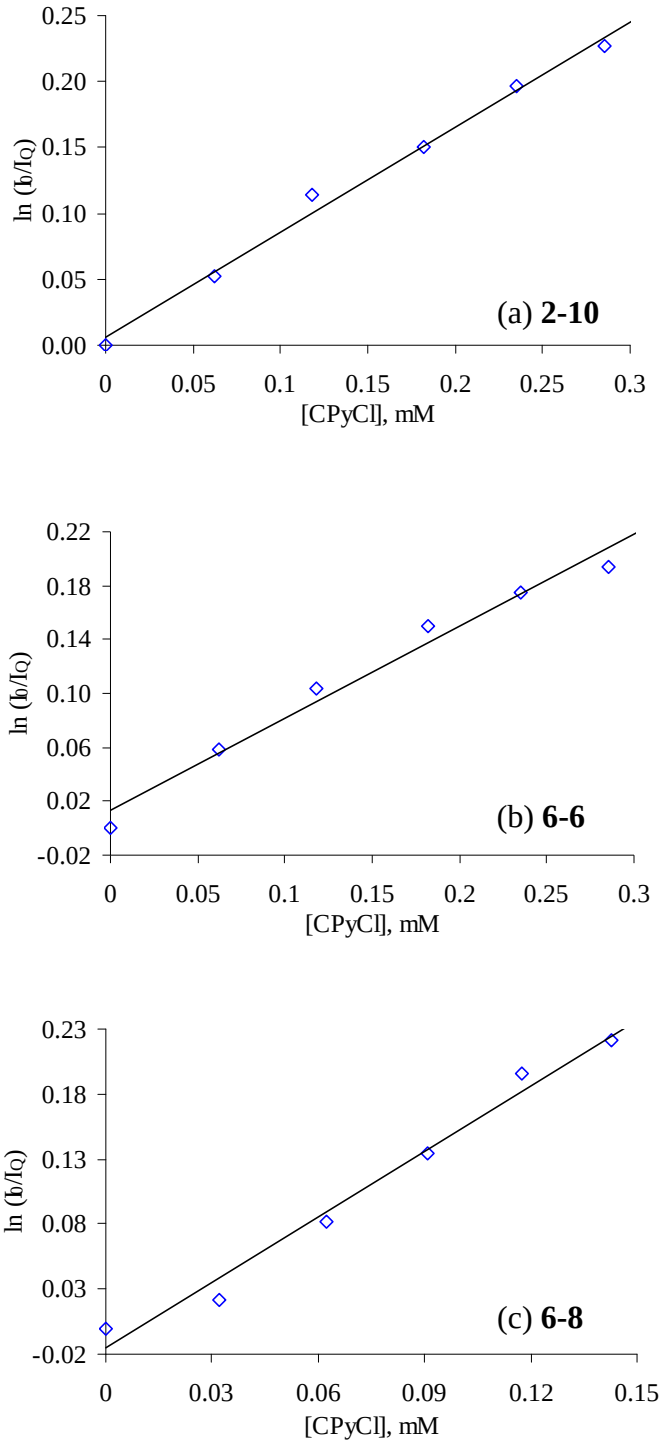

Figure 1.16. Plots of $\ln(I_0/I_Q)$ versus [CPyCl] at the fifth vibronic peak (λ = 395 nm) for thioether-modified systems (with pyrene/CPyCl as the probe/quencher pair)

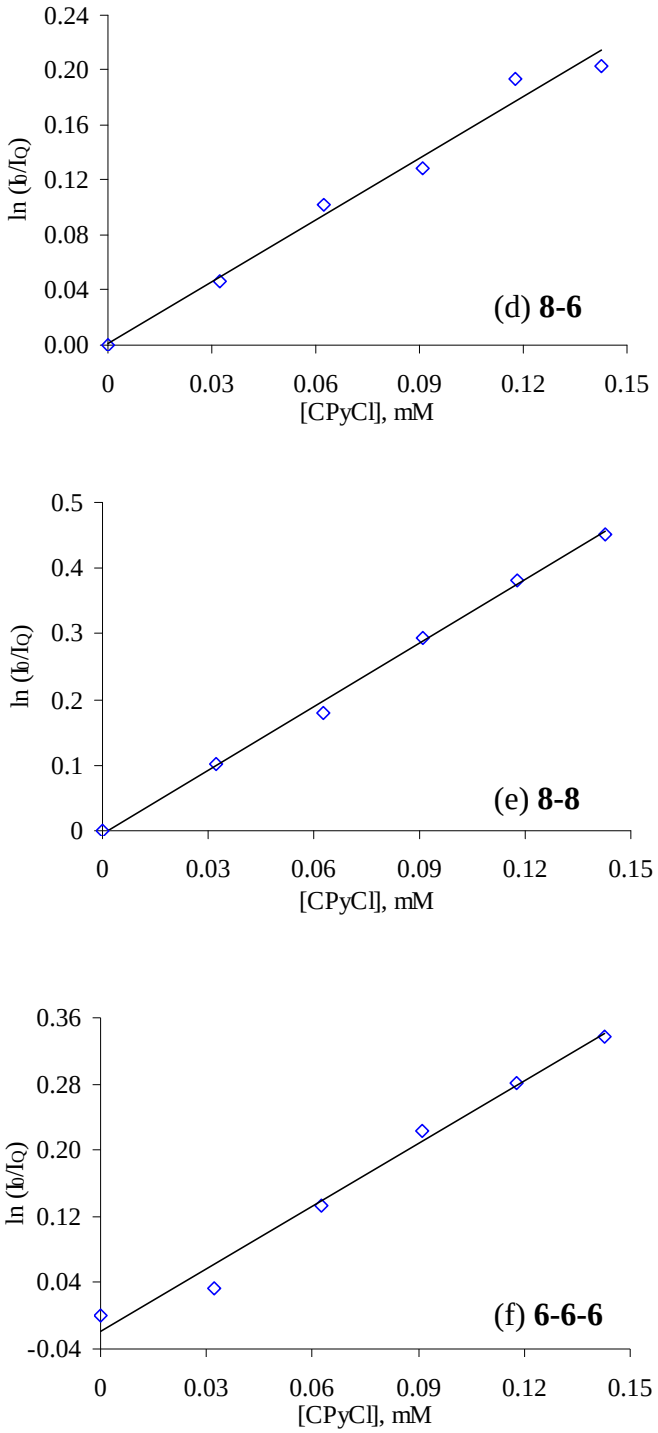

Figure 1.16. Plots of $\ln(I_0/I_Q)$ versus [CPyCl] at the fifth vibronic peak (λ = 395 nm) for thioether-modified surfactant systems (with pyrene/CPyCl as the probe/quencher pair)

In general, all plots show a good linearity of ln (I_0/I_Q) versus [Q], indicating that the experimental conditions are appropriate. Except **2-10** and **6-6-6**, the aggregation numbers (46–60) of thio-surfactants reveal normal micelle sizes. More importantly, all N_{agg} parameters prove that the self-assemblies are micelles instead of loose, small aggregates. For **6-6-6**, intramolecular and enhanced intermolecular S/S interactions may contribute to the small aggregation number (29). Another interesting trend is the N_{agg} decreases with increasing chain length for thio-surfactants, which is opposite to that of conventional surfactants. This probably is caused by the same reason discussed in the surface tension part that longer alkyl chain is prone to sulfur disruption.

Besides, as mentioned in Table 1.4, the polarities of intramicelles can be estimated by measuring the ratio of the first and third vibronic peaks, I_1/I_3. The I_1/I_3 values of thio-surfactants (~ 1.4–1.5) are higher than the all-carbon cationic surfactants (~ 1.3), indicating a less nonpolar microenvironment (the micelle interior) where the pyrene molecules reside.

NMR

NMR-based measurements have offered insights into a range of physico-chemical properties including size, shape, and complexation for the study of self-assemblies in solution for decades.[113,114] Multiple NMR techniques (^{1}H, ^{13}C, and NMR diffusometry) are adopted for investigating four selected thio-surfactants **2-10**, **6-6**, **8-6**, and **8-8**. The results are compared to DTAB and CTAB in water within the same concentration range. In this section, two systems: I. Solutions of Single Thio-surfactant and II. Mixtures of **2-10** or **6-6** with DTAB are studied.

I. Solutions of Single Thio-surfactant

Viscosity and ^{1}H-NMR.

All samples except solutions of **8-8** in concentrations of about 500 mM and above are of low viscosity and show high-resolution peaks in ^{1}H-NMR spectra. These features indicate that no or a very limited micellar growth occurs in the samples. In concentrated solutions of **8-8**, on the other hand, there is a notable increase in viscosity with increasing concentration (Figure 1.17).

Solutions of large micelles exhibit behavior that is analogous to that of solutions of linear polymers. In fact, large micelles can in many senses be regarded as "living polymers" (since the "degree of polymerization" show a strong dependence on the conditions), and concepts and theories developed for polymer solutions can successfully be applied when analyzing their behavior.[10] At concentrations above the so-called overlap concentration, polymer-like micelles form a transient entangled network and the zero-shear viscosity of the solution, η, is expected to depend on the micellar aggregation number, N, and the volume fraction of aggregates, Φ, according to:[10]

$$\eta = \text{constant } N^3 \Phi^{3.75} \tag{1.23}$$

If the concentrated **8-8** samples are compared to solutions of CTAB, the micelles of which are known to show notable growth into thread-like aggregates with increasing concentration,[115] solutions of the former consistently have a significantly lower viscosity than those of the latter at comparable concentrations. Considering the similarities between **8-8** and CTAB – the compounds have the same type of head-group and hydrophobic tails of similar size – this observation gives strong indication that, at a given concentration (at concentrations where aggregate growth occurs), the micelles of **8-8** are smaller than those of CTAB.

This notion is also supported by a comparison of ^{1}H-NMR spectra of the two compounds at different concentrations. The peaks in a ^{1}H-NMR spectrum of a surfactant that reside in large micelles are broad and show a characteristic band-shape with a broad base and a narrow apex. This appearance of the peaks is due to the presence of slow motion components.[115,116] Figure 1.17 shows the spectra of **8-8** and CTAB, both at a concentration of 16 wt% (i.e. approximately 440 and 480 mM of **8-8** and CTAB, respectively). It is clear that, although the observed peak broadening for **8-8** is significant, it is much smaller than for CTAB. This observation is consistent with a smaller micelle size for **8-8**.

Taken together, the results from ^{1}H-NMR and the differences in the viscosity of solutions of **8-8** or CTAB clearly indicate that the presence of a sulfide group in the hydrocarbon tail of a surfactant decreases the tendency for micellar growth. In other words, the inclusion of the sulfur renders the surfactant a smaller effective packing parameter and the surfactant film a higher spontaneous curvature.[10] From a molecular

point of view, this observation may be rationalized by the sulfide group having a slightly higher propensity to reside close to the aggregate surface as compared to a methylene group in the same position. This would give a surfactant containing a sulfide group a slightly larger area per molecule that is exposed to the aqueous surroundings as well as decreased effective hydrophobe volume and hence a somewhat lower spontaneous packing parameter as compared to that of an all-methylene counterpart.[117]

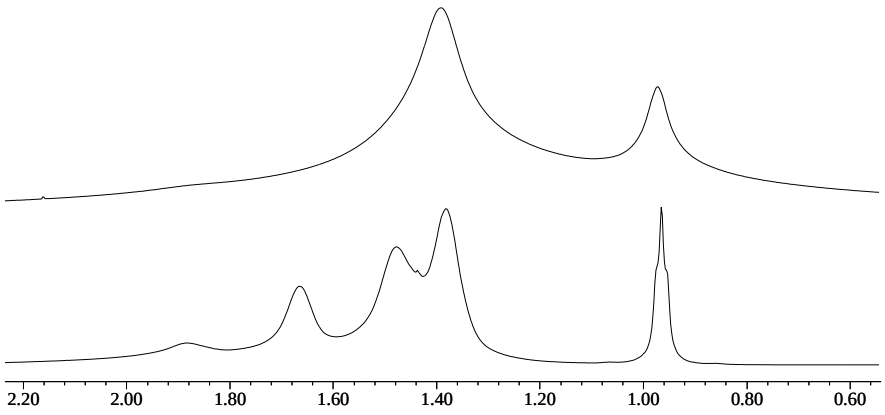

Figure 1.17. ^{1}H-NMR spectra of 16 wt% solutions of CTAB (top) and **8-8** (bottom) at 28℃. The peaks at 0.9 ppm arise from the terminal methyl group, and the signals between 1.2 and 2.0 ppm arise from the majority of the tail methylene groups.

NMR Diffusometry

The translational mobility of a surfactant in solution depends on the formation of micelles and other aggregates, and self-assembly is manifested by a decrease in the self-diffusion coefficient of the surfactant as the effective size of the diffusing entities increases. Hence, by determining the concentration dependence of a surfactant's self-

diffusion coefficient, it is possible to estimate the size of its micelles as well as to probe the process by which these are formed. In this work, the diffusion coefficients were measured using the Pulsed Gradient Spin-Echo (PGSE) NMR technique, a well-established method for studying surfactant self-assembly.[114,118]

Generally, the exchange between surfactant monomers and surfactant molecules that reside in aggregates occurs at a rate much faster than the time-scale of the NMR diffusion experiment. Thus, the observed self-diffusion coefficient, D_{obs}, is a population-weighted average of the self-diffusion coefficients at the different sites where the surfactant resides. Under the assumption that the micellization can be described by the phase-separation model,[10] and that the micelles can be approximated as discrete monodisperse aggregates, D_{obs} can be expressed as follows:

$$D_{obs} = \frac{c_{mono}}{c} D_{mono} + \frac{c_{mic}}{c} D_{mic} \tag{1.24}$$

where D_{mono} and D_{mic} are the diffusion coefficients for the surfactant monomers and the micelles, respectively, while c_{mono} is the concentration of surfactant monomers, c_{mic} the concentration of surfactant molecules that reside in the aggregates, and c the total surfactant concentration. It follows from eq 1.23 that a plot of the experimental values of D_{obs} versus c^{-1} should give two straight lines that intersect at the CMC – a horizontal line with $D_{obs} = D_{mono}$ for concentrations up to the CMC, and a line with a slope of approximately $(D_{mono}–D_{mic})\times$CMC for higher concentrations. For a conventional, micelle-forming surfactant this is generally a good approximation of reality.

Figure 1.18 presents the results from diffusion measurements on the four studied thioether surfactants, along with the corresponding data for DTAB. One can see that all surfactants indeed give two sharply intersecting, straight lines. To simplify the

comparison between the results on the different surfactants, the concentrations are normalized to the CMC values of the respective surfactants (i.e. the x-axis shows (c/CMC)$^{-1}$ rather than c^{-1}). The CMC values, which were obtained from the intersection of the horizontal and sloping lines in plots of D_{obs} vs. c^{-1}, are presented in Table 1.6. With the exception of the values for **2-10**, these diffusometry-based values correspond well with those obtained from surface tension measurements. We cannot explain the discrepancy of the CMC values obtained from the surface tension measurements and the other used techniques. However, since the NMR-techniques and the conductivity measurements all investigate the bulk, and hence are more direct than a surface tension study, and all give reasonable agreement, we assume that the CMCs obtained from these methods are closer to the true value.

Table 1.6. Data on the studied thio-surfactants and surfactant mixtures

surfactant	**2-10**	**6-6**	**8-6**	**8-8**	DTAB	**2-10**+ DTAB[a]	**6-6**+ DTAB[a]
CMC from NMR Diff., mM	39	30	6.8	2.2	16	18	17
CMC from ^{13}C-NMR, mM	42	31	7.1	2.0	15	18	18
CMC from conductivity, mM	46	33	8.2	2.8	16	/	/
ionization degree, α	0.35	0.40	0.28	0.28	0.30	/	/
CMC from S.T., mM	14	22	6.6	2.7	15	/	/

[a] Equimolar mixtures.

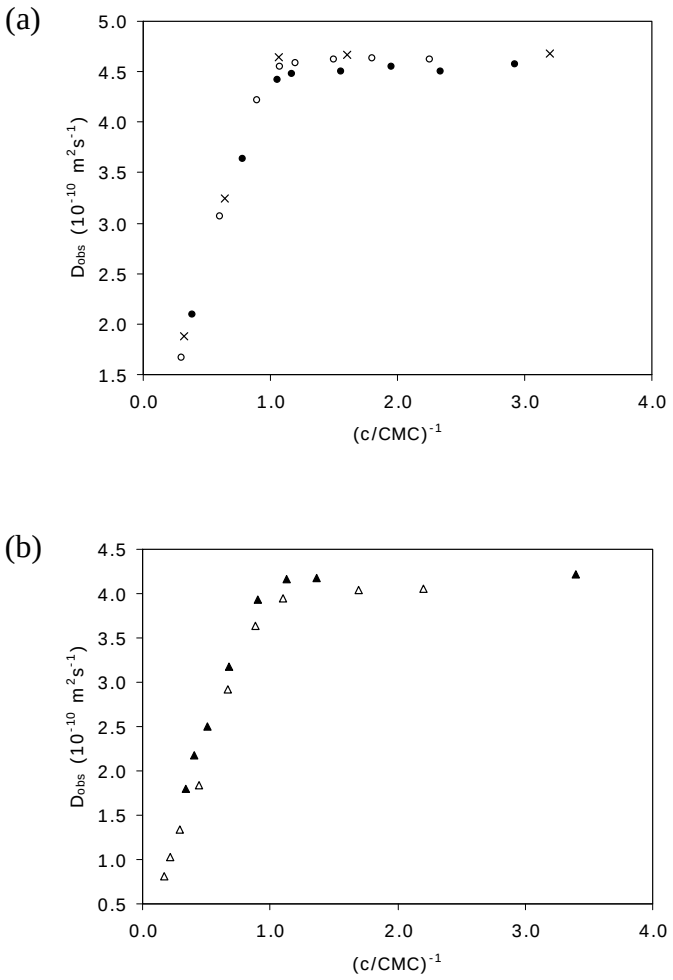

Figure 1.18. The observed self-diffusion coefficients, D_{obs}, of (a) **2-10** (●), **6-6** (○), and DTAB (×), and (b) **8-6** (▲) and **8-8** (△) vs. the inverse normalized surfactant concentration. The concentration, *c*, is normalized to the CMC of the respective surfactants.

Another important observation that can be made in Figure 1.18a is the fact that the variation of D_{obs} with $(c/\mathrm{CMC})^{-1}$ for **2-10** and **6-6** practically overlaps with that for DTAB. The radius of a spherical micelle, which is inversely proportional to D_{mic}, is by

geometrical constraints forced to be approximately the length of one extended surfactant molecule, l_{max}, for an effectively packed micelle.[117] Thus, since l_{max} of **2-10** and **6-6** are similar to that of DTAB, which is known to form spherical micelles up to concentrations of about 450 mM,[119] the overlapping data support that these two thioether surfactants form essentially normal, spherical micelles with a degree of cooperativity similar to that in the assembly of a conventional analog.

If one compares the CMC values for **2-10**, **6-6**, and DTAB (all with 12 carbons in their hydrophobic parts) one can see that insertion of a sulfide group in the chain raises the CMC by 2 to 3 fold. A decreased propensity for micellization (as manifested by an increased CMC) might reflect a perturbation on either side of the monomer-micelle equilibrium (or both). Furthermore, if the larger CMC (~ 40 mM) by NMR and conductivity method of **2-10**, compared to 14 mM by surface tension, is closer to the real CMC, then the previous explanation on the effect of sulfur position would be inappropriate. Sulfur in **6-6** is 4-carbon closer toward the head group than in **2-10**. The longer hydrocarbon between sulfur and the ionic group in **2-10** makes itself more flexible to bend, and thereby shortens the effective chain length. This may also rationalize the fact that **2-10** has larger area per molecule (due to the looping at the interface).

^{13}C-NMR

The chemical shifts in NMR spectra of surfactants in aqueous solution commonly show pronounced concentration dependencies. This phenomenon can be explained by differences between monomers and micellized surfactant in both the direct effects of the environment (medium effects) and in the average conformation of the molecules (conformation effects). It has been shown that the changes in the ^{13}C-NMR shifts for

carbon atoms along an alkyl chain show only a very weak dependence on medium effects and to a good approximation can be ascribed exclusively to changes in the average chain conformation.[120-122] Thus, a downfield ^{13}C-NMR shift can be related to an increase in the average ratio of gauche to trans conformations in the chains. A concentration-dependence study of the ^{13}C-NMR shifts of a surfactant is valuable for revealing structural changes in its aggregates with concentration.

If only one peak for each nonequivalent carbon in a molecule appears at all concentrations, as is the case for all of the herein discussed compounds, then the observed chemical shift, δ_{obs}, for an atom at a given position in the studied molecule is, in a similar way as D_{obs}, a population-weighted average of the values at the different sites where the molecule can reside. Accordingly, δ_{obs} can be described by an expression of the same form as eq 1.24, given as eq 1.25:

$$\delta_{obs} = \frac{c_{mono}}{c}\delta_{mono} + \frac{c_{mic}}{c}\delta_{mic} \tag{1.25}$$

where δ_{mono} and δ_{mic} are the average chemical shifts of surfactant molecules present as monomers or residing in micelles, respectively, while c_{mono}, c_{mic} and c have the same meanings as above.

Since a majority of the peaks in ^{13}C-NMR spectra of the studied compounds show quite similar chemical shifts, it is difficult to assign all carbons along the hydrophobic tails. However, as is also the case for surfactants with a normal hydrocarbon tail,[123] signals from most of the “mid-chain” methylene groups in the thioether surfactants show similar changes in shift with concentration; these are all larger than the shift changes for signals from methylene groups close to either the terminal methyl groups or the head groups.

Figure 1.19 shows the change in chemical shift, $\Delta\delta$, where $\Delta\delta = \delta_{obs} - \delta_{mono}$, for the methylene signal that gives the largest shift change with increasing concentration. Plots of $\Delta\delta$ vs. $(c/CMC)^{-1}$ are similar for all the studied surfactants. As seen in the Table 1.6, the CMC values obtained from the data underlying Figure 1.18 agree well with those obtained from the NMR diffusometry experiments. Most importantly, the plots for **2-10** and **6-6** closely resemble that for DTAB. These findings suggest that the inclusion of a sulfide group into the tail of a surfactant does not cause any significant change in the average conformation of the surfactant molecules in micelles.

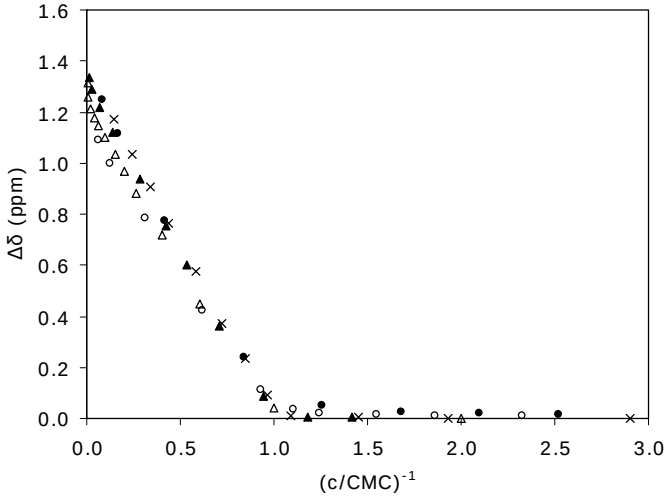

Figure 1.19. Maximum observed change in chemical shifts, $\Delta\delta = \delta_{obs} - \delta_{mono}$, for peaks from methylene carbons in ^{13}C-NMR spectra of **2-10** (●), **6-6** (○), **8-6** (▲), **8-8** (△), and DTAB (×) with the inverse normalized surfactant concentration. The shifts in samples with concentrations below the CMC, are 29.5 ppm for **2-10**, 29.6 ppm for **6-6**, 29.1 ppm for **8-6**, 29.0 ppm for **8-8**, and 29.8 ppm for DTAB.

II. Mixtures of **2-10** or **6-6** with DTAB

In order to investigate the behavior of the thioether surfactants in mixtures with a conventional surfactant, in particular the possible occurrence of conformational changes in the surfactant chains with changing micelle composition, equimolar mixtures of **2-10** or **6-6** with DTAB at different total surfactant concentrations were studied.

NMR Diffusometry

Figure 1.20 shows the results from a diffusion study on equimolar aqueous mixtures of **2-10** and DTAB at different total surfactant concentrations. The fact that D_{obs} for both surfactants departs from D_{mono} at the same total concentration suggests that the two surfactants form true mixed micelles. Furthermore, the observed difference in D_{obs} for the compounds at concentrations above the CMC, i.e. at $(c/\mathrm{CMC})^{-1} < 1$, can be explained by the CMC difference of the two surfactants (about 40 mM and 15 mM for **2-10** and DTAB, respectively). Due to this difference, the fraction of DTAB in the first formed micelles is higher than the global fraction, but approaches the bulk composition with increasing total surfactant concentration, i.e. with decreasing $(c/\mathrm{CMC})^{-1}$. Consequently, D_{obs} for the two surfactants approach each other at higher concentrations. The effect of the CMC difference, as well as the fact that the CMC of the mixture is similar to that of the surfactant with the lower CMC (i.e. DTAB), are in line with what is expected for the formation of ideal mixed micelles.[10] A corresponding study on a mixture of **6-6** and DTAB gives essentially the same result, except that the difference in D_{obs} for the components at concentrations above the CMC is somewhat smaller. Since the difference in CMC for the pure **6-6** and DTAB is smaller than that for **2-10** and DTAB, this result is in line with the expectations.

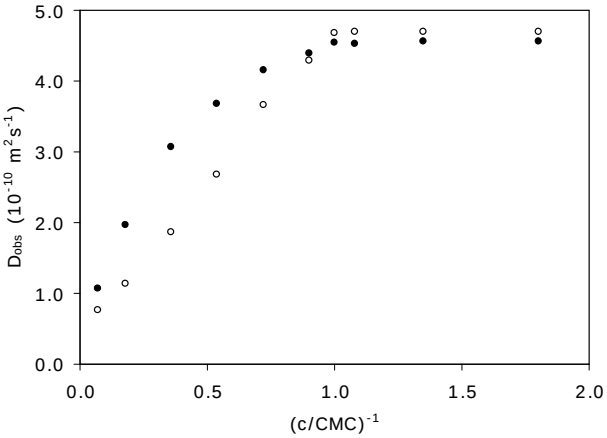

Figure 1.20. Observed self-diffusion coefficients, D_{obs}, of **2-10** (●) and DTAB (○) in equimolar mixtures vs. the inverse normalized total surfactant concentration. The total concentration, *c*, is normalized to the critical micelle concentration, CMC, of the surfactant mixture.

^{13}C-NMR

Figure 1.21 presents the change in chemical shift of methylene peaks from **2-10** and DTAB with $(c/CMC)^{-1}$ when they are present in equimolar mixtures of the two. The signals were selected mainly because they were clearly distinguishable, and not too much attention should be drawn to the absolute values of $\Delta\delta$; what is most important in this context is the functional form of $\Delta\delta$ vs $(c/CMC)^{-1}$. A corresponding plot for the ^{13}C-NMR data on a mixture of **6-6** and DTAB has a very similar appearance.

From eq 1.24, in a situation where the average conformation of the hydrophobic tails in micelles does not change with the total surfactant concentration, $\Delta\delta$ for a component *i* in a surfactant mixture should show a roughly linear dependence on the fraction *p* of *i* that resides in micelles, i.e. $p = c_{mic,i}/c_i$ where $c_{mic,i}$ is the concentration of

micellized i and c_i the total concentration of i. If one assumes that the micelle size is constant with changing total surfactant concentration, p can be estimated from eq 1.23 and the experimental values of D_{mono} and D_{mic} for each component (the latter is approximated by extrapolating D_{obs} to $c^{-1} = 0$). Since it is unlikely that a mixture of two cationic surfactants that both give spherical micelles when present as the lone solutes would form elongated micelles, a plot of $\Delta\delta$ vs. p, as calculated from the diffusion data, should reveal possible bending of the thioether surfactant tails in the mixed micelles. As discussed above, the difference in CMC causes a gradual increase in the micellar fraction of the thioethers from a low value up to the bulk compositions, i.e. equimolarity, as the total surfactant concentration is increased.

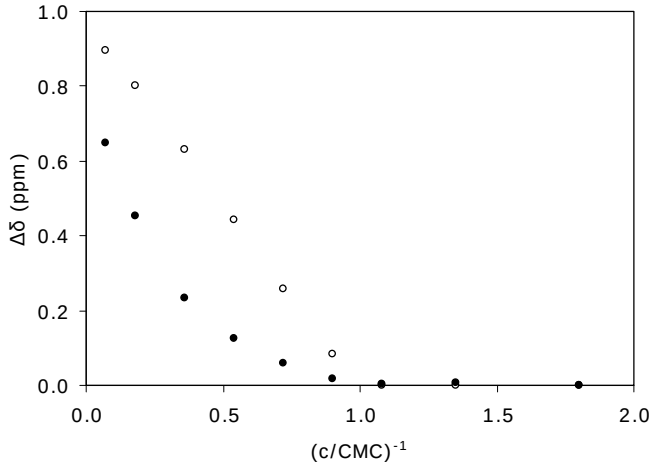

Figure 1.21. The observed change in the chemical shifts, $\Delta\delta = \delta_{obs} - \delta_{mono}$, for peaks from methylene carbons in ^{13}C-NMR spectra of **2-10** (●) and DTAB (○) in equimolar aqueous mixtures of the two with the inverse normalized total surfactant concentration. The total surfactant concentration, c, is normalized to the critical micelle concentration, CMC, of the surfactant mixture.

Figure 1.22 shows a plot of $\Delta\delta$ vs. *p* of the respective surfactant components for the equimolar mixtures of **2-10** and DTAB. One can see that for DTAB $\Delta\delta$ does indeed show a roughly linear dependence of *p*, whereas for **2-10** it shows a slight curvature. This curvature indicates an, on average, more gradual changeover from gauche to trans conformations in the chain with an increasing *p* for the thioether surfactant. It is consistent with the chains of **2-10** being more bent at low *p*, and does hence support the idea that a sulfur atom has a slightly higher preference for the micellar surface as compared to a methylene group. Again, a corresponding result is obtained for the mixtures of **6-6** and DTAB.

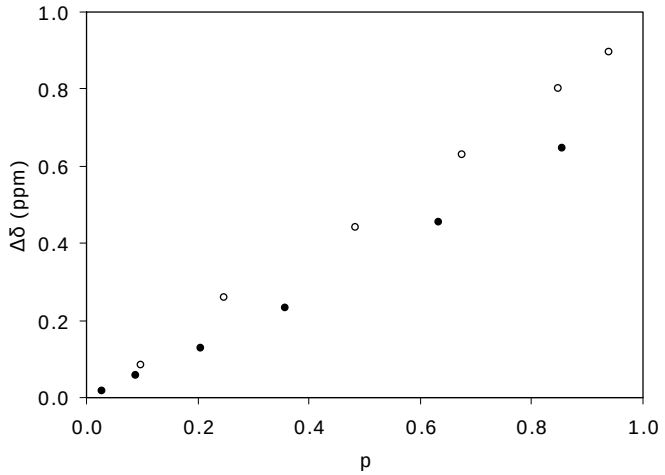

Figure 1.22. A plot of $\Delta\delta$ vs. the fraction of micellized surfactant, *p*, for **2-10** (●) and DTAB (○) in equimolar aqueous mixtures of the two substances

Micellar Structure

Micelles are of great importance for both commercial and academic interest, and many subjects concerning the structure of micelles including micelle shape, water penetration, surface roughness, and chain conformation have been intensely studied.[124] In history, several different opinions on the micellar structure have been developed. G. S. Hartley pioneered in the exploration to understand the nature of spherical micelles.[125] As illustrated in Figure 1.23a, the structure proposed by Hartley has been commonly portrayed in organic chemistry and biochemistry texts as the "spokes of a wheel".[126,127] This Hartley model described some characteristics of micelles: counterions tightly bound to a fraction of the head groups to reduce their repulsion caused by the close proximity; spherical micelles have a radius approximately equal to the length of the fully extended hydrophobic chain.[1,11] In the 1980s, Dill et al.[128,129] presented another micellar structure based on their interphase theory. As shown in Figure 1.23b, the Dill-Flory lattice model possesses a smooth surface, no chain looping or terminal methyl at the surface, and a crystalline interior. However, both the Hartley and Dill-Flory model oversimplify the micellar structure since they fail to adequately explain many experimentally observed phenomena.

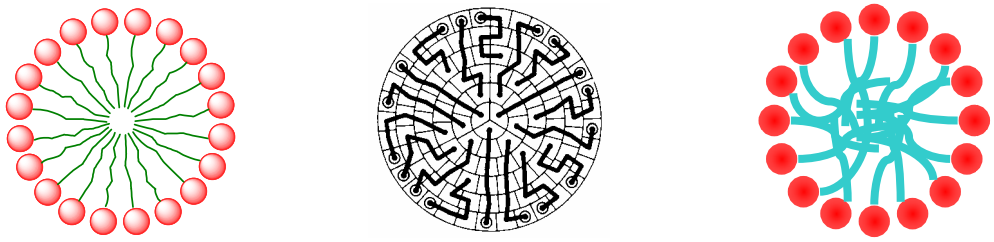

(a) Hartley model (b) Dill-Flory lattice model (c) real model

Figure 1.23. Various models on the structure of micelle

Menger et al.[130-134] proposed a new model which is now universally accepted (Figure 1.23c). More realistically, the model depicts the fluid nature of the micelle interior: micelle is a highly disorganized structure with multiple bent chains, cavities, hydrocarbon/water contact, and deviations from an exact spherical shape. This model has successfully been supported by many experiments.[132,133,135] For example, Breslow et al.[135] reported that the photolysis of benzophenone-4-carboxylate in SDS or CTAB micelles leads predominantly to oxygen insertion at the terminal methylene of the surfactant tails. As much as 27% of the functionalization occurs at C-11 of SDS. It can be interpreted as evidence of micelle looping which bring into proximity the chain termini and carbonyls near the micelle surface.

As discussed previously, sulfur serves as a reasonably innocuous entity in thio-surfactants. In a solution of either single thioether surfactant or a mixture of thio-surfactant/DTAB, the self assembly behavior of surfactant is not dramatically altered by their sulfur content. Meanwhile, sulfide can be oxidized to sulfoxide at a reasonable rate. Therefore, measuring oxidation rate of thioether surfactant provides a new kinetic approach for investigating the chain exposure in micelles. In our experiments, rate constants for thioether oxidation to sulfoxide were determined by in-situ ^{1}H NMR under the following conditions: thio-surfactant (8 mM) was admixed with a 10 fold molar excess of a conventional anionic surfactant, sodium dodecyl sulfate (SDS). The 80 mM SDS concentration was also 10 fold higher than its own CMC. These conditions were deliberately chosen because a low thio-surfactant concentration minimized any (inherently minor) perturbation by the sulfur to the overall SDS micelle structure.

Adding 8 mM thio-surfactant **8-6** to 80 mM SDS had only a small effect on N_{agg} (increasing it from 81 to 88).

Table 1.7. Oxidation rates of thio-surfactants, co-micellized into SDS micelles, by IO_4^- or H_2O_2 at 20 ℃ in D_2O

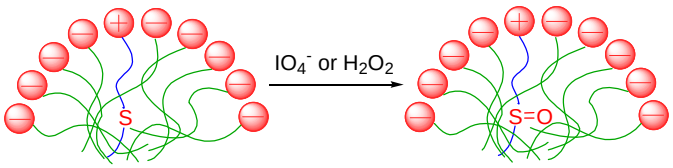

thio-surfactant	IO_4^- k_2,[a,c] 10^{-3} $sec^{-1}M^{-1}$	rel. k_2	H_2O_2 k_2,[b,c] 10^{-3} $sec^{-1}M^{-1}$	rel. k_2
3-3	2300	190	5.0	3.8
2-10	26	2.2	2.4	1.8
6-6	28	2.3	2.2	1.7
6-8	18	1.5	1.9	1.5
8-6	16	1.3	1.4	1.1
8-8	12	1.0	1.3	1.0
6-6-6	23, 31	1.9, 2.6	1.6, 2.9	1.2, 2.2

[a] **3-3** was studied without SDS and served as a control. All thio-surfactants (8 mM) were studied with SDS (80 mM) and at five IO_4^- concentrations (80-240 mM). [b] Thio-surfactants (8 mM) were studied with SDS (80 mM) and at five H_2O_2 concentrations (800-2400 mM). [c] Plots of k_{obs} vs [oxidant] were linear (R^2 = 0.97); their slopes gave k_2 values with uncertainties of <10%. [d] The two numbers represent oxidation rates of the two sulfurs in **6-6-6**.

The percentage of thio-surfactant residing in the free solution was considered kinetically insignificant. This implies that rate constants reflect only micelle-bound substrates. Three factors favor total binding of the thio-surfactants to the excess SDS: (a) Association constants between SDS and even mildly "hydrophobic" cations are large (e.g. K_{assoc} = 1.6 × 104 for Bu_4N^+).[136] Similarly, a "very large synergetic effect" was noted between cationic and anionic surfactants.[136] (b) Cooperative hydrophobic and electrostatic attraction between comparable quantities of cationic and anionic surfactants leads to huge micellar growth, vesicular association, or outright precipitation.[95,137] (c) Most convincingly, our rate constants are independent of the excess SDS concentration, an observation consistent with an absence of external monomeric substrate and subsequent non-micellar reactivity.

After adding periodate (80–240 mM) to the above micellar system, we quantitatively monitored the ensuing appearance of sulfoxide α-methylenes in the NMR for more than two half-lives. (After several days sulfone was formed, but it was not followed). Data from linear pseudo-first-order plots gave the second-order rate constants (k_2) recorded in Table 1.7.[138] One sees from columns 2 and 3 that monomeric **3-3**, with no SDS present, is oxidized two orders of magnitude faster than any of the micellized thio-surfactants. By way of comparison, SDS micelles inhibit hydroxide-catalyzed hydrolysis of a hydrophobic ester by a factor of 15.[139] Importantly, all the thio-surfactants react at roughly the same rates, indicating that oxidation rates are largely independent of the sulfur position within the chains. The simplest explanation is that the anionic SDS micelle surface electrostatically repels anions, and that all the chain loci access this periodiate-depleted surface at about the same frequency. Alternatively,

oxidation may originate in part from low levels of IO_4^- entering concavities within a porous self-assembly. Either way, the kinetics provide strong evidence for chain disorder within SDS micelles, a point that have previously been touted.[124,131,133]

A quite different behavior emerges when H_2O_2, a non-ionic oxidant, was used instead of anionic IO_4^- (Table 1.7, columns 4 and 5). In this case, all six thio-surfactants were oxidized at a rate only slightly smaller than that of monomeric **3-3** in the free solution. We interpret this result as indicating that H_2O_2 (which would be excluded from the hydrocarbon regions of the micelle interior)[140] is not electrostatically repulsed from the SDS micelle surface. Our kinetic data also indicate that the H_2O_2 at the micelle surface, or possibly in aqueous micellar concavities, has roughly equal access to the sulfurs independent of their positions on the surfactant chains. Oxidation of "interior" sulfur groups manifests itself not only in anionic SDS micelles but in cationic TTAB (tetradecyltrimethylammonium bromide) micelles as well (Table 1.8).

Table 1.8. Oxidation rates of thio-surfactants, co-micellized into TTAB micelles, by H_2O_2 at 20 ℃ in D_2O

thio-surfactant	**2-10**	**6-6**	**6-8**	**8-6**	**8-8**	**6-6-6**
H_2O_2 k_2,[a]						
10^{-3} $sec^{-1}M^{-1}$	7.0	6.6	2.4	2.0	0.73	1.0, 1.2
rel. k_2	9.6	9.0	3.3	2.7	1.0	1.4, 1.6

[a] All thio-surfactants (8 mM) were studied with TTAB (80 mM) and at five IO_4^- concentrations (800-2400 mM).

The 100-fold rate decrease with IO_4^- oxidation compared to no substantial decrease with H_2O_2 oxidation (Table 1.7) is basic to the understanding of our micellar systems. If the slow IO_4^- oxidation rates with SDS micelles were attributed to low levels of rapidly-reacting material in the free solution, then the corresponding H_2O_2 oxidation rates would have been similarly inhibited. Thus, there is only one explanation consistent with both sets of data: All sulfur loci have equal access to the SDS micelle surface, a surface that has a diminished IO_4^- concentration but a relatively normal H_2O_2 concentration. The picture that emerges, therefore, is a micelle in which disordered chains are rapidly rearranging to equalize chain exposure to water and the elements therein.

We have assumed, based on the properties of thioethers,[57-59,63,64] that the thio-surfactant chains buried within the SDS micelles possess conformational populations comparable to those of their SDS neighbors. Only if our assumption is correct can the results be extrapolated to conventional surfactants. But whether the thio-surfactants fold and twist anomalously or not, it is instructive that sulfur exposure at the micelle surfaces is independent of the sulfur atom position within the chains.

Conclusions

In conclusion, a series of six thioether-modified cationic surfactants plus a non-aggregating ammonium salt (**3-3**) were synthesized. Self-assemblies of these surfactants in aqueous solutions have been investigated by surface tension, fluorescence, conductivity, and NMR.[141,142] The introduction of a sulfur atom to the hydrophobic tail causes an increase in the critical micelle concentration but has a rather limited effect on the aggregate structure, and real micelles are formed for all of the studied surfactants. This is true for both the single thio-surfactant systems and the mixtures of thio-surfactants with DTAB. Compared to other non-hydrocarbon functionalities such as ester and ether, thioether is a weaker hydrating group and the aqueous behaviors of segmented surfactants are only slightly influenced.

Finally, oxidation rate constants of sulfide to sulfoxide by IO_4^- or H_2O_2 were measured through a kinetic approach: in-situ ^1H NMR. The results show a 100 fold difference in oxidation rate constant between the co-micellized thioether and the monomeric one. This indicates how a hydrophobic environment such as micelles can protect the interior species from external oxidants and may assist researchers in further understanding the physiological functions of methionine. More importantly, thio-surfactants with different sulfur position and chain length give roughly equal oxidation rate constants in SDS micelles. It confirms the highly disordered structure of micelle in which chain reversals, cavities, and hydrocarbon/water contact are permitted. The sulfur labeling method can be used to assess chain exposure to the external medium not only in micelles but in a variety of other self-assemblies and polymeric systems wherever the NMR resolution so permits.

Experiments

Materials

All reagents were purchased from Aldrich or Acros and used without additional purification. All solvents used were reagent or HPLC grade and, if required dried over 4 Å molecular sieves. Deionized water with a resistivity of 18 MΩ cm was obtained using Milli-Q Water System from Millipore.

Methods

Normal ^{1}H and ^{13}C NMR spectra were acquired on a Varian INOVA 400 mHz (100 mHz for ^{13}C) instrument. Melting points were measured on a Thomas Hoover Capillary Melting Point Apparatus. Mass spectra experiments were completed by the Emory University Mass Spectrometry Center. Elemental analyses were performed by Atlantic Microlabs in Norcross, GA.

Conductivity

All experiments were conducted at room temperature using a sample volume of 10 mL. A Fischer Scientific Traceable™ Conductivity Meter was used and calibrated with three standard solutions of 100, 1000, and 10,000 μS/cm from Fischer Scientific.

Tensiometry

Surface tension measurements were conducted at room temperature on a Fisher Surface Tensiomat following the Du Nouy ring procedure. All solutions were prepared using deionized water in a 25 mL volumetric flask. Each solution was measured 10 times in a 50 mL crystallizing dish and the obtained values were averaged. Between each solution, the platinum ring (mean circumference: 5.920 cm) was rinsed by 0.1 M HCl solution and deionized water and flame dried.

Aggregation Numbers Measurements

Fluorescence measurements were obtained on a Shimadzu RF-5301 PC Spectrofluorophotometer at room temperature with sensitivity of 1 nm. The excitation and emission wavelengths were set at 335 nm and 393 nm, respectively. Pyrene and cetylpyridinium chloride (CPyrCl) were used as the fluorescent probe/quencher pair. A 1.0×10^{-3} M stock solution of pyrene was prepared in methanol. A 2.0×10^{-3} M stock solution of the quencher was prepared in deionized water. A known volume of the probe stock solution was pipetted into a clean volumetric flask, a gentle stream of nitrogen gas then evaporated methanol and then aqueous surfactant solution was added to achieve 2.0×10^{-6} M pyrene (solution 1). After sonicating for 50 min, solution 1 was stored in dark and left to equilibrate overnight. The equilibrated solution was divided in two halves. The first half was diluted with deionized water to give a 1.0×10^{-6} M probe and half of initial concentration surfactant (solution 2), while the other half was mixed with quencher stock solution to give a solution containing 1.0×10^{-3} M quencher, 1.0×10^{-6} M probe, and half of initial concentration surfactant (quencher solution). The quencher solution was added to the probe solution 2 (3 mL) in increasing volume increments of 100 μL and allowed to equilibrate for 3 minutes before fluorescence measurements. The emission spectra of pyrene from 350 nm to 410 nm were recorded after addition of each aliquot of the quencher solution and the logarithm of the intensity ratio of the fifth vibronic band ($\ln(I_0/I_Q)$ at λ = 395 nm) was plotted vs. the quencher concentration. The aggregation number, N_{agg}, is obtained from the slope of the plot of $\ln (I_0/I_Q)$ vs. [CPyCl] by N_{agg} = slope × ([surf.] – CMC). The fluorescence molecule, pyrene, stays in the core and is sensitive to the polarity of the environment. The ratio of the intensity of vibronic

band I at 375 nm to band III at 385 nm (I_1/I_3) of pyrene without quenching was used to determine the polarity of the micelle.

NMR

All NMR experiments were performed at 25 °C (except ^{1}H NMR experiments on concentrated solutions of **8**-**8** and CTAB, which were performed at 28 °C) on a INOVA 600 MHz NMR equipped with a pulsed field gradient (PFG) generator and a PFG amplifier. Each sample was placed into the NMR for at least 20 minutes prior to the experiments to allow thermal equilibration. The ^{13}C NMR spectra were recorded in ^{1}H-decoupled mode. It was assumed that the chemical shift of the ^{2}H lock signal was independent of the amphiphile concentration (which has been shown to be a good approximation for other ionic amphiphiles in a similar concentration range).[143] Because the frequency offset was kept constant, the changes in the ^{13}C NMRchemical shifts with concentration could be calculated directly from the measured frequencies of the respective resonances. The ^{13}C NMR ppm scale was calibrated using an external sample of methanol in D_2O; the shift of the methyl carbon peak was set equal to 50 ppm.[144] The diffusion experiments were run using a Hahn-echo sequence with intervening pulsed field gradients (PG). The pulse sequence was 90°-PG-180°-PG with the delays between the PG (Δ) fixed to 140ms. The width (δ) of PG was set to 7 ms and the strength of the pulsed gradient (G) was increased linearly from 0.01 up to 0.4 T/m (with the maximum varying among experiments and samples) in 16 steps. The gradient strength and gradient amplifier linearity in the applied gradient strength interval were calibrated by measurements on a trace amount of H_2O in D_2O (D = 1.902×10^{-9} m^2 s^{-1}) and on poly(ethylene glycols) with known self-diffusion coefficients.[145] The self-diffusion

coefficients (*D*) of the amphiphiles were obtained from the attenuation of relevant echo peaks by linear least squares fits to the Stejskal-Tanner equation:[13]

$$\ln(I / I_0) = -(\gamma G\delta)^2 D(\Delta - \delta / 3) \qquad (1.26)$$

where I is the measured signal intensity, I_0 is the signal intensity in the absence of gradient pulses, and γ is the magnetogyric ratio of protons and the rest of the parameters are defined above. In all experiments, the observed echo decays gave good fits to eq 1.26, which shows that they represent single self-diffusion coefficients.

Oxidation Rate Measurements

A 0.16 M stock solution of SDS was prepared in D_2O. The thioether trimethylammonium surfactant (0.064 mmol) was dissolved in SDS stock solution (4 mL). The concentrations of SDS and the thioether trimethylammonium surfactant were 0.16 M and 0.016 M (solution 1). $NaIO_4$ stock solutions of 5 concentrations (0.16 M, 0.24 M, 0.32 M, 0.40 M, and 0.48 M) were prepared in D_2O. A NMR tube containing solution 1 (500 μL) was placed in a Varian INOVA 600 instrument. When the temperature was equilibrated at 20 ℃ for at least 15 minutes, the NMR tube was ejected and a $NaIO_4$ stock solution (500 μL) was added quickly. In-situ ^1H spectra were recorded after certain time intervals and the percentage of converting thioether to sulfoxide was tracked by integration of the peaks from the methylene groups near sulfur (Figure 1.23).

When the oxidant is in great excess, the second-order reaction, sulfide + IO_4^- → sulfoxide + IO_3^-, becomes a pseudo-first-order reaction. The pseudo-first-order rate constant, k_{obs}, is defined by:[71]

$$\ln c_t = -k_{obs}t + \ln c_0 \tag{1.27}$$

or

$$\ln(\frac{c_t}{c_0}) = -k_{obs}t \tag{1.28}$$

where c_0 and c_t are the initial surfactant concentration and the concentration at time, t, respectively. The ratio of c_t/c_0 is calculated based on ^1H NMR integration (Figure 1.24). Then, pseudo-first-order rate constants (k_{obs}) are determined by plotting $\ln(c_t/c_0)$ vs. time. Since $k_{obs} = k_2[IO_4^-]$, plotting k_{obs} against $[IO_4^-]$ gives the second-order rate constant (k_2 = slope, Figure 1.25).

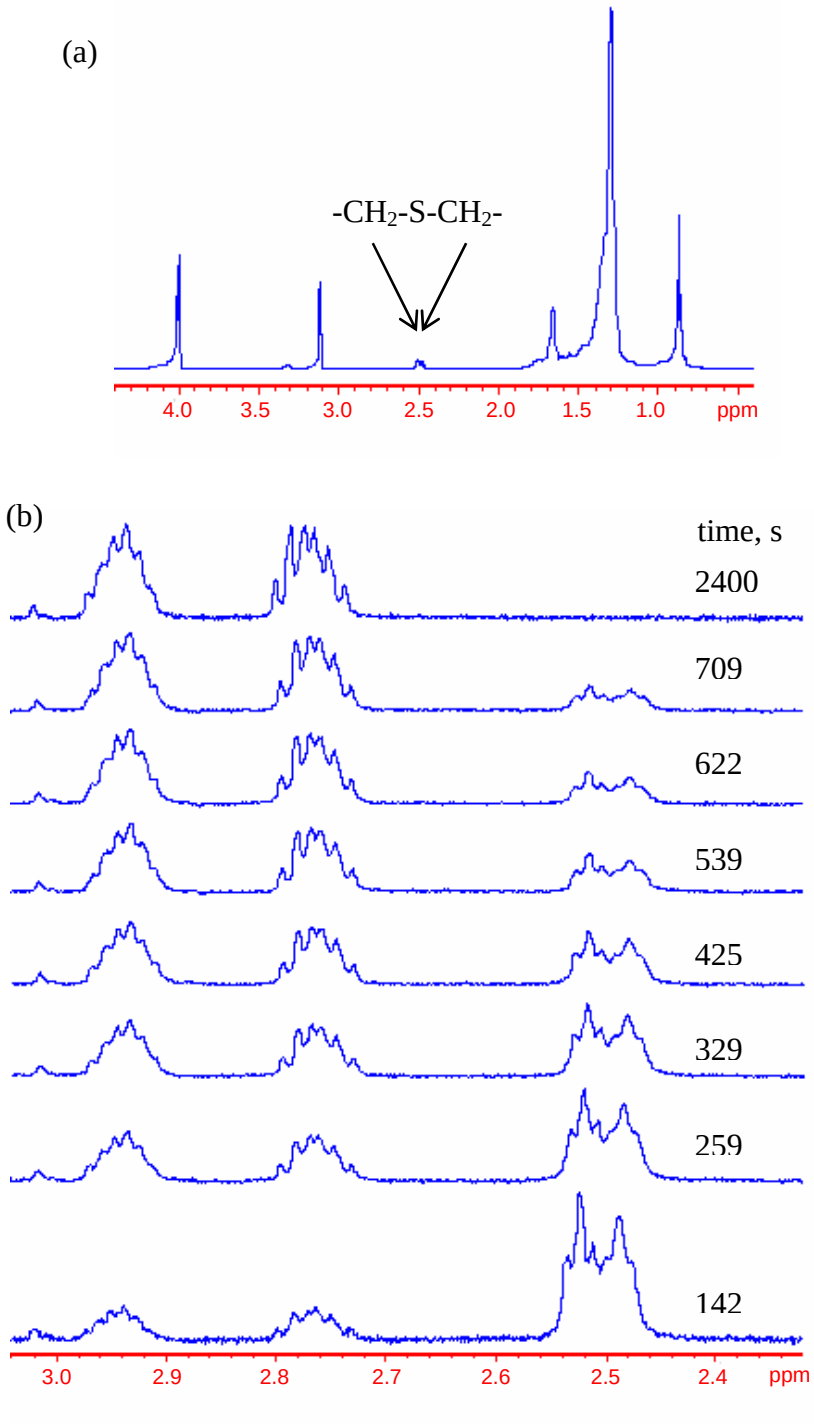

Figure 1.24. Partial ^{1}H NMR (600 M Hz) spectra of **8-6**/SDS system at 20 ℃. (a) [**8-6**] = 8 mM, [SDS] = 80 mM. (b) [**8-6**] = 8 mM, [SDS] = 80 mM, [IO_4^-] = 160 mM.

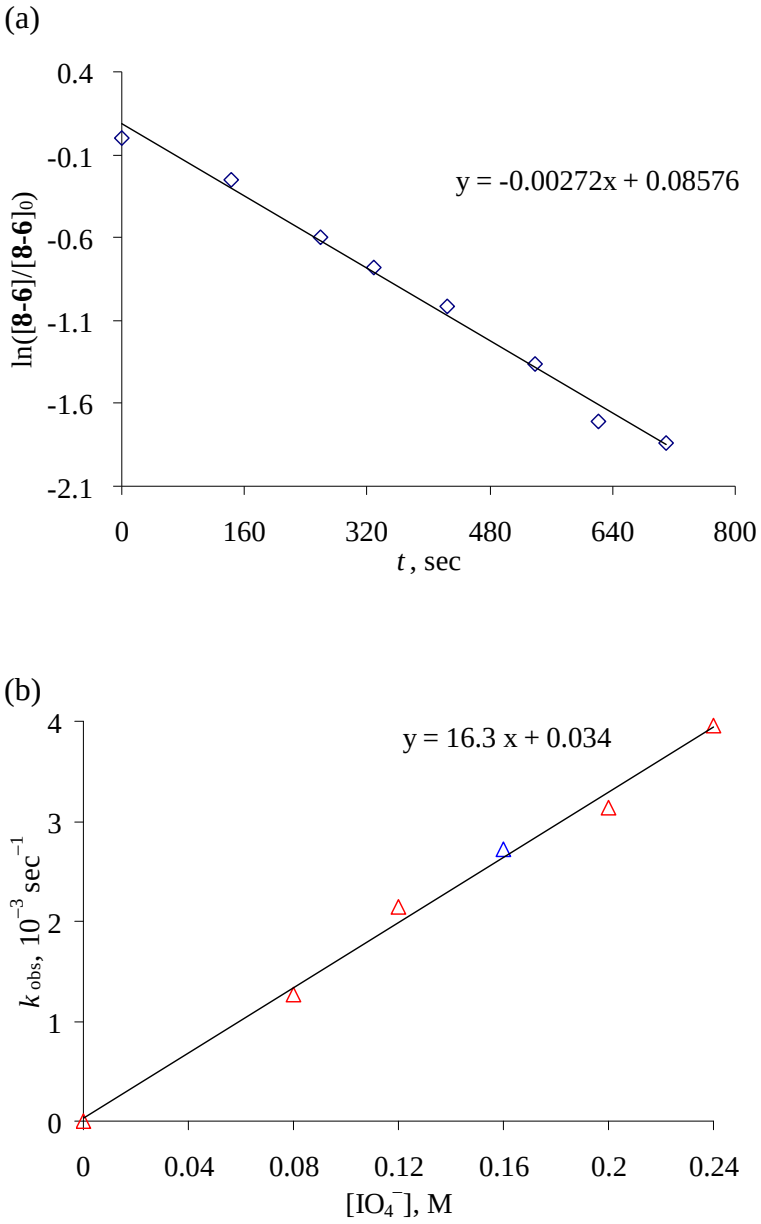

Figure 1.25. Oxidation rate constant of **8-6** by IO_4^- in the solution of **8-6**/SDS at 20 ℃. $[\mathbf{8\text{-}6}]_0$ = 0.008 M, [SDS] = 0.080 M. (a) Plotting of ln($[\mathbf{8\text{-}6}]/[\mathbf{8\text{-}6}]_0$) vs. time. $[IO_4^-]$ = 0.16 M, $k_{obs} = 2.72 \times 10^{-3}\ sec^{-1}$. (b). Plotting of k_{obs} vs. IO_4^- concentration. $k_2 = 0.016\ sec^{-1}M^{-1}$.

Syntheses and Purification

General Procedure for Bromides

The corresponding thiol (25 mmol) was added to NaOEt, 21 wt % solution in ethanol (30 mmol), and was stirred at room temperature for 1 hour. The mixture was slowly injected to the dibromoalkane (30 mmol, dissolved in 150 mL of ethanol) with a syringe pump under stirring. The solution was stirred for 24 hours and was monitored by TLC. Then H_2O (200 mL) was added, and the resulting mixture was extracted with CH_2Cl_2 (3 × 100 mL). The organic phase was dried and rotary evaporated. The final product was purified on a silica column (CH_2Cl_2/hexane) and the solvent was removed under vacuum.

1-Bromo-3-(propylthio)propane. Yield = 31.6%, colorless oil. ^{1}H NMR (400 mHz, $CDCl_3$): δ 3.53 (t, 2H), 2.67 (t, 2H), 2.51 (t, 2H), 2.16-2.09 (m, 2H), 1.67-1.58 (m, 2H), 1.00 (t, 3H). ^{13}C NMR (100 mHz, $CDCl_3$): δ 34.18, 32.40, 32.35, 30.16, 22.98, 13.51.

1-Bromo-10-(ethylthio)decane. Yield = 49.5%, colorless oil. ^{1}H NMR (400 mHz, $CDCl_3$): δ 3.39-3.34 (m, 2H), 2.53-2.46 (m, 4H), 1.86-1.77 (m, 2H), 1.69-1.50 (m, 2H), 1.44-1.16 (m, 15H). ^{13}C NMR (100 mHz, $CDCl_3$): δ 34.05, 32.90, 31.73, 29.71, 29.49, 29.45, 29.29, 28.99, 28.82, 28.24, 25.98, 14.92.

1-Bromo-6-(hethylthio)hexane. Yield = 76.7%, colorless oil. ^{1}H NMR (400 mHz, $CDCl_3$): δ 3.41 (t, 2H), 2.53-2.48 (m, 4H), 1.90-1.83 (m, 2H), 1.64-1.54 (m, 4H), 1.49-1.23 (m, 10H), 0.89 (t, 3H). ^{13}C NMR (100 mHz, $CDCl_3$): δ 34.06, 32.86, 32.41, 32.21, 31.68, 29.90, 29.67, 28.85, 28.22, 28.00, 22.79, 14.27.

1-Bromo-8-(hexylthio)octane. Yield = 54.1%, colorless oil. ^{1}H NMR (400 mHz, $CDCl_3$): δ 3.40 (t, 2H), 2.49 (t, 4H), 1.88-1.81 (m, 2H), 1.60-1.53 (m, 4H), 1.48-1.22 (m, 14H),

0.88 (t, 3H). ^{13}C NMR (100 mHz, $CDCl_3$): δ 34.08, 32.92, 32.32, 32.25, 31.60, 29.82, 29.77, 29.18, 28.93, 28.77 (2C), 28.23, 22.70, 14.20.

1-Bromo-6-(octylthio)hexane. Yield = 58.7%, colorless oil. ^{1}H NMR (400 mHz, $CDCl_3$): δ 3.41 (t, 2H), 2.52-2.47 (m, 4H), 1.90-1.83 (m, 2H), 1.63-1.53 (m, 4H), 1.49-1.21 (m, 14H), 0.88 (t, 3H). ^{13}C NMR (100 mHz, $CDCl_3$): δ 34.03, 32.83, 32.37, 32.17, 32.01, 29.91, 29.65, 29.41, 29.40, 29.15, 28.20, 27.97, 22.85, 14.30.

1-Bromo-8-(octylthio)octane. Yield = 56.3%, colorless oil. ^{1}H NMR (400 mHz, $CDCl_3$): δ 3.41 (t, 2H), 2.50 (t, 4H), 1.89-1.82 (m, 2H), 1.61-1.54 (m, 4H), 1.49-1.20 (m, 18H), 0.88 (t, 3H). ^{13}C NMR (100 mHz, $CDCl_3$): δ 34.22, 33.00, 32.41, 32.34, 32.05, 29.95, 29.86, 29.45, 29.42, 29.27, 29.19, 29.02, 28.86, 28.32, 22.88, 14.33.

Synthesis of 6-(Hexylthio)-1-hexanethiol

NaOEt, 21 wt % solution in ethanol (12 mmol), was slowly added to 1,6-hexanedithiol (14 mmol) under stirring. The mixture was stirred for 1 hour. 1-Bromohexane (12 mmol) was slowly injected to the mixture with a syringe pump. Reaction continued at room temperature for 24 hours. Then H_2O (15 mL) was added, and the resulting mixture was extracted with $CHCl_3$ (6 × 10 mL). The organic phase was washed with brine (2 × 8 mL), dried and rotary evaporated. The final product was purified on a silica column (hexane) and the solvent was removed under vacuum. Yield = 41.7%, colorless oil. ^{1}H NMR (400 mHz, $CDCl_3$): δ 2.56-2.48 (m, 6H), 1.66-1.52 (m, 6H), 1.45-1.24 (m, 11H), 0.89 (t, 3H). ^{13}C NMR (100 mHz, $CDCl_3$): δ 34.07, 32.40, 32.25, 31.66, 29.88, 29.72, 28.83, 28.52, 28.15, 24.76, 22.76, 14.26.

Synthesis of 1-Bromo-6-[6-(hexylthio)hexylthio]hexane

6-(Hexylthio)-1-hexanethiol (4 mmol) was added to NaOEt, 21 wt % solution in ethanol (5 mmol) and stirred for 1 hour. The mixture was slowly injected to 1,6-dibromohexane (5 mmol, dissolved in ethanol (40 mL)) with a syringe pump. Reaction continued at room temperature for 24 hours. Then H_2O (40 mL) was added, and the resulting mixture was extracted with CH_2Cl_2 (3 × 20 mL). The organic phase was dried and rotary evaporated. The final product was purified on a silica column (hexane) and the solvent was removed under vacuum. Yield = 50.6%, colorless oil. ^{1}H NMR (400 mHz, $CDCl_3$): δ 3.41 (t, 2H), 2.70-2.34 (m, 8H), 1.90-1.83 (m, 2H), 1.66-1.53 (m, 8H), 1.50-1.22 (m, 14H), 0.89 (t, 3H). ^{13}C NMR (100 mHz, $CDCl_3$): δ 33.72, 32.52, 32.08, 31.97 (2C), 31.90, 31.35, 29.58, 29.45 (2C), 29.33, 28.52, 28.41 (2C), 27.88, 27.66, 22.45, 13.93.

General Procedure for Ammonium Bromides

The corresponding bromide (12 mmol) and ethanol (25 mL) was placed in a round-bottom flask and stirred. Trimethylamine, 30 wt % solution in ethanol (15 mmol), was added. Reaction continued for 4 days at room temperature, and trimethylamine (10 mmol) was added every 24 hours. After the solvent was stripped, ether (30 mL) was added to the crude product followed by an extraction of the desired product with H_2O (3 × 30 mL). Water was removed by sublimation to yield a flakey white powder. The powder was stirred in ether (150 mL) for 24 hours, filtrated, and dried at 100 ℃ under vacuum for 12 hours. (3-(Propylthio)propyl-trimethylammonium Bromide was dried at 40 ℃.)

*3-(Propylthio)propyl-trimethylammonium Bromide (**A**)*. Yield = 93.2%, white hygroscopic powder. Mp: 55-58 °C. ^{1}H NMR (400 mHz, D_2O): δ 3.46-3.41 (m, 2H), 3.14

(s, 9H), 2.63 (t, 2H), 2.58 (t, 2H), 2.14-2.05 (m, 2H), 1.66-1.56 (m, 2H), 0.96 (t, 3H). ^{13}C NMR (100 mHz, $CDCl_3$): δ 66.28, 54.05 (3C), 34.85, 28.76, 23.73, 23.28, 13.87. Mass spec. $(M\text{-}Br)^+$: theory 176.14675 amu, found 176.14664 amu. Elemental analysis: theory (21surfactant + $10H_2O$) 40.81% C, 8.73% H, 5.29% N, 12.10% S; found 41.07% C, 8.72% H, 5.21% N, 11.86% S.

*10-(Ethylthio)decanyl-trimethylammonium Bromide (**B**)*. Yield = 90.9%, white powder. Mp: 194-197 °C. ^{1}H NMR (400 mHz, D_2O): δ 3.31-3.26 (m, 2H), 3.08 (s, 9H), 2.59-2.53 (m, 4H), 1.81-1.72 (m, 2H), 1.61-1.53 (m, 2H), 1.41-1.26 (m, 12H), 1.21 (t, 3H). ^{13}C NMR (100 mHz, $CDCl_3$): δ 66.99, 53.45 (3C), 31.69, 29.66, 29.37, 29.34, 29.25, 29.20, 28.93, 26.22, 25.97, 23.26, 14.91. Mass spec. $(M\text{-}Br)^+$: theory 260.24065 amu, found 260.24039 amu. Elemental analysis: theory 52.93% C, 10.07% H, 4.11% N, 9.42% S; found 52.81% C, 10.22% H, 4.17% N, 9.42% S.

*6-(Hexylthio)hexyl-trimethylammonium Bromide (**C**)*. Yield = 94.1%, white powder. Mp: 200-203 °C. ^{1}H NMR (400 mHz, D_2O): δ 3.31-3.26 (m, 2H), 3.08 (s, 9H), 2.58-2.54 (m, 4H), 1.81-1.73 (m, 2H), 1.63-1.53 (m, 4H), 1.47-1.23 (m, 10H), 0.84 (t, 3H). ^{13}C NMR (100 mHz, $CDCl_3$): δ 66.58, 53.19 (3C), 32.01, 31.64, 31.25, 29.46, 29.05, 28.42, 28.16, 25.59, 22.93, 22.36, 13.87. Mass spec. $(M\text{-}Br)^+$: theory 260.24065 amu, found 260.24068 amu. Elemental analysis: theory 52.93% C, 10.07% H, 4.11% N, 9.42% S; found 52.91% C, 10.24% H, 4.12% N, 9.41% S.

*6-(Octanylthio)hexyl-trimethylammonium Bromide (**D**)*. Yield = 95.0%, white powder. Mp: 213-214 °C. ^{1}H NMR (400 mHz, D_2O): δ 3.46-3.34 (m, 2H), 3.16 (s, 9H), 2.64-2.48 (m, 4H), 1.88-1.74 (m, 2H), 1.67-1.55 (m, 4H), 1.53-1.23 (m, 14H), 0.89 (t, 3H). ^{13}C NMR (100 mHz, $CDCl_3$): δ 66.98, 53.54 (3C), 32.38, 32.01, 31.98, 29.86, 29.39 (2C),

29.37, 29.12, 28.50, 25.95, 23.29, 22.81, 14.28. Mass spec. $(M\text{-}Br)^+$: theory 288.27195 amu, found 288.27197 amu. Elemental analysis: theory 55.42% C, 10.40% H, 3.80% N, 8.70% S; found 55.37% C, 10.56% H, 3.80% N, 8.53% S.

*8-(Hexylthio)octanyl-trimethylammonium Bromide (**E**).* Yield = 92.7%, white hygroscopic powder. Mp: 205-206 °C. ^{1}H NMR (400 mHz, D_2O): δ 3.31-3.27 (m, 2H), 3.08 (s, 9H), 2.57-2.53 (m, 4H), 1.82-1.71 (m, 2H), 1.62-1.52 (m, 4H), 1.43-1.24 (m, 14H), 0.85 (t, 3H). ^{13}C NMR (100 mHz, $CDCl_3$): δ 67.07, 53.51 (3C), 32.34, 32.20, 31.60, 29.82, 29.68, 29.24, 29.09, 28.80, 28.77, 26.23, 23.30, 22.70, 14.20. Mass spec. $(M\text{-}Br)^+$: theory 288.27195 amu, found 288.27170 amu. Elemental analysis: theory (3surfactant + $1H_2O$) 54.53% C, 10.41% H, 3.74% N, 8.56% S; found 54.50% C, 10.54% H, 3.83% N, 8.59% S.

*8-(Octanylthio)octanyl-trimethylammonium Bromide (**F**).* Yield = 90.6%, white powder. Mp: 212-214 °C. ^{1}H NMR (400 mHz, D_2O): δ 3.42-3.38 (m, 2H), 3.16 (s, 9H), 2.56-2.49 (m, 4H), 1.84-1.75 (m, 2H), 1.64-1.53 (m, 4H), 1.47-1.23 (m, 18H), 0.89 (t, 3H). ^{13}C NMR (100 mHz, $CDCl_3$): δ 66.84, 53.37 (3C), 32.19, 32.07, 31.80, 29.71, 29.56, 29.21, 29.19, 29.12, 28.96 (2C), 28.68, 26.01, 23.17, 22.64, 14.12. Mass spec. $(M\text{-}Br)^+$: theory 316.30325 amu, found 316.30338 amu. Elemental analysis: theory 57.55% C, 10.68% H, 3.53% N, 8.09% S; found 57.47% C, 10.82% H, 3.40% N, 8.06% S.

*6-[6-(Hexylthio)hexylthio]hexyl-trimethylammonium Bromide (**G**).* Yield = 90.0 %, white powder. Mp: 187-189 °C. ^{1}H NMR (400 mHz, D_2O): δ 3.45-3.39 (m, 2H), 3.18 (s, 9H), 2.62-2.50 (m, 8H), 1.88-1.77 (m, 2H), 1.69-1.28 (m, 22H), 0.93 (t, 3H). ^{13}C NMR (100 mHz, $CDCl_3$): δ 67.33, 53.89 (3C), 32.67, 32.59, 32.56, 32.32, 31.94, 30.17, 30.05 (2C), 29.71, 29.12, 29.02 (2C), 28.81, 26.27, 23.61, 23.05, 14.55. Mass spec. $(M\text{-}Br)^+$: theory

376.30662 amu, found 376.30650 amu. Elemental analysis: theory 55.24% C, 10.15% H, 3.07% N, 14.04% S; found 54.96% C, 10.27% H, 3.12% N, 14.04% S.

References

(1) Myers, D. *Surfactant Science and Technology*, 3rd ed.; Wiley: Hoboken, NJ, 2005.

(2) Bhardwaj, A.; Hartland, S. *J. Dispersion Sci. Technol.* **1993,** *14*, 87-116.

(3) Somasundaran, P.; Chakraborty, S.; Qiang, Q.; Deo, P.; Wang, J.; Zhang, R. *J. Cosmetic Sci.* **2004,** *55*, S1-S17.

(4) Swarup, S.; Schoff, C. K. *Prog. Org. Coat.* **1993,** *23*, 1-22.

(5) Schmidt, G. *Tenside, Surfactants, Deterg.* **1990,** *27*, 324-328.

(6) Dwars, T.; Paetzold, E.; Oehme, G. *Angew. Chem., Int. Ed.* **2005,** *44*, 7174-7199.

(7) Lawrence, M. J.; Rees, G. D. *Adv. Drug Deliver. Rev* **2000,** *45*, 89-121.

(8) Berthod, A.; Garcia-Alvarez-Coque, C., Eds. *Micellar Liquid Chromatography*; Marcel Dekker: New York, 2000; Vol. 83.

(9) Holmberg, K. *J. Colloid Interf. Sci* **2004,** *274*, 355-364.

(10) Holmberg, K.; Lindman, B.; Joensoon, B.; Kronberg, B. *Surfactants and Polymers in Aqueous Solution*, 2nd ed.; Wiley: Chichester, UK, 2002.

(11) Rosen, M. J. *Surfactants and Interfacial Phenomena*, 3rd ed.; Wiley: Chichester, UK, 2004.

(12) Tadros, T. F. *Applied Surfactants: Principles and Applications*; Wiley: Chichester, UK, 2005.

(13) Tanford, C. *The Hydrophobic Effect: Formation of Micelles and Biological Membranes*, 2nd ed.; Wiley: New York, 1980.

(14) Lindman, B.; Wennerstroem, H. *Top. Curr. Chem.* **1980,** *87*, 1-83.

(15) Esumi, K.; Ueno, M., Eds. *Structure-Performance Relationships in Surfactants*, 2nd ed.; Marcel Dekker: New York, 2003; Vol. 112.

(16) Holmberg, K.; Shah, D. O.; Schwuger, M. J., Eds. *Handbook of Applied Surface and Colloid Chemistry*; Wiley: Chichester, UK, 2002; Vol. 1.

(17) Farn, R. J., Ed. *Chemistry and Technology of Surfactants*; Blackwell: Oxford, UK, 2006.

(18) Balzer, D.; Luders, H., Eds. *Nonionic Surfactants: Alkyl Polyglucosides*; Marcel Dekker: New York, 2000.

(19) Menger, F. M.; Zhang, H. *Langmuir* **2005,** *21*, 10428-10438.

(20) Fuhrhop, J. H.; Fritsch, D. *Acc. Chem. Res.* **1986,** *19*, 130-137.

(21) Fuhrhop, J.-H.; Wang, T. *Chem. Rev.* **2004,** *104*, 2901-2937.

(22) Escamilla, G. H.; Newkome, G. R. *Angew. Chem., Int. Ed.* **1994,** *33*, 1937-1940.

(23) Fuhrhop, J. H.; Mathieu, J. *Angew. Chem., Int. Ed.* **1984,** *23*, 100-113.

(24) Zana, R. *Curr. Opin. Colloid Interface Sci.* **1996,** *1*, 566-571.

(25) Menger, F. M.; Keiper, J. S. *Angew. Chem., Int. Ed.* **2000,** *39*, 1907-1920.

(26) Zana, R.; Xia, J., Eds. *Gemini Surfactants: Synthesis, Interfacial and Solution-Phase Behavior, and Applications*; Marcel Dekker: New York, 2003; Vol. 117.

(27) Piirma, I., Ed. *Polymeric Surfactants*; Marcel Dekker: New York, 1992; Vol. 42.

(28) Garnier, S.; Laschewsky, A.; Storsberg, J. *Tenside, Surfactants, Deterg.* **2006,** *43*, 88-102.

(29) Halperin, A. *Polym. Rev.* **2006,** *46*, 173-214.

(30) Monduzzi, M. *Curr. Opin. Colloid Interface Sci.* **1998,** *3*, 467-477.

(31) Hill, R. M., Ed. *Silicone Surfactants*; Marcel Dekker: New York, 1999; Vol. 86.

(32) Myers, D. *Surfaces, Interfaces, and Colloids: Principles and Applications*, 2nd ed.; Wiley: New York, 1999.

(33) Holmberg, K.; Shah, D. O.; Schwuger, M. J., Eds. *Handbook of Applied Surface and Colloid Chemistry*; Wiley: Chichester, UK, 2002; Vol. 2.

(34) Laughlin, R. G. *The Aqueous Phase Behavior of Surfactants*; Academic Press: San Diego, CA, 1996.

(35) Menger, F. M.; Chlebowski, M. E. *Langmuir* **2005,** *21*, 2689-2695.

(36) Menger, F. M.; Galloway, A. L. *J. Am. Chem. Soc.* **2004,** *126*, 15883-15889.

(37) Menger, F. M.; Galloway, A. L.; Chlebowski, M. E. *Langmuir* **2005,** *21*, 9010-9012.

(38) Lundberg, D.; Unga, J.; Galloway, A. L.; Menger, F. M. *Langmuir* **2007,** *23*, 11434-11442.

(39) Ruiz, C. C., Ed. *Sugar-based Surfactants; Fundamentals and Applications*; CRC Press: Boca Rotan, FL, 2009; Vol. 143.

(40) Holmberg, K., Ed. *Novel Surfactants: Preparation, Applications, and Biodegradability*, 2nd ed.; Marcel Dekker: New York, 2003.

(41) Pauling, L. *The Nature of the Chemical Bond*, 3rd ed.; Cornell University Press: Ithaca, NY, 1960.

(42) Patai, S., Ed. *The Chemistry of Functional Groups, Suppl. E: The Chemistry of Ethers Crown Ethers, Hydroxyl Groups and Their Sulfur Analogs, Pt. 1*; Wiley: Chichester, UK, 1980.

(43) Patai, S., Ed. *The Chemistry of Functional Groups, Suppl. E: The Chemistry of Ethers, Crown Ethers, Hydroxyl Groups and Their Sulfur Analogs, Pt. 2*; Wiley: Chichester, UK, 1980.

(44) Chen, H.; Li, Y. P.; Huo, F. W.; Wang, Z. Q.; Zhang, X. *Chem. Lett.* **2003,** *32*, 1094-1095.

(45) Nishijo, J.; Miyazaki, A.; Enoki, T. *Bull. Chem. Soc. Jpn.* **2004,** *77*, 715-727.

(46) Itoh, S.; Takayama, S.; Arakawa, R.; Furuta, A.; Komatsu, M.; Ishida, A.; Takamuku, S.; Fukuzumi, S. *Inorg. Chem.* **1997,** *36*, 1407-1416.

(47) Rudnick, L. R.; Shubkin, R. L., Eds. *Synthetic Lubricants and High-Performance Functional Fluids*; Marcel Dekker: New York, 1999; Vol. 77.

(48) Jaoued, N. G.; Hedhli, A. *J. Dispersion Sci. Technol.* **2003,** *24*, 749-753.

(49) Gilles, P. P.; Milano, J. C.; Vernet, J. L. *Eur. Polym. J.* **2003,** *39*, 1875-1882.

(50) Matsumura, S.; Kihara, N.; Takata, T. *High Perform. Polym.* **2001,** *13*, S293-S304.

(51) Lippert, E.; Prigge, H. *Ann.* **1962,** *659*, 81-89.

(52) Bystrov, V. F.; Lezina, V. P.; Shostakovskii, S. M. *Optika i Spektroskopiya (Akademiya Nauk SSSR, Otdelenie Fiziko-Matematicheskikh Nauk)* **1967,** *3*, 339-345.

(53) Kunz, D.; Fischer, M. *Zeitschrift fuer Chemie* **1969,** *9*, 307.

(54) Sheridan, J. P.; Martire, D. E.; Tewari, Y. B. *J. Am. Chem. Soc.* **1972,** *94*, 3294-3298.

(55) Liao, H. L.; Martire, D. E. *J. Am. Chem. Soc.* **1974,** *96*, 2058-2062.

(56) Martire, D. E.; Sheridan, J. P.; King, J. W.; O'Donnell, S. E. *J. Am. Chem. Soc.* **1976,** *98*, 3101-3106.

(57) Allen, F. H.; Bird, C. M.; Rowland, R. S.; Raithby, P. R. *Acta Crystallogr. B* **1997,** *B53*, 696-701.

(58) Leo, A.; Hansch, C.; Elkins, D. *Chem. Rev.* **1971,** *71*, 525-616.

(59) Sokolowski, A. *J. Phys. Chem.* **1989,** *93*, 8223-8226.

(60) Miesiac, I.; Merkwitz, H.; Szymanowski, J.; Beger, J. *J. Colloid Interf. Sci* **1986,** *114*, 425-431.

(61) Sokolowski, A.; Burczyk, B.; Beger, J. *Colloids Surf.* **1990,** *44*, 89-100.

(62) Lehinger, A. L. *Biochemistry: The Molecular Basis of Cell Structure and Function*, 4th ed.; Worth: New York, 1989.

(63) O'Neil, K. T.; DeGrado, W. F. *Trends Biochem. Sci.* **1990,** *15*, 59-64.

(64) Gellman, S. H. *Biochemistry* **1991,** *30*, 6633-6636.

(65) Brot, N.; Weissbach, H. *Arch. Biochem. Biophys.* **1983,** *223*, 271-281.

(66) Jacob, C.; Giles, G. I.; Giles, N. M.; Sies, H. *Angew. Chem., Int. Ed.* **2003,** *42*, 4742-4758.

(67) Levine, R. L.; Moskovitz, J.; Stadtman, E. R. *Iubmb Life* **2000,** *50*, 301-307.

(68) Levine, R. L.; Berlett, B. S.; Moskovitz, J.; Mosoni, L.; Stadtman, E. R. *Mech. Ageing. Dev.* **1999,** *107*, 323-332.

(69) Levine, R. L.; Mosoni, L.; Berlett, B. S.; Stadtman, E. R. *Proc. Natl. Acad. Sci. U.S.A.* **1996,** *93*, 15036-15040.

(70) Yao, Y.; Yin, D.; Jas, G. S.; Kuczer, K.; Williams, T. D.; Schoneich, C.; Squier, T. C. *Biochemistry* **1996,** *35*, 2767-2787.

(71) Smith, M. B.; March, J. *March's Advanced Organic Chemistry: Reactions, Mechanisms, and Structure*, 6th ed.; Wiley: Hoboken, New Jersey, 2007.

(72) Anklam, E. *Synthesis* **1987**, 841-843.

(73) MacLeod, A. J.; MacLeod, G. *Phytochemistry.* **1977,** *16*, 907-909.

(74) Gray, A. P.; Schlieper, D. C.; Spinner, E. E.; Cavallito, C. J. *J. Am. Chem. Soc.* **1955,** *77*, 3648-3649.

(75) du Nouy, P. L. *J. Gen. Physiol.* **1919,** *1*, 521-524.

(76) Freud, B. B.; Freud, H. Z. *J. Am. Chem. Soc.* **1930,** *52*, 1772-1782.

(77) Harkins, W. D.; Jordan, H. F. *J. Am. Chem. Soc.* **1930,** *52*, 1751-1772.

(78) Zana, R. *J. Colloid Interface Sci.* **1980,** *78*, 330-337.

(79) Evans, D. F.; Allen, M.; Ninham, B. W.; Fouda, A. *J. Solution Chem.* **1984,** *13*, 87-101.

(80) Barry, B. W.; Russell, G. F. J. *J. Colloid Interface Sci.* **1972,** *40*, 174-194.

(81) Berr, S. S.; Caponetti, E.; Johnson, J. S., Jr.; Jones, R. R. M.; Magid, L. J. *J. Phys. Chem.* **1986,** *90*, 5766-5770.

(82) Alami, E.; Beinert, G.; Marie, P.; Zana, R. *Langmuir* **1993,** *9*, 1465-1467.

(83) Devinsky, F.; Lacko, I.; Bittererova, F.; Tomeckova, L. *J. Colloid Interface Sci.* **1986,** *114*, 314-322.

(84) Attwood, D.; Natarajan, R. *J. Pharm. Pharmacol.* **1980,** *32*, 460-462.

(85) Gomez-Diaz, D.; Navaza, J. M.; Sanjurjo, B. *J. Chem. Eng. Data* **2007,** *52*, 2091-2093.

(86) Rosen, M. J.; Mathias, J. H.; Davenport, L. *Langmuir* **1999,** *15*, 7340-7346.

(87) Callaghan, A.; Doyle, R.; Alexander, E.; Palepu, R. *Langmuir* **1993,** *9*, 3422-3426.

(88) Seredyuk, V.; Alami, E.; Nyden, M.; Holmberg, K.; Peresypkin, A. V.; Menger, F. M. *Langmuir* **2001,** *17*, 5160-5165.

(89) Zana, R., Ed. *Surfactant Solutions. New Methods of Investigation*; Marcel Dekker: New York, 1987; Vol. 22.

(90) Dederen, J. C.; Van der Auweraer, M.; De Schryver, F. C. *J. Phys. Chem.* **1981,** *85*, 1198-1202.

(91) Hansson, P.; Joensson, B.; Stroem, C.; Soederman, O. *J. Phys. Chem. B* **2000,** *104*, 3496-3506.

(92) Infelta, P. P.; Gratzel, M.; Thomas, J. K. *J. Phys. Chem.* **1974,** *78*, 190-195.

(93) Rizvi, S. A. A.; Shamsi, S. A. *Electrophoresis.* **2003,** *24*, 2514-2526.

(94) Turro, N. J.; Yekta, A. *J. Am. Chem. Soc.* **1978,** *100*, 5951-5952.

(95) Li, G.-Z.; Li, F.; Zheng, L.-Q.; Wang, H.-L. *Colloids Surf., A* **1993,** *76*, 257-265.

(96) Panmai, S.; Prud'homme, R. K.; Peiffer, D. G.; Jockusch, S.; Turro, N. J. *Langmuir* **2002,** *18*, 3860-3864.

(97) Sierra, M. L.; Rodenas, E. *J. Phys. Chem.* **1993,** *97*, 12387-12392.

(98) Zhai, L.; Lu, X.; Chen, W.; Hu, C.; Zheng, L. *Colloids Surf., A* **2004,** *236*, 1-5.

(99) Almgren, M.; Hansson, P.; Mukhtar, E.; Van Stam, J. *Langmuir* **1992,** *8*, 2405-2412.

(100) Marangoni, D. G.; Rodenhiser, A. P.; Thomas, J. M.; Kwak, J. C. T. *Langmuir* **1993,** *9*, 438-443.

(101) Reekmans, S.; Luo, H.; Van der Auweraer, M.; De Schryver, F. C. *Langmuir* **1990,** *6*, 628-637.

(102) Jayakumar, R.; Murugesan, M.; Selvi, S.; Scibioh, M. A. *Langmuir* **2000,** *16*, 3019-3021.

(103) Alargova, R. G.; Kochijashky, I. I.; Sierra, M. L.; Zana, R. *Langmuir* **1998,** *14*, 5412-5418.

(104) Gehlen, M. H.; De Schryver, F. C. *Chem. Rev.* **1993,** *93*, 199-221.

(105) Li, W.; Han, Y. C.; Zhang, J. L.; Wang, B. G. *Colloid J.* **2005,** *67*, 159-163.

(106) Croonen, Y.; Gelade, E.; Van der Zegel, M.; Van der Auweraer, M.; Vandendriessche, H.; De Schryver, F. C.; Almgren, M. *J. Phys. Chem.* **1983,** *87*, 1426-1431.

(107) Roelants, E.; De Schryver, F. C. *Langmuir* **1987,** *3*, 209-214.

(108) Malliaris, A.; Le Moigne, J.; Sturm, J.; Zana, R. *J. Phys. Chem.* **1985,** *89*, 2709-2713.

(109) Zana, R.; Binana-Limbele, W.; Kamenka, N.; Lindman, B. *J. Phys. Chem.* **1992,** *96*, 5461-5465.

(110) Ridriguez Prieto, M. F.; Rios Rodriguez, M. C.; Gonzalez, M. M.; Rios Rodriguez, A. M.; Mejuto Fernandez, J. C. *J. Chem. Educ.* **1995,** *72*, 662-663.

(111) Turner, D.; Gracie, K.; Taylor, T.; Palepu, R. *J. Colloid Interf. Sci* **1998,** *202*, 359-368.

(112) van Stam, J.; Depaemelaere, S.; De Schryver, F. C. *J. Chem. Educ.* **1998,** *75*, 93-98.

(113) Stilbs, P. *Prog. Nucl. Magn. Reson. Spectrosc.* **1987,** *19*, 1-45.

(114) Soederman, O.; Stilbs, P.; Price, W. S. *Concepts Magn. Reson., Part A* **2004,** *23A*, 121-135.

(115) Ulmius, J.; Wennerstrom, H. *J. Magn. Reson.* **1977,** *28*, 309-312.

(116) Olsson, U.; Soederman, O.; Guering, P. *J. Phys. Chem.* **1986,** *90*, 5223-5232.

(117) Israelachvili, J. N. *Intermolecular and Surface Forces*, 2nd ed.; Academic Press: London, UK, 1991.

(118) Furo, I. *J. Mol. Liq.* **2005,** *117*, 117-137.

(119) Minardi, R. M.; Schulz, P. C.; Vuano, B. *Colloids Surf., A* **2002,** *197*, 167-172.

(120) Stothers, J. B. *Carbon-13 NMR Spectroscopy*; Academic Press: New York, 1972; Vol. 24.

(121) Persson, B. O.; Drakenberg, T.; Lindman, B. *J. Phys. Chem.* **1976,** *80*, 2124-2125.

(122) Grant, D. M.; Cheney, B. V. *J. Am. Chem. Soc.* **1967,** *89*, 5315-5318.

(123) Drakenberg, T.; Lindman, B. *J. Colloid Interface Sci.* **1973,** *44*, 184-186.

(124) Menger, F. M. *Acc. Chem. Res.* **1979,** *12*, 111-117.

(125) Hartley, G. S. *Aqueous Solutions of Paraffin-chain Salts. A Study in Micelle Formation*; Hermann & Cie: Paris, FR, 1936.

(126) Carey, F. A., Ed. *Organic Chemistry*, 3rd ed.; McGraw-Hill: New York, 1996.

(127) Lehninger, A. L.; Nelson, D. L.; Cox, M. M. *Principles of Biochemistry*, 2nd ed.; Worth: New York, 1993.

(128) Dill, K. A.; Flory, P. J. *Proc. Natl. Acad. Sci. U.S.A.* **1981,** *78*, 676-680.

(129) Dill, K. A.; Koppel, D. E.; Cantor, R. S.; Dill, J. D.; Bendedouch, D.; Chen, S. H. *Nature* **1984,** *309*, 42-45.

(130) Menger, F. M. *Acc. Chem. Res.* **1979,** *12*, 111-117.

(131) Menger, F. M. *Nature* **1985,** *313*, 603.

(132) Menger, F. M.; Carnahan, D. W. *J. Am. Chem. Soc.* **1986,** *108*, 1297-1298.

(133) Menger, F. M.; Doll, D. W. *J. Am. Chem. Soc.* **1984,** *106*, 1109-1113.

(134) Menger, F. M.; Zana, R.; Lindman, B. *J. Chem. Educ.* **1998,** *75*, 115.

(135) Breslow, R.; Kitabatake, S.; Rothbard, J. *J. Am. Chem. Soc.* **1978,** *100*, 8156-8160.

(136) Pradines, V.; Lavabre, D.; Micheau, J.-C.; Pimienta, V. *Langmuir* **2005,** *21*, 11167-11172.

(137) Kaler, E. W.; Murthy, A. K.; Rodriguez, B. E.; Zasadzinski, J. A. *Science* **1989,** *245*, 1371-1374.

(138) Yao, H.; Richardson, D. E. *J. Am. Chem. Soc.* **2003,** *125*, 6211-6221.

(139) Behme, M. T. A.; Fullington, J. G.; Noel, R.; Cordes, E. H. *J. Am. Chem. Soc.* **1965,** *87*, 266-270.

(140) Walton, J. H.; Lewis, H. A. *J. Am. Chem. Soc.* **1916,** *38*, 633-638.

(141) Lundberg, D.; Shi, L.; Menger, F. M. *Langmuir* **2008,** *24*, 4530-4536.

(142) Menger, F. M.; Shi, L. *J. Am. Chem. Soc.* **2006,** *128*, 9338-9339.

(143) Odberg, L.; Svens, B.; Danielsson, I. *J. Colloid Interface Sci.* **1972,** *41*, 298-304.

(144) Gottlieb, H. E.; Kotlyar, V.; Nudelman, A. *J. Org. Chem.* **1997,** *62*, 7512-7515.

(145) Hakansson, B.; Nyden, M.; Soderman, O. *Colloid Polym. Sci.* **2000,** *278*, 399-405.

II. Electrostatic Binding among Equilibrating 2-D and 3-D Self-Assemblies

Introduction

Intermolecular interactions are dominated by noncovalent forces including hydrogen-bonding, π-stacking, metal-ligand coordination, hydrophobic effect and van der Waals forces. In recent years, supramolecular chemistry has become an area of intense research and offers insight into applications of noncovalent forces.[1-5]

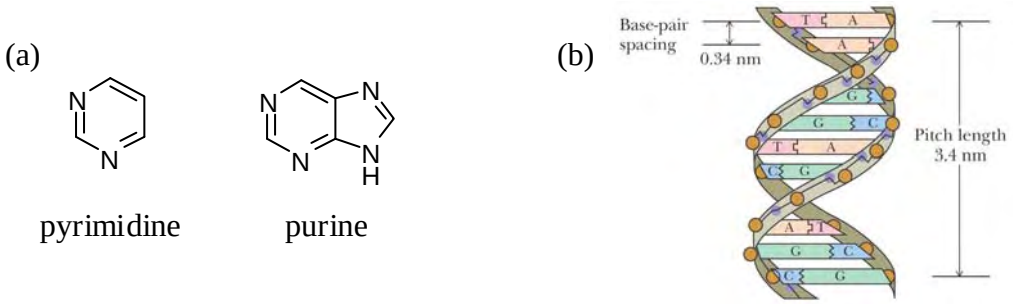

Figure 2.1. (a) Structures of pyrimidine and purine. (b) Double-stranded DNA. A = adenine, C = cytosine, G = guanine, and T = thymine.

π-Stacking, or aromatic interaction, is caused by intermolecular overlapping of p-orbitals in π-conjugated moieties. π-Stacking plays an important role in many areas such as, in particular, biology and electronic materials.[6,7] For instance, the bases of nucleotides and nucleic acids are derivatives of either pyrimidine or purine, both containing a six-membered heterocyclic aromatic ring (Figure 2.1a). Within DNA, the aromatic rings align nearly perpendicular to the DNA double-strand, so the planes of aromatic rings are positioned parallel to each other. This allows the electron clouds, extending from atoms participating in double bonds, overlap with those of adjacent bases. Single π-stacking is much weaker than a covalent bond, but the sum of π-stacking

between adjacent nucleotides can create a large net stabilizing energy for the helix structure of DNA (Figure 2.1b). Currently, π-stacking is widely utilized in biological areas such as molecular recognition[8-10] and creating membrane channels.[11-16]

π-Conjugated polymers are the most promising functional materials owing to their potential applications in field-effect transistors (FET), light-emitting diodes (LED), plastic lasers, and photovoltaic cells. In the past twenty years, investigation of π-conjugated oligomers and polymers has flourished and received many reviews.[17-24] It was found that π-stacking can direct molecular organization in solid or liquid crystal state (i.e. crystal engineering) and may generate organic nanodevices with improved electronic properties.[25] A general hypothesis about the molecular design of such materials is the following: low dimensional (1-D and 2-D) larger π-core enhance π-stacking and reduce steric hindrance, thereby reducing the intermolecular distance between molecules within the stack (Figure 2.2).[26,27]

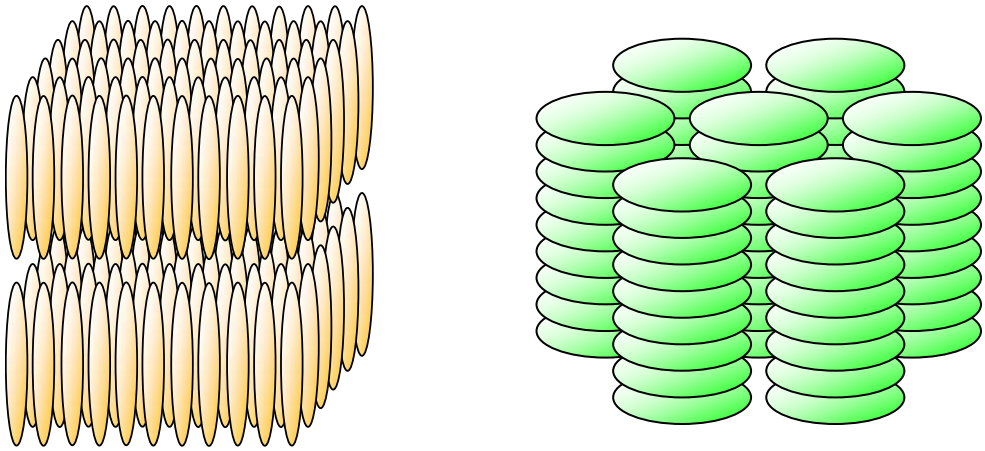

(a) 1-D molecular structure
Smectic phases

(b) 2-D molecular structure
Columnar or discotic phases

Figure 2.2. Schematic drawing of liquid crystal phases formed by π-conjugated polymers

Driven by the possibility of control supramolecular architectures in aqueous solution, the design of amphiphilic π-conjugated systems has also attracted increasing interest.[28-30] Much effort has been devoted to create well-defined supramolecular structures using π-conjugated systems as the building block. For example, Iverson and co-workers developed "aedamers", self-folding supramolecules between electron rich 1,5-dialkoxynaphthalens (DAN) and electron-poor 1,4,5,8-naphthalene-tetracarboxylic-bisimides (NDI).[31,32] The loss of highly ordered solvent molecules upon assembling is overcompensated by the reinforced rigidity of the aromatic cores, contributing to the overall negative Gibbs free energy. Stoddart et al.[29,30] utilized the similar method in constructing supramolecules such as catenane.

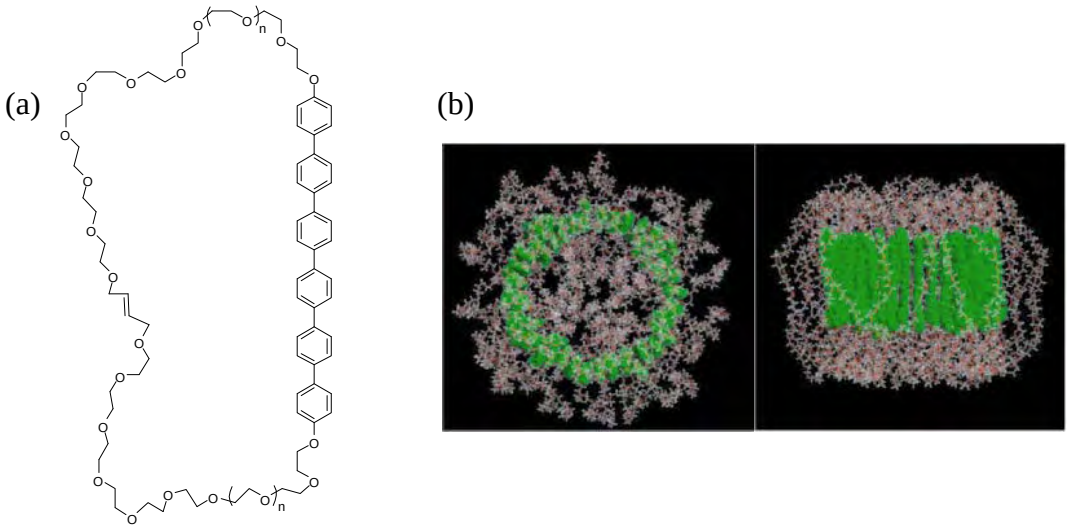

Figure 2.3. (a) Example of an amphiphile with a rigid linear π-conjugated core. (b) Top view (left) and side view (right) of a barrel-like structure by molecular modeling (rod segments are coloured green, oxygens and hydrocarbons are coloured red and grey, respectively).

More recently, Lee et al.[15,33-36] synthesized water-soluble amphiphilic molecules with a rigid linear π-conjugated core. The molecule shown in Figure 2.3a consists of a hexa-*p*-phenylene rod and a poly(ethylene oxide) chain that are fused together into a macrocyclic ring. In aqueous solution, the rod-coil macrocycles aggregate into a barrel-like structure with hydrophilic exterior and interior (Figure 2.3b). Other types of amphiphiles with various cores (flexible linear, cyclic, rigid star or T-shape) have also been studied by Lee's group.[37-42]

Mullen et al.[43] used planar π-conjugated building block for preparing disk-like molecules. Figure 2.4 illustrates an amphiphile with a rigid hexabenzocoronene (HBC) core and six oligo(ethylene glycol) chains. These molecules were shown to form ordered columnar self-assembly not only in bulk, but more importantly in aqueous solution and can serve as template for preparing porous silica with aligned nanochannels.

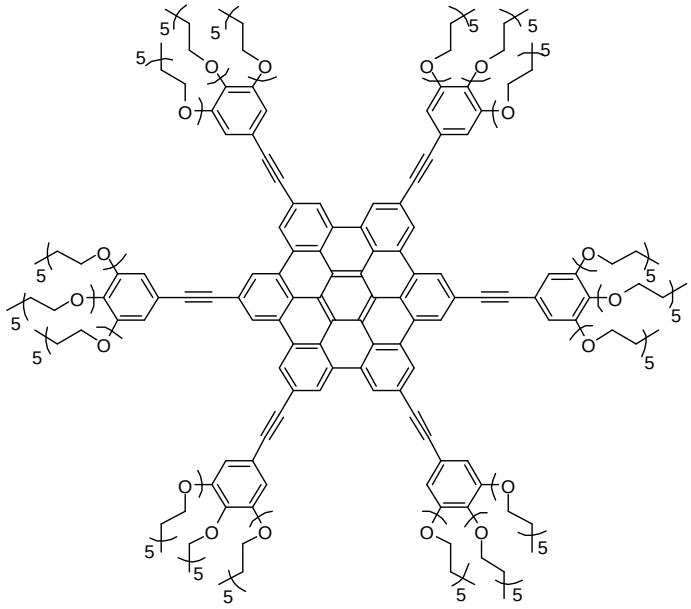

Figure 2.4. Example of an amphiphile with a rigid planar π-conjugated core

Our group had also studied a rigid amphiphile.[44] It can be seen from Figure 2.5a that this compound (**A**) has two sulfate groups on one face and a rigid wall of hydrophobicity on the other. Amphiphile **A** showed some unusual properties: (1) **A** is surface active in water (surface tension decrease with increasing concentration), but the plot of surface tension vs. log *c* has no sharp break corresponding to the CMC, indicating a stepwise rather than cooperative aggregation behavior (Figure 2.5b). (2) **A** dramatically stabilizes an o/w (toluene in water) emulsion. No change in the size distribution of the droplets was observed during a period of more than six months. No doubt, the rigidity of the structure dramatically affects the colloidal properties of **A** (e.g. The packing density at the air/water interface might be impaired and causes lower surface activity).

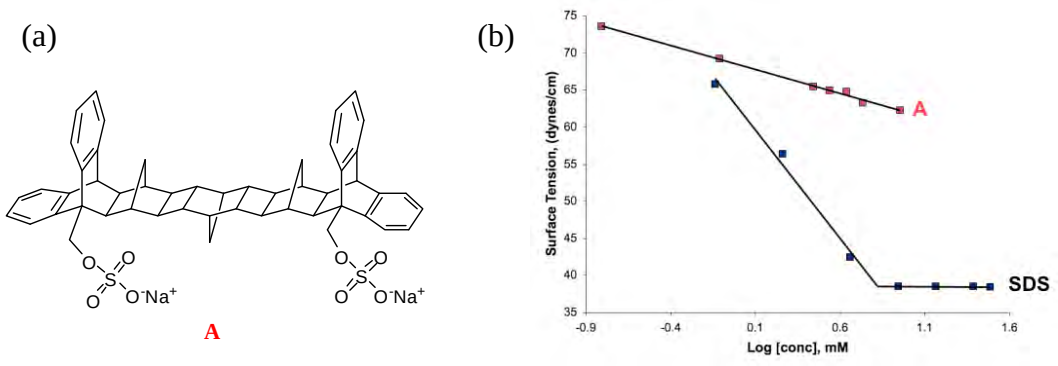

Figure 2.5. (a) Structure of a rigid amphiphile (**A**). (b) Surface tension vs. log *c* of **A** and sodium dodecyl sulfate (SDS).

Therefore, it is significant to explore how an enhanced π-stacking in rigid amphiphiles affects self-assembly. However, in most previously described systems, other non-covalent interactions such as hydrogen-bonding are combined with π-stacking and the strength of the overall binding is the result of many cooperative processes.[45-47] Thus,

the situation is too complicated to isolate and study the π-stacking effect. Furthermore, the damage on the surface activity from the rigid structure of amphiphiles has not been fully studied. In this context, we propose to synthesize a planar amphiphile **1'** which possesses a large π-conjugated core (HBC) surrounded by six ionic groups (Figure 2.6). This rigid characteristic of compound **1'** promotes the π-stacking interaction while minimizing other non-covalent forces. Another compound, **1**, has a hexaphenylbenzne (HPB) core which is relatively more flexible than **1'**, and thereby can be used as a non-conjugated amphiphile for comparison.

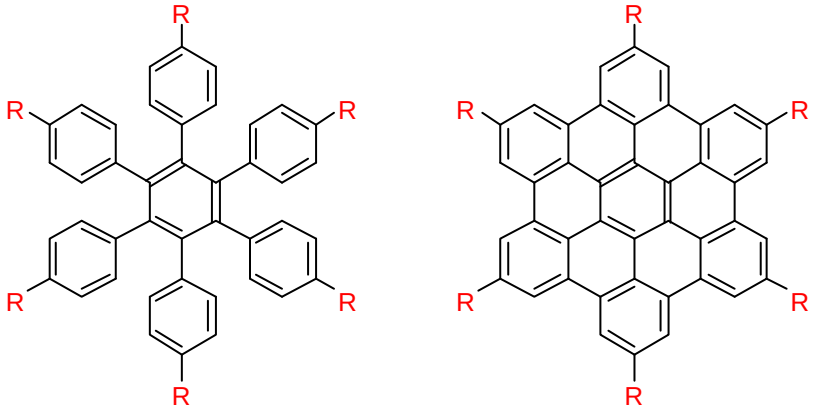

Non-Facial Amphiphile **1** Facial Amphiphile **1'**

Figure 2.6. Target molecules with a rigid π-conjugated core. R = ionic group.

Synthesis

By retrosynthetic analysis and searching literature, several synthetic routes were proposed and shown in Scheme 2.1.

Scheme 2.1. Proposed synthetic routes for **1** and **1'**. R = ionic group and R' = group that can be converted to R.

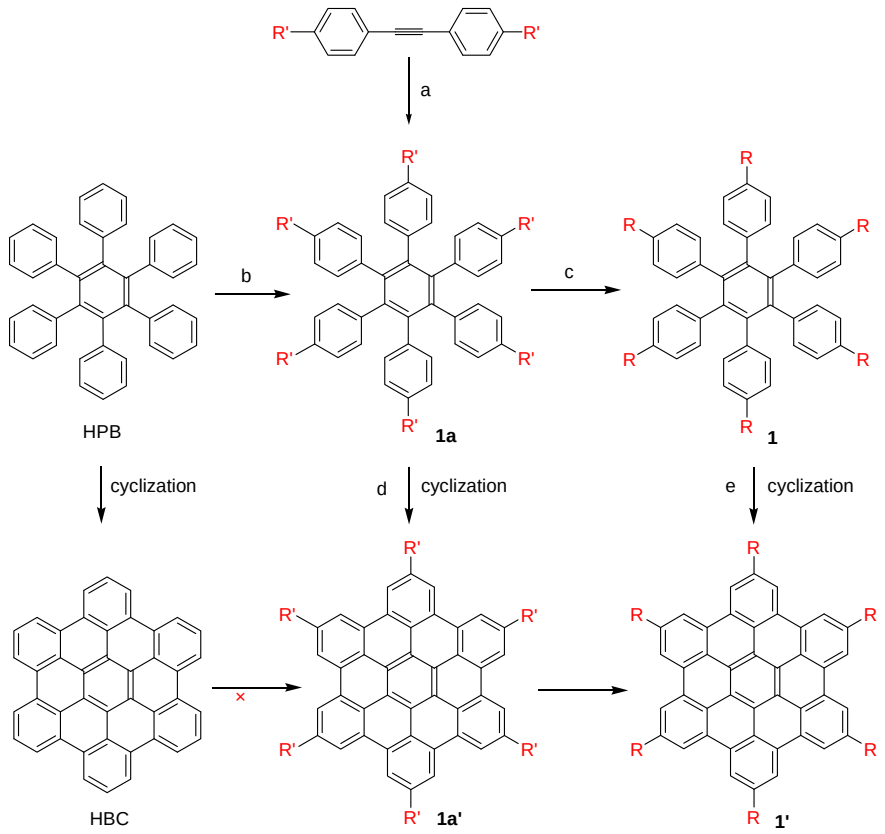

Compound **1** can be synthesized through an intermediate **1a** (c), which can be achieved by either (a) cyclotrimerization of a functionized tolane[48-51] or (b) direct functionization of hexaphenylbenzne (HPB). Correspondingly, compound **1'** can be synthesized by either (d) cyclization of 1a to give **1a'** followed by transforming R' to an

ionic group R or (e) cyclization of **1**. Although HPB can undergo Scholl reaction[52-60] to give hexabenzocoronene (HBC), due to the insolubility of HBC in either organic solvent or water, it is unlikely to directly place functional groups onto HBC. Details of the experiments are discussed in the following.

Route a

It was reported that 4,4'-bis(methyl)tolane can react with N-bromosuccimide (NBS) in the presence of azobisisobutyronitrile (AIBN) to get 4,4'-bis(bromomethyl)tolane (Scheme 2.2).[61-63] The reaction was carried out in tetrachloromethane (highly toxic) under reflux. Purification of 4,4'-bis(bromomethyl)tolane by recrystallization is difficult since it co-recrystallizes with byproduct such as 4-methyl-4'-bromomethyltolane and 4,4,4',4'-Bis(dibromomethyl)tolane. Flash column chromatography can purify 4,4'-bis(bromomethyl)tolane but only in a low yield (15%) due to the close polarity between the byproducts and the desired compound.

Scheme 2.2. Cyclotrimerization of 4,4'-bis(bromomethyl)tolane

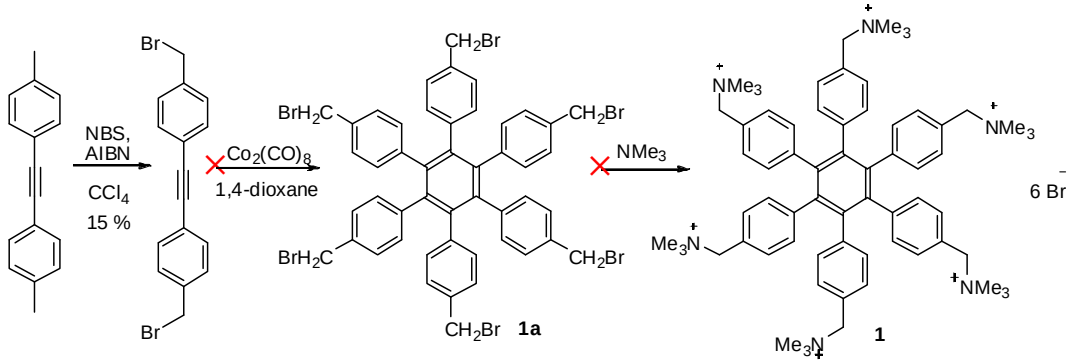

The following cyclotrimerization of 4,4'-bis(bromomethyl)tolane to form intermediate **1a** failed, giving a mixture of unknown byproducts. Thus, the next transformation of bromide group to ammonium group could not continue.

Route b

First, by following the literature,[43] HPB was treated with $PhI(O_2CCF_3)_2$ and iodine to give hexaiodohexaphenylbenzene (HPB-I, Scheme 2.3). Scholl reaction of HPB-I produced insoluble hexaiodohexabenzocoronene (HBC-I). However, Sonogashira reaction[52,64-67] did not work for either HPB-I or HPC-I to provide the desired intermediate **1a** or **1a'**.

Scheme 2.3. Sonogashira reaction of HPB-I and HBC-I

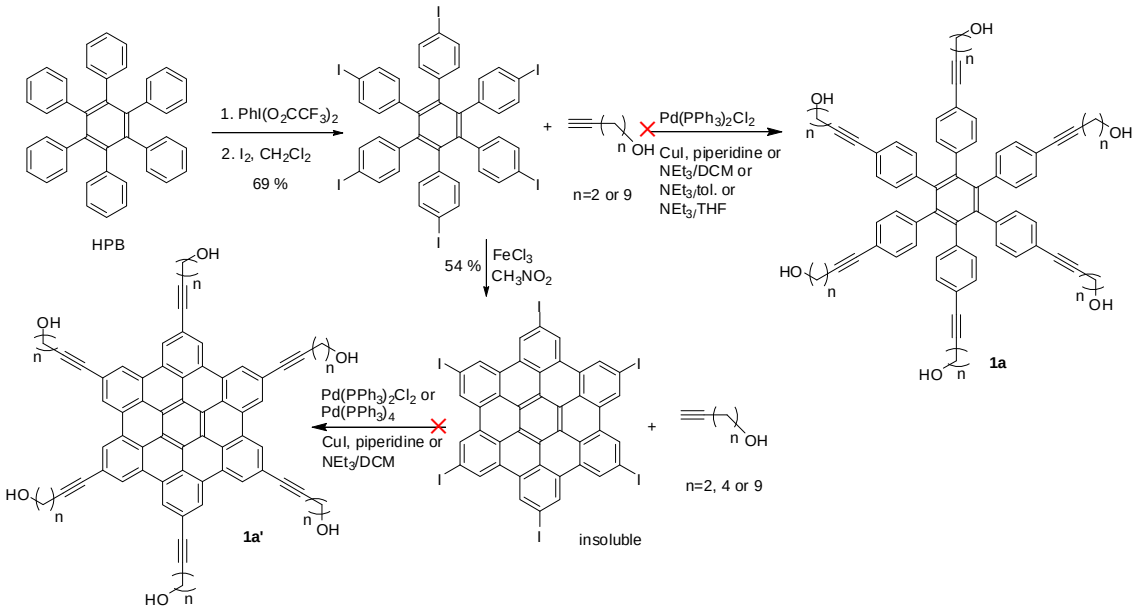

Fortunately, we found that according to Robello et al.,[68-70] HPB can be directly sulfonated by chlorsulfonic acid in dichloromethane (Scheme 2.4). This reaction was

repeated successfully in a high yield (97 %). The intermediate **1a** (hexaphenylbenzene hexasulfonyl chloride, HPB-SO_2Cl) was then dissolved in a large excess sodium hydroxide solution at 50 ℃. Purification of **1**, hexaphenylbenzene hexasulfonyl acid hexasodium, with the reported recrystallization method[71] failed. The final product **1** was purified by long time dialysis (yield: 16 %). The structure and purity of **1** (pale yellow crystal) was proved by ^{1}H and ^{13}C NMR and high-resolution FAB-MS.

Scheme 2.4. Synthesis of **1** by sulfonation of HPB

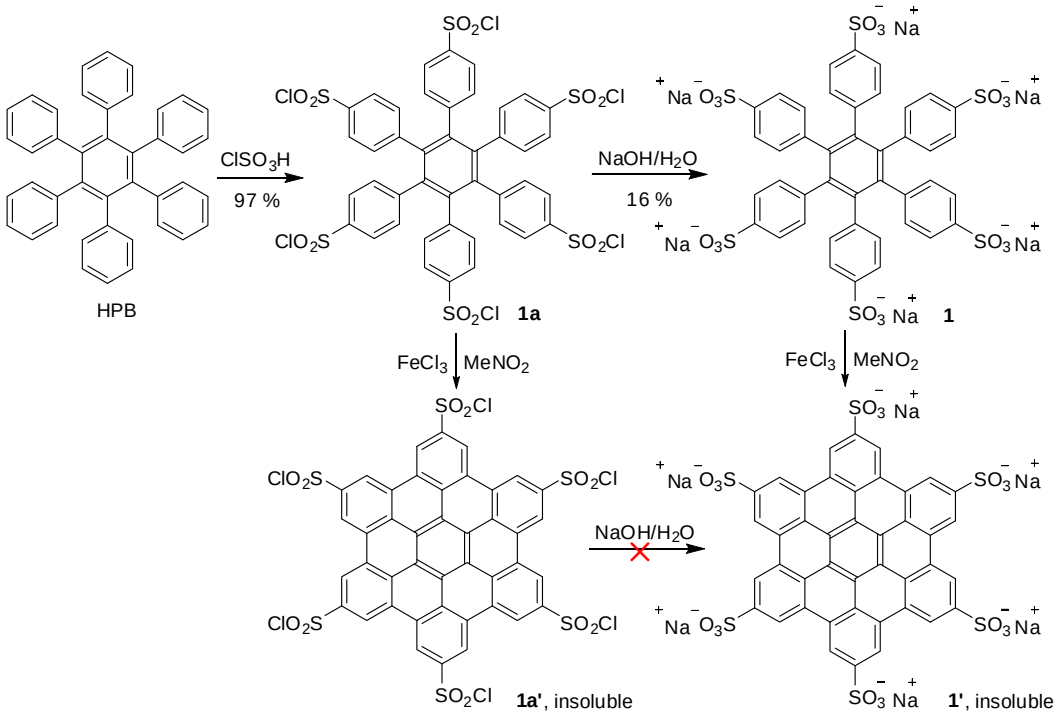

However, cyclization of **1a** and **1** using ferric chloride in nitromethane (route d and e) both give insoluble (in water or organic solvent including chloroform, toluene, tetrahydrofuran, acetone, ethyl acetate, and dimethylsulfoxide) yellow/brown solid. Currently, the only reported technique for characterizing such polycyclic aromatic

hydrocarbons is matrix assisted laser desorption/ionization time-of-flight (MALDI-TOF).[72,73] This technique requires additional instruments and materials which are not available to us. Therefore, the initial idea of exploring enhanced π-stacking of rigid facial amphiphile in self-assembly was not successful due to the problem of insolubility and only compound **1** was continued with the following colloidal study.

Results and Discussions

Surface Tension and Conductivity

The study of compound **1** started with surface tension measurement by the Du Nouy ring method. With concentration increasing (up to 20 mM), the surface tension of aqueous solution of **1** remained at ~ 72 mN/m (≈ the surface tension of water). This constant surface tension reveals that the amphiphilic compound **1** is not surface active. Thus, **1** has no tendency to either preferably adsorb at the air/water interface or at high concentrations, aggregate to form self-assembly such as micelle.

In comparison, when **1** was admixed with a cationic surfactant, dodecyltrimethylammonium bromide (DTAB), some unusual phenomena were observed. As shown in Figure 2.7, adding a mere 3.3 mole-% of hexanion **1** substantially lowers the apparent surface-tension-based critical micelle concentration (CMC) of DTAB by a factor of 10. Moreover, solutions of DTAB/**1** = 30:1 were cloudy from 0.7—13 mM DTAB, indicating formation of large aggregates. Thereby, although by itself **1** is both surface-inactive and non-aggregating, **1** shifts downward the "break" in the surface tension plots (commonly taken as the CMC).[74,75] It is as if 3.3 mole-% **1** "seeds" micelle formation by the excess DTAB.[76] As will be shown, however, the effect is in fact unrelated to micelle "seeding". Rather, it reflects a more entangled colloidal behavior than we first realized.

Studies of an ionic amphiphile in the presence of an oppositely-charged additive are common enough, but generally both components self-assemble individually, e.g. a cationic and an anionic surfactant. Such combinations tend to ion-pair,[77] resulting in a reduced head-group area that causes spontaneous formation of stable vesicles.[78-82] When

the anionic/cationic ratio is precisely unity, a precipitate is possible. Long micellar lifetimes and low surface tensions also arise from anionic/cationic interactions.[83] These interactions have been further explored at the air/water interface.[84-87] As mentioned, our curiosity centered around low levels of non-aggregating anionic additives, bearing one to six negative charges (Figure 2.8), in the presence of a large excess of cationic amphiphile.

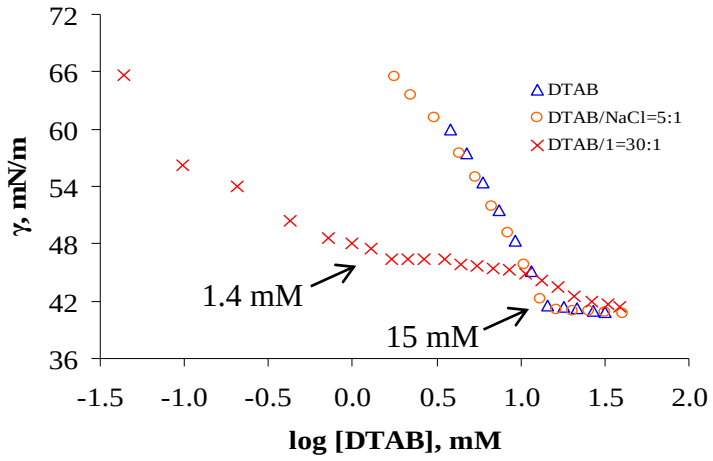

Figure 2.7. Surface tension vs. log [DTAB] in solutions of constant DTAB/**1** ratio of 30:1, DTAB and DTAB/NaCl (5:1) with no added **1**

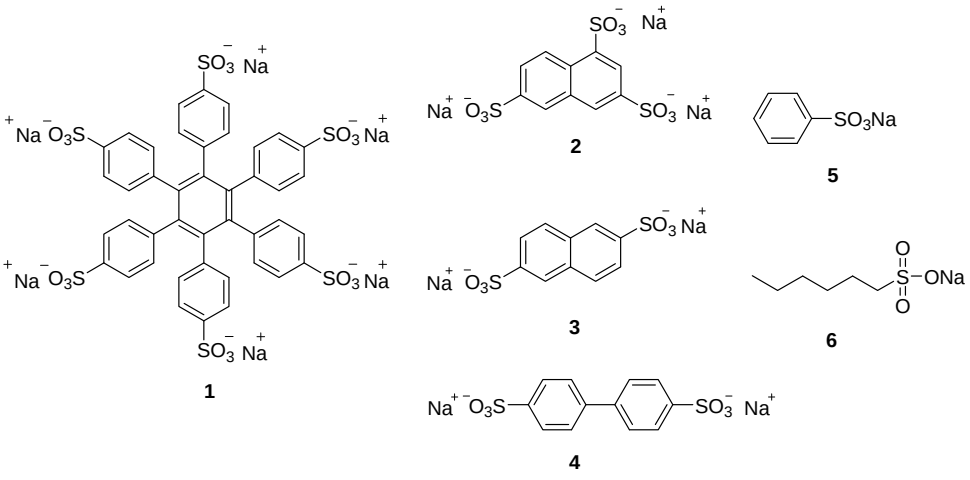

Figure 2.8. Surface-inactive anionic additives with one to six negative charges

Figure 2.9 shows surface-tension vs. log [DTAB] plots for anions **2-5**. All solutions were optically clear and pure **2** is surface-inactive as high as 15 mM. Ratios were changed to keep DTAB/anion charge-ratios constant. For instance, a DTAB/**2** ratio was maintained at 15:1 throughout (Figure 2.9a). For comparison purposes, Figure 2.9a shows the corresponding plot for 5:1 DTAB/NaCl. As seen, breaks are located at 2.9 mM and 15 mM for DTAB/2 and DTAB/NaCl, respectively. If conventional thought is accepted at face value, then 6.7 mole-% of **2** lowers the CMC of DTAB by a factor of 5.

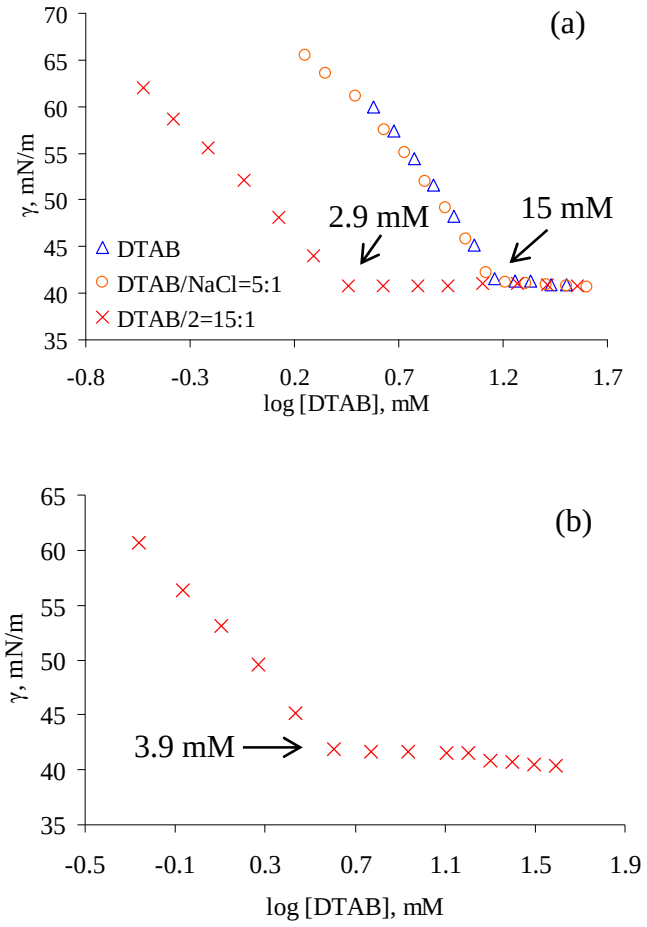

Figure 2.9. Surface tension vs. log [DTAB] in solutions of (a) DTAB/**2** = 15:1, (b) DTAB/**3** =10:1, (c) DTAB/**4** =10:1, (d) DTAB/**5** = 5:1, and (e) DTAB/**6** =5:1

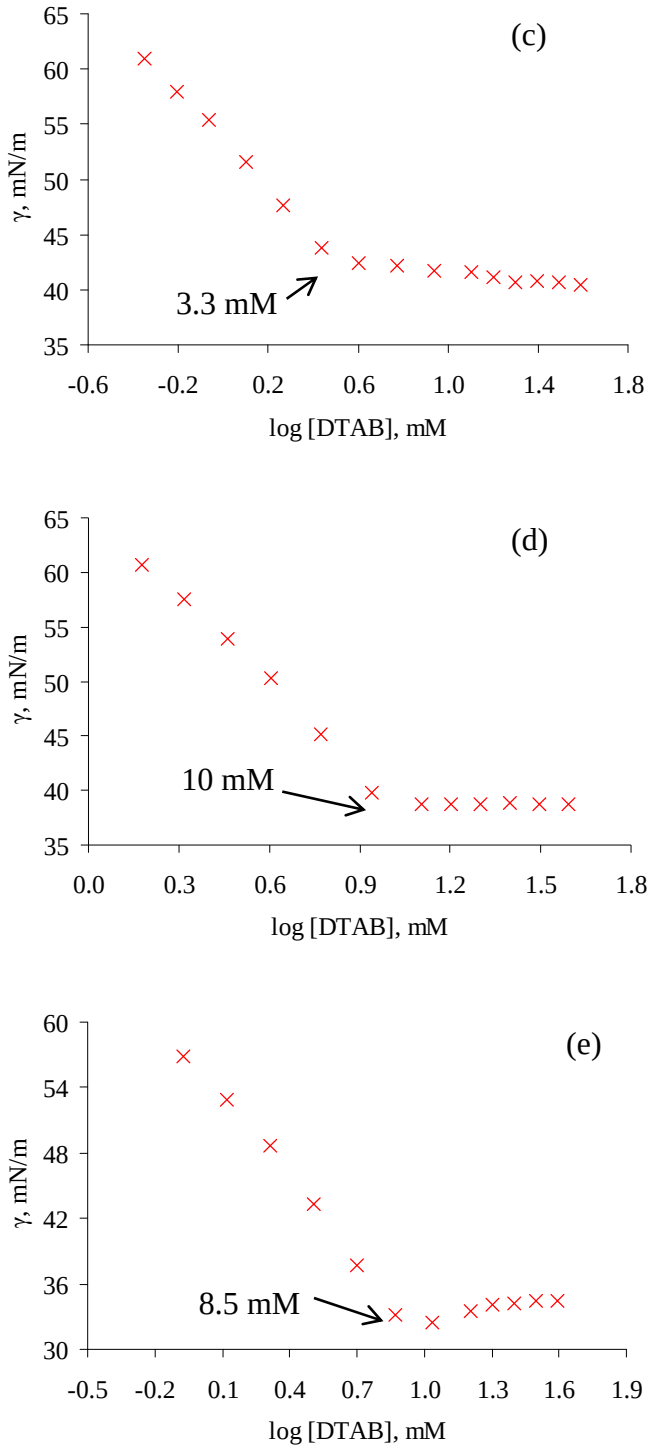

Figure 2.9. Surface tension vs. log [DTAB] in solutions of (a) DTAB/**2** = 15:1, (b) DTAB/**3** =10:1, (c) DTAB/**4** =10:1, (d) DTAB/**5** = 5:1, and (e) DTAB/**6** =5:1

In Figure 2.10b, surface tension is plotted vs. log [**2**] using a constant sub-micellar [DTAB] of 1.8 mM. The surface tension reaches a minimum when [**2**] = 0.39 mM. Yet in the absence of **2**, a [DTAB] of 15 mM (CMC) is required to lower the surface tension to a comparable value. These data suggest a profound effect of **2** upon the assembly at the air/water interface, a fact relevant to our subsequent analysis below.

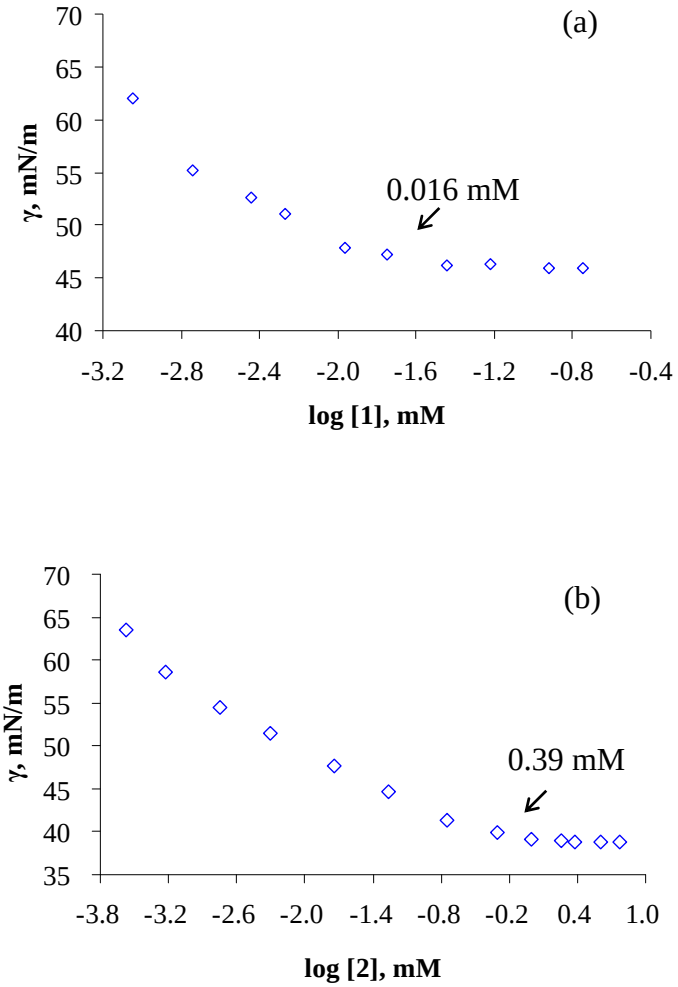

Figure 2.10. Surface tension vs. log [anion] at a constant sub-micellar [DTAB] of 1.8 mM

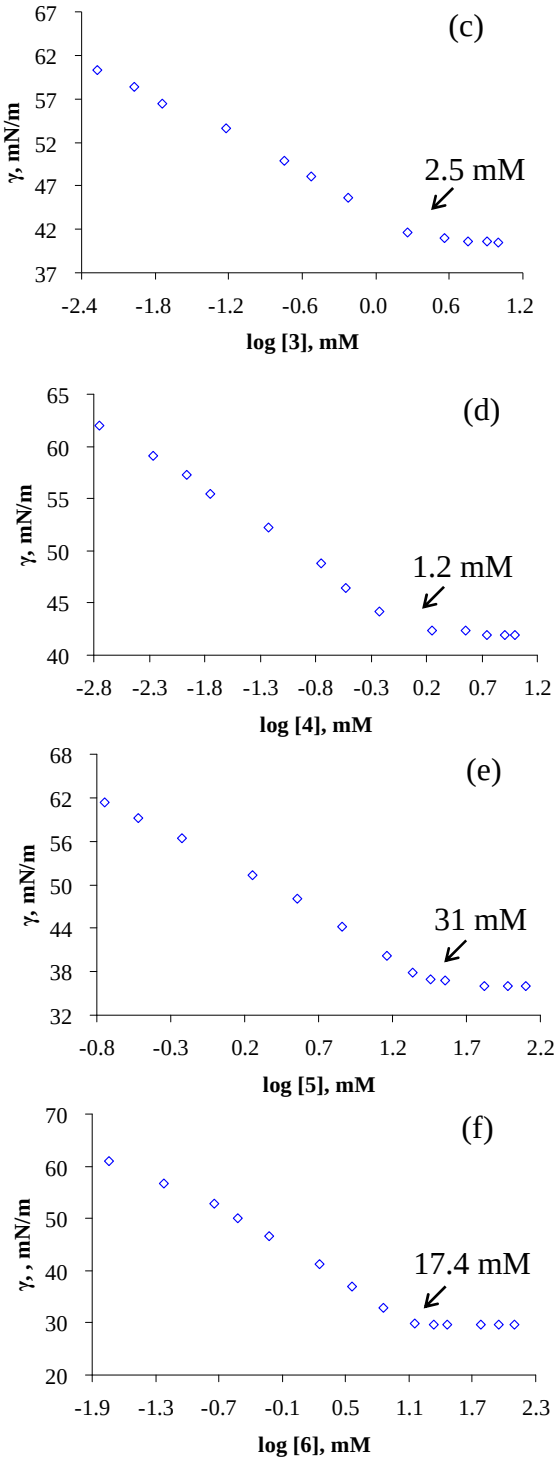

Figure 2.10. Surface tension vs. log [anion] at a constant sub-micellar [DTAB] of 1.8 mM

Conductivity, a second major technique for measuring CMC values,[74,75,88] tells a different story. As seen in Figure 2.11b, both DTAB/**2** and pure DTAB have similar plots of conductivity vs. [DTAB], indicating now that **2** has a negligible effect upon the CMC. Since the surface tension and conductivity methods generally give identical CMC values, a $CMC_{surface\ tension}$ = 2.9 mM vs. $CMC_{conductivity}$ = 14 mM constitutes a major departure from common experience. Note that all anionic additives listed in Table 2.1 likewise display method-based inequalities with magnitudes directly dependent upon the charge-content of the anions.

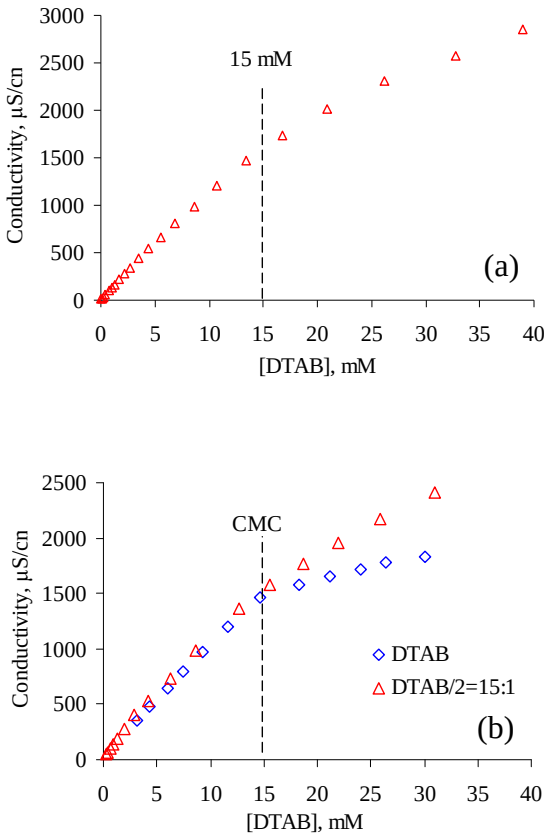

Figure 2.11. Conductivity vs. [DTAB] in solutions of (a) DTAB/**1** = 30:1, (b) DTAB/**2** = 15:1, (c) DTAB/**3** = 10:1, (d) DTAB/**4** = 10:1, (e) DTAB/**5** = 5:1, and (f) DTAB/**6** = 5:1

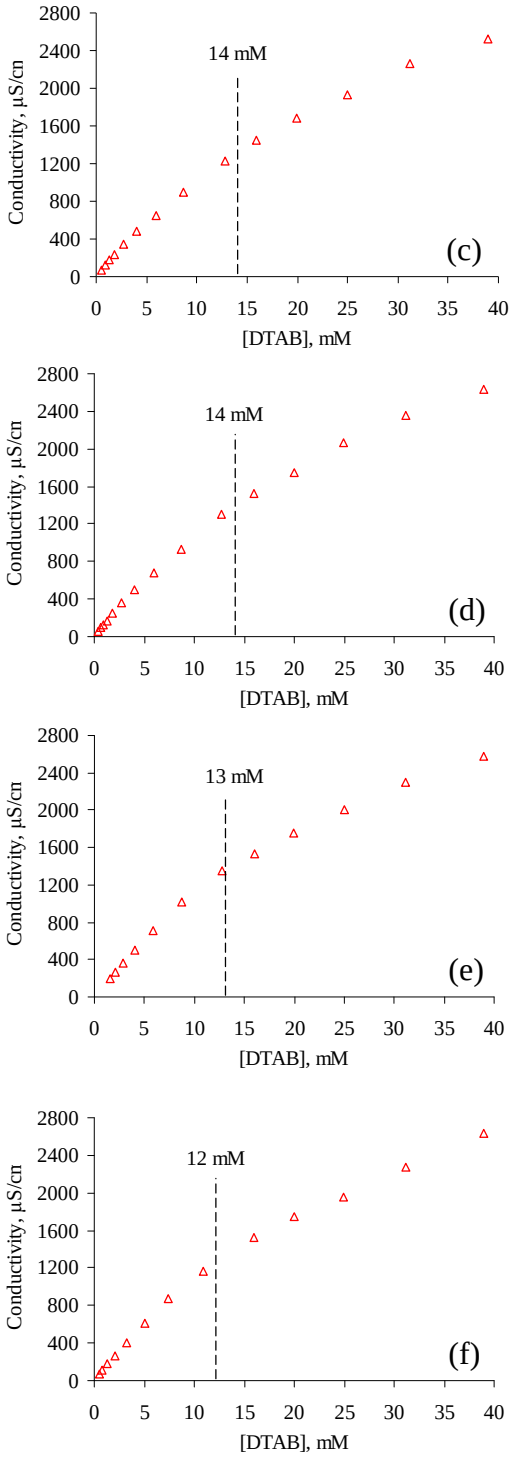

Figure 2.11. Conductivity vs. [DTAB] in solutions of (a) DTAB/**1** = 30:1, (b) DTAB/**2** = 15:1, (c) DTAB/**3** = 10:1, (d) DTAB/**4** = 10:1, (e) DTAB/**5** = 5:1, and (f) DTAB/**6** = 5:1

Table 2.1. Properties of anion/DTAB self-assemblies

anion	DTAB/anion	"CMC" by surface tension, mM	CMC by conductivity, mM	[anion] at ST_{min}, mM[a]
1	30:1	1.4	15	0.016
2	15:1	2.9	14	0.39
3	10:1	3.9	14	2.5
4	10:1	3.3	14	1.2
5	5:1	10	13	31
6	5:1	8.5	12	17.4

[a] Anion concentration at minimum surface tension with [DTAB] = 1.8 mM.

Classical theory has it that sharp breaks in surface tension plots, such as in Figure 2.9a, stem from the following: Surface tension declines as added surfactant adsorbs to the air/water interface. At some point (i.e. the CMC) micelles begin to assemble. Since additional surfactant molecules then prefer to join the micelles rather than bind further to the air/water interface, the surface tension plot levels off abruptly. But our data support an entirely different mechanism: According to Figure 2.9a, when a mixed-monolayer of absorbed DTAB/**2** reaches a surface tension minimum at 41 mN/m, the interface becomes saturated. Consequently, the plot levels off at 2.9 mM DTAB, prior to any micelle formation. Since at saturation the surface tension has already reached its minimum, micelles that form at 15 mM DTAB are never detected by surface tension. Normal micelle formation at 15 mM is, however, revealed by a "bulk" property such as

conductivity (Figure 2.11b). A schematic of binding to the 2-D air/water interface is given in Figure 2.12.

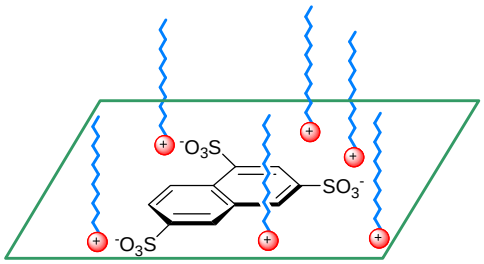

Figure 2.12. Schematic showing a trianion (**2**) absorbed at the air/water interface in which DTAB molecules are present

Therefore, rather than reflecting the early "seeding" of DTAB micelles, Figure 2.9a reveals entry of trianions into the air/water interface. The drop of surface tension as seen in Figure 2.10 is caused by the closer packing of surfactant at the air/water interface toward saturation promoted by electrostatic attraction. This mechanism is similar to that reported in the study on mixtures of ionic surfactant/oppositely charged polymers.[89-91] Micellization at higher DTAB concentrations is unaffected by the trianions, as seen from Figure 2.11. As shown in Figure 2.12, large, flat multi-anionic species can readily insert into a gaseous 2-D monolayer. But they probably bind loosely and tangentially to a spherical micelle surface so as to avoid penetration deep into the Stern layer and, thereby, cause an unfavorable chain-spreading. In any event, the mechanism serves as a cautionary note: The sharp "leveling off" routinely seen in surface tension-based "CMC plots" need not in fact attest to micelle formation.

Furthermore, our study gave rise to two fundamental and related questions: What is the reason for decrease in surface tension with increasing surfactant concentration and

is the surface saturated with surfactant before the dramatic surface tension reduction? Plots of surface tension vs. log [surfactant] display three regions (Figure 2.13):[92] Region-A, where the surface tension hardly changes with concentration; Region-B, a steep, almost linear, decline; (C) an abrupt leveling at the critical micelle concentration (CMC).

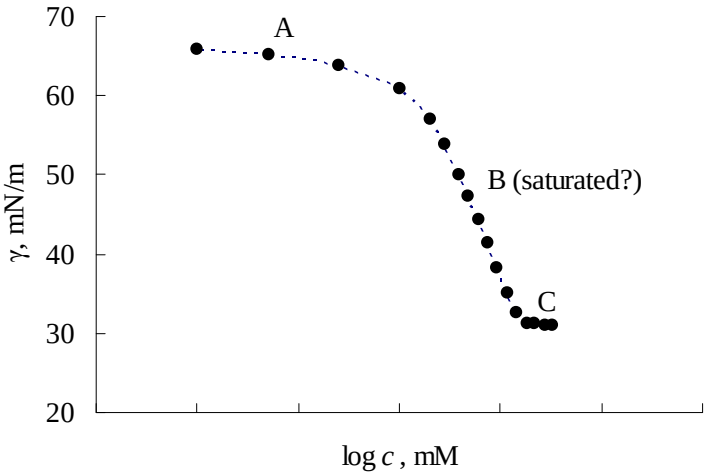

Figure 2.13. The three regions of a typical surface tension vs. log [surfactant] plot

Conventional theory assumes that the air/water interface is saturated with surfactant throughout Region-B.[93] It is this key assumption that allows the calculation of the area-per-molecule (*A*) via application of the Gibbs equation (eq 2.1 and 2.2):

$$\Gamma_2 = -\frac{1}{2.303RT}\frac{d\gamma}{d\log c} \tag{2.1}$$

$$A = \frac{10^3}{N \times \Gamma_2} \tag{2.2}$$

where Γ_2 = the surface excess concentration; dγ/dlog *c* = the slope of line-B; and *N* = Avogadro's number. If the area-per-molecule were continuously decreasing in Region-B, instead of remaining constant owing to saturation, a unique area would obviously be unattainable. The Gibbs analysis is now accepted dogma in colloid/interface chemistry

as revealed by its prevalence in the textbooks[94,95] and by the hundreds of Gibbs-based areas published in the literature.[96-104] We count ourselves among the many who have innocently applied the Gibbs equation to the surface tension of air/water interfaces.[105,106] The purpose of the following discussion is to revise current thought on the subject.

Puzzling questions emerge from the Gibbs analysis. One wonders, for example, why the surface tension remains unaltered in Region-A only to decline precipitously once saturation at the air/water interface is finally reached at the beginning of Region-B. It seems strange that the surface tension responds far more sensitively at concentrations exceeding saturation than it does while the interface is in the process of becoming saturated. The large surface tension change in Region-B is commonly explained (rather vaguely) by an "increased activity of the surfactant in the bulk phase rather than at the interface."[96] More specifically, the water/surfactant interaction close to the interface is gradually replaced by weaker surfactant/surfactant interaction with higher concentration until micelles begin to form. But there exists an alternative explanation that to our knowledge has not yet been explicitly considered.

Several concepts must be clarified first: Surface excess (n_2), surface excess concentration (Γ_2), saturated surface concentration (c_{sat}). According to Mitropoulos[107], "surface excess is the difference between the amount of a component actually present in the system, and that which would be present in a reference system if the bulk concentration in the adjoining phases were maintained up to a chosen geometrical dividing surface: i.e. as though the interface has no effect."

Schematically:

$$n_2 = n_{\text{real}} - n_{\text{reference}} \tag{2.3}$$

where $n_{real} = n^{\alpha} + n^{\beta}$ is the total amount of that component (surfactant) in the real system and $n_{reference}$ is the amount of the same component in a reference system having the same volume (V) as the real system which is divided by a hypothetical surface into two volumes $V^{\alpha} + V^{\beta} = V$ each one containing $C_2{}^{\alpha}V^{\alpha} = n^{\alpha}$ and $C_2{}^{\beta}V^{\beta} = n^{\beta}$ moles with $C_2{}^{\alpha}$ and $C_2{}^{\beta}$ as the bulk concentrations in the real system, respectively (Figure 2.14).

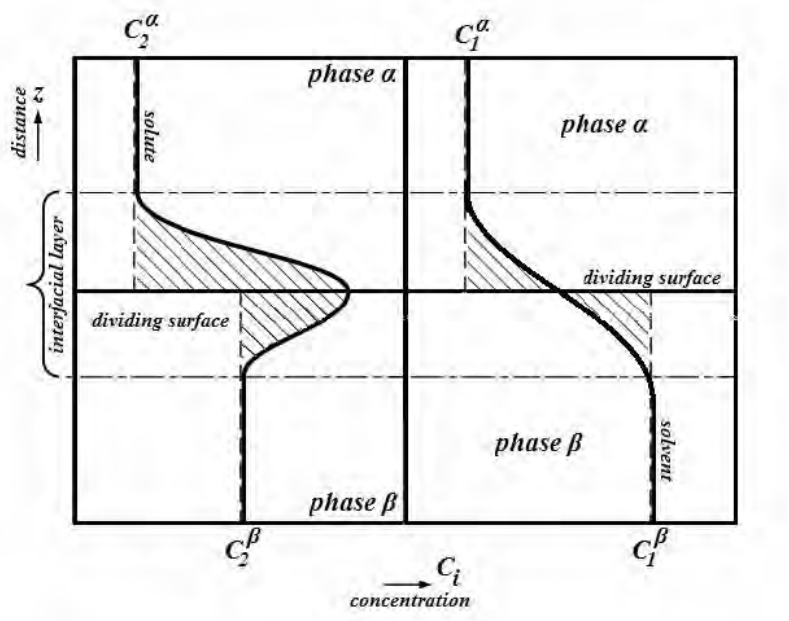

Figure 2.14.[107] Concentration profiles of a binary system as a function of distance normal to the phase boundary. Bold curved lines, in both frames, are the concentration profiles of the solute and the solvent in the real system, respectively, and again vertical broken lines are the concentrations in the reference system (being actually the extend of the bulk concentrations up to the dividing surface). Chain dotted lines indicate the boundaries of the interfacial layer. Bold horizontal line is the dividing surface and dotted horizontal line is another choice for the location of the dividing surface. The surface excess is the sum of the shaded areas above and under the dividing surface.

If more precisely, phase α is divided into two parts: one with constant bulk concentration (C_2^{α}) and bulk volume ($V^{\alpha b}$) and one with an interfacial concentration ($C_2^{\alpha i}$) and interfacial volume ($V^{\alpha i}$), then $V^{\alpha} = V^{\alpha b}+V^{\alpha i}$. Similarly, phase β is divided into two parts with corresponding parameters C_2^{β}, $V^{\beta b}$, $C_2^{\beta i}$, $V^{\beta i}$, and $V^{\beta} = V^{\beta b}+V^{\beta i}$. The total amount of surfactant in the real system is given by:

$$n_{\text{real}} = C_2^{\alpha}V^{\alpha b} + C_2^{\alpha i}V^{\alpha i} + C_2^{\beta}V^{\beta b} + C_2^{\beta i}V^{\beta i} \tag{2.4}$$

The amount of surfactant in the reference system is given by:

$$n_{\text{reference}} = C_2^{\alpha}V^{\alpha} + C_2^{\beta}V^{\beta} = C_2^{\alpha}(V^{\alpha b} + V^{\alpha i}) + C_2^{\beta}(V^{\beta b} + V^{\beta i}) \tag{2.5}$$

Substituting eq 2.4 and 2.5 in eq 2.3, surface excess (n_2) is obtained as:

$$n_2 = (C_2^{\alpha i} - C_2^{\alpha})V^{\alpha i} + (C_2^{\beta i} - C_2^{\beta})V^{\beta i} \tag{2.6}$$

If A_s is the area of the interface, the surface excess concentration (Γ_2) is defined as:

$$\Gamma_2 = \frac{n_2}{A_s} \tag{2.7}$$

and the saturated surface concentration (c_{sat}) is defined as:

$$c_{sat} = \frac{n_{sat}}{A_s} \tag{2.8}$$

where n_{sat} is the total amount of surfactant molecules at the interface when it is saturated with surfactant. Theoretically, the area-per-molecule at the interface (A) should be:

$$A = \frac{1}{c_{sat}} = \frac{A_s}{n_{sat}} \tag{2.9}$$

For aqueous solution of surfactant, α and β represent air and water phase, respectively and it is assumed that $C_2^{\alpha i} \gg C_2^{\alpha}$ and $C_2^{\beta i} \gg C_2^{\beta}$. In Figure 2.13, region-B generally shows a constant slope (= Γ_2). Hence, it is commonly thought that Γ_2 approximately equals to C_{sat} and eq 2.2 is used to calculate A.

However, C_{sat} is obviously larger than Γ_2 and the difference between C_{sat} and Γ_2 might have been excessively neglected. In general, Region-B covers a broad concentration range which means that the bulk solution concentration, C_2^{β}, can increase by more than 10 fold and subsequently cause a non-neglectable difference between C_{sat} and Γ_2.

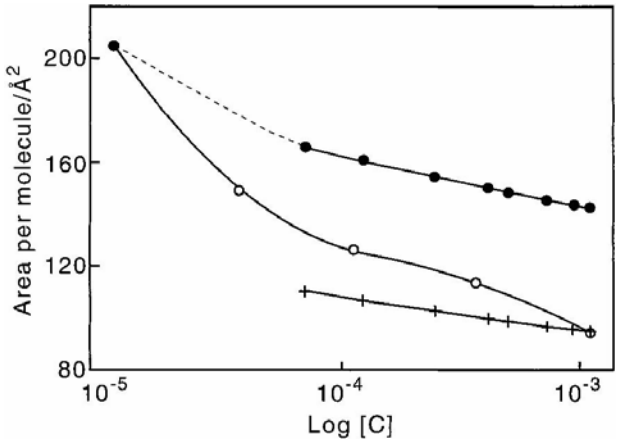

Figure 2.15.[108] Comparison of the surface coverage of a gemini surfactant determined by neutron reflection (○) and surface tension with Gibbs prefactors of 2 (+) and 3 (●)

Figure 2.15 compared area-per-molecule of a gemini surfactant determined by neutron reflection and surface tension.[108] In the concentration range corresponding to Region-B, neutron reflection gives 20 % larger area than that achieved by surface tension using prefactor (n) of 2 in

$$\Gamma_2 = -\frac{1}{2.303nRT}\frac{d\gamma}{d\log c} \qquad (2.10)$$

The neutron reflection values would be more than 30 % smaller than those from surface tension method if n = 3 is used. Only at concentrations close to the CMC, the two methods provide a consistent area-per-molecule. This result implies that the air/water

interface is not really saturated in Region-B and that, therefore, the commonplace Gibbs calculations of molecular areas (dependent upon a fortuitous linear section of the surface tension plots) are inaccurate.

We are arguing for a continuously increasing occupancy of the interface in Region-B that corresponds smoothly to the decline in surface tension. Can one ever observe saturation of the air/water interface by surfactant? Unfortunately, micelle formation often precedes and obscures interfacial saturation. When micelles form at the CMC, additional surfactant molecules prefer to join the micelles rather than enter the interface, and the surface tension no longer decreases (Region C in Figure 2.13). If the CMC lies near or below the saturation point, then the latter becomes unobservable by the surface tension method.

Incredulousness (however legitimate) over a saturated Region-B in the Gibbs analysis does not constitute a disproof. In order to obtain evidence for or against the saturation assumption, we turned to the behavior of insoluble monolayers at the air/water interface. Insoluble monolayers differ from the soluble monolayers formed from most surfactants in two ways: (a) Insoluble monolayers have the adsorbent delivered from the air phase, while soluble monolayers have the adsorbent delivered from the aqueous phase. (b) A soluble monolayer cannot be compressed because molecules under compression will simply depart from the air/water interface and enter the bulk water phase. But otherwise the morphologies of the two monolayers are similar. Thus, an insoluble monolayer of hexadecanol will have its hydroxyl in the water and its hydrocarbon tail projecting in the air…the identical situation found with a soluble monolayer of octanol.

A plot of surface tension vs. area-per-molecule for hexadecanol, obtained from a Langmuir surface balance, is given in Figure 2.16.

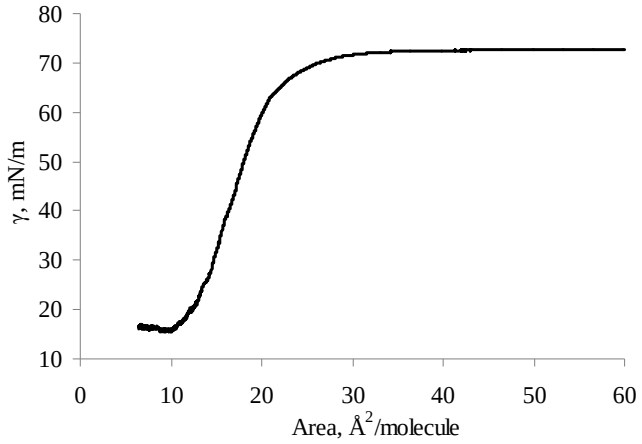

Figure 2.16. Plot of surface tension vs. area/molecule for an insoluble monolayer of hexadecanol

It is seen that the surface tension has a constant "water value" of 72 mN/M between 60 and 40 $Å^2$ per hexadecanol molecule. But Gibbs-determined areas for single-chained surfactants fall into this range (e.g. $C_{12}H_{25}SO^{3-}Na^{+}$, 65 $Å^2$/mol; $C_{18}H_{37}N(CH_3)^{3+}Br^{-}$, 64 $Å^2$/mol; $C_{12}H_{25}Pyr^{+}Cl^{-}$, 62 $Å^2$/mol; $C_{12}H_{25}(OC_2H_4)_4OH$, 46 $Å^2$/mol).[96] This means that when the Gibbs method is applied to steeply declining surface tension plots (Region-B), the resulting areas correspond, according to Figure 2.16, to zero surface tension change. This contradiction can be avoided by assuming cooperative binding at the air/water interface, leading to only minor adsorption at low concentrations followed by an abrupt increase in adsorption (and precipitous decline in surface activity) as the interface becomes saturated. Implied by this model is an air/water interface in Region-B that is merely filling up with adsorbent on its way toward

saturation. By assuming total saturation throughout Region-B, the Gibbs analysis greatly overestimates the true areas per molecule at saturation.

In summary, we have shown that molecular areas calculated by applying the Gibbs equation to Region-B are based on an incorrect assumption, namely that the interface is already saturated when the surface tension first begins its precipitous decline. The surface tension decreases and levels off at higher added anion concentrations in solutions of [DTAB] = 1.8 mM. Normally, the phenomenon is ascribed to micelle formation, but in this case the leveling effect occurs far below the CMC, which can be explained only by saturation subsequent to the Gibbs Region-B.

UV-Vis Spectroscopy

Ultraviolet-Visible (UV-Vis) spectroscopy can be a useful tool in monitoring self-assembly process.[109] UV-Vis absorbance depends on the Beer–Lambert–Bouguer expression commonly known as Beer's Law[110]

$$A = \varepsilon bc \tag{2.11}$$

where A is the absorbance, ε is the absorptivity or molar extinction coefficient, b is the pathlength, and c is the concentration of the absorbing substance. Actually, the absorbance is calculated by taking the negative logarithm of the fraction of light transmitted through a sample. Thereby, A is usually given by

$$A = -\log T = \log \frac{p_0}{p} \tag{2.12}$$

where P is the strength of the light passing through a sample, P_0 is the power of the light detected when the concentration of the absorbing material is zero, and T (= p/p_0) is the fraction of light transmitted.

All the anions studied (except **6)**, with at least one aromatic ring, have strong absorption bands accessible in the UV-Vis region. As shown in Figure 2.17, the plot of A vs. concentration of pure **1** shows a good linearity as high as 20 mM, indicating that **1** is non-aggregating which is consistent with the surface tension results. When **1** mixed with DTAB, owing the cloudy solutions caused by large aggregates formation ([DTAB] ranging from ~ 1-15 mM), the adsorption curve is irregular and gives no useful information. Plots of A vs. [DTAB] of other UV-Vis active anions (**2** to **5**) admixed with DTAB are given in Figure 2.18. Similar to solutions of pure **1**, the slope kept constant for all the mixture solutions in the whole [DTAB] range. This result reveals that no self-assembly of anions occurs either above or below the CMC of DTAB. More importantly,

it supports that the aggregates are formed between anion and DTAB by electrostatic interaction which will not dramatically change the absorbance of aromatic cores.

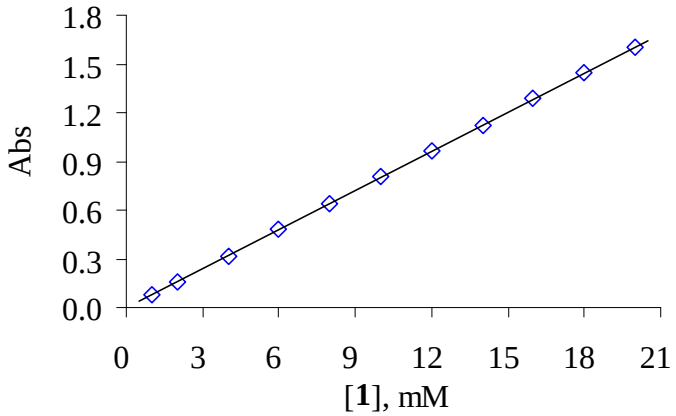

Figure 2.17. UV-Vis absorption of **1** vs. concentration at λ = 392.5 nm

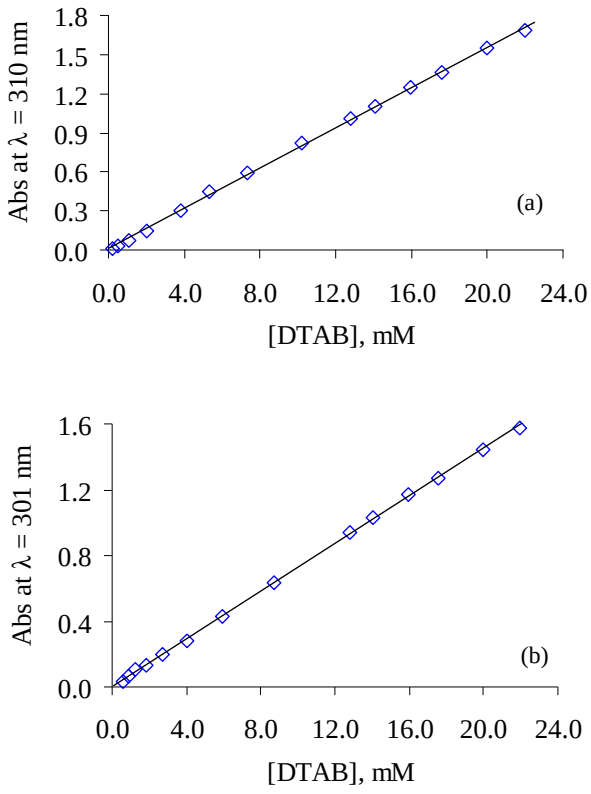

Figure 2.18. UV-Vis absorption of anion vs. [DTAB] in (a) DTAB/**2** = 15:1, (b) DTAB/**3** = 10:1, (c) DTAB/**4** = 10:1, and (d) DTAB/**5** = 5:1

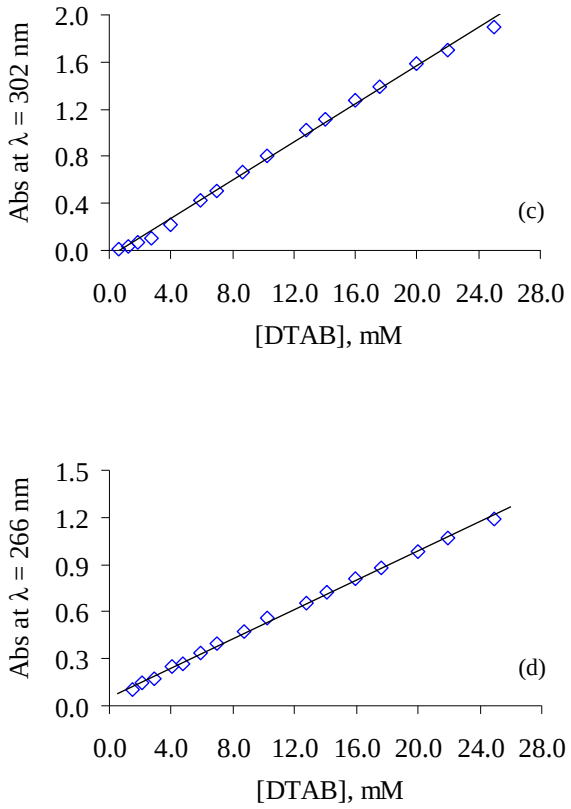

Figure 2.18. UV-Vis absorption of anion vs. [DTAB] in (a) DTAB/**2** = 15:1, (b) DTAB/**3** = 10:1, (c) DTAB/**4** = 10:1, and (d) DTAB/**5** = 5:1

PGSE-NMR

Defining the aggregate size by dynamic light scattering (DLS)[111] was not successful because of the following reasons. (1) Anion **1** form large associated complex with DTAB when DTAB/**1** = 30:1 and [DTAB] ranges ~1-15 mM. Prior to measurements, to eliminate dust interference, all samples (except the standard solutions) must be filtered through a sterile syringe filter with a pore size of 200 nm which is smaller than the DTAB/**1** aggregates formed below the CMC of DTAB. Otherwise, the data would be highly polydispersed. Surfactant solutions without added inorganic salt (e.g. NaBr) often have the polydispersity problem as well. (2) Diluted solutions of DTAB/**1** = 30:1 has a weak light scattering intensity that is out of the required range. (3) The size limit of the instrument ranges from 3 to 3000 nm in diameter, and thus particles smaller than or close to 3 nm are difficult to measure.

Although by DLS, 30 mM DTAB in a 100 mM NaBr solution was found to have an average micellar diameter of 5.6 nm which matches the reported value,[112,113] no reliable data was achieved from DLS for optically clear solutions of DTAB/anion system.

Another powerful tool, Pulse gradient spin echo NMR (PGSE-NMR or "diffusion NMR"),[114-116] was used to investigate the aggregation of DTAB/anion. PGSE-NMR provides diffusion coefficients which, when plotted vs. the reciprocal DTAB concentration, give lines intersecting at a CMC of about 14 mM with or without added **2** (Figure 2.19). Thus, both PGSE-NMR and our other "bulk" method, conductivity, affirm that Figure 2.9a represent solely an interfacial effect. NMR studies also show that the diffusion coefficient of **2** decreases from 4.5×10^{-10} m^2/s in water to 0.80×10^{-10} m^2/s in

15:1 DTAB/**2** at 32 mM DTAB. Thus, **2** binds to the 3-D micelles, following saturation of the 2-D air/water interface, but the CMC is affected little.

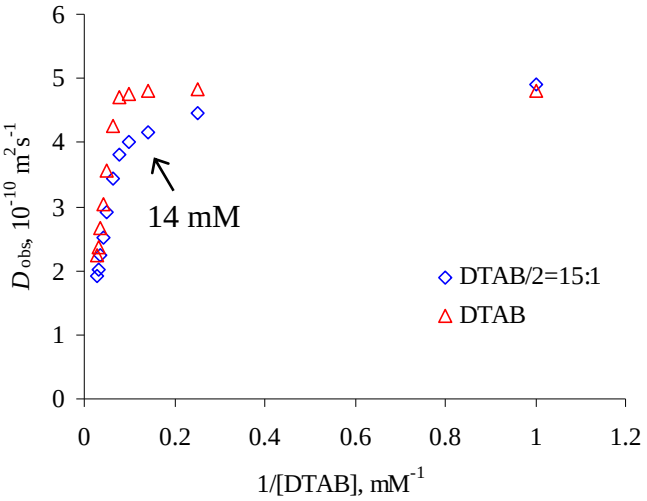

Figure 2.19. Diffusion coefficients vs. reciprocal [DTAB] in solutions of pure DTAB and DTAB/**2** = 15:1

From PGSE-NMR, diffusion coefficients of trianion **2** were also obtained and plotted vs. reciprocal [**2**] (Figure 2.20). For solutions of pure **2** with concentrations ranging from 1 to 15 mM, D_{obs} remains approximately the same (4.5×10^{-10} m^2s^{-1}, close to that of free DTAB molecules), confirming that molecules of compound **2** stay as free monomers. For solutions of DTAB/**2** = 15:1, the signal intensity of 2 is substantially reduced due to the binding between **2** and DTAB or DTAB micelles. As a result, PGSE-NMR can only provide D_{obs} of **2** from two concentrated DTAB/**2** solutions ([DTAB] = 36 and 32 mM). The other samples in lower concentration show an irregular signal decay against pulse gradient which can not be used to calculate D_{obs}.

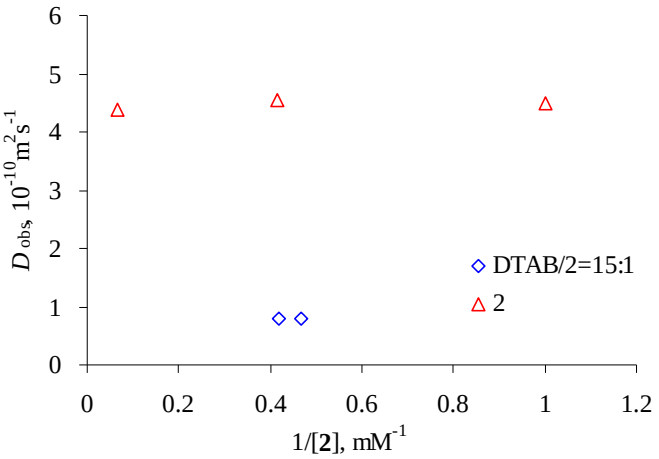

Figure 2.20. Diffusion coefficients vs. reciprocal [**2**] in solutions of pure **2** and DTAB/**2** = 15:1

Since **2** can not only bind to DTAB micelle but also form small aggregate with DTAB molecules, it would be valuable to examine the distribution of **2** among the two types of aggregates by PGSE-NMR. The following discussion, starting from the simplest system, analyzes diffusion coefficient data in details.

(1) For pure DTAB solutions when [DTAB] < CMC, there is only one species - free DTAB molecule. The diffusion coefficient of free DTAB molecule, $D_{Df} = D_{obs} = 4.8\times10^{-10}$ m^2s^{-1}.

(2) For pure **2** solutions, there is only one species - free **2** molecules. The diffusion coefficient of free **2** molecule $D_{2f} = D_{obs} = 4.5\times10^{-10}$ m^2s^{-1}.

(3) In pure DTAB solutions when [DTAB] > CMC, there are two species - free DTAB molecules (D_{Df}) and micellar DTAB molecules (D_{Dm}). Since there is an dynamic exchange between free and micellized DTAB, the observed diffusion coefficient is the weight average of the two species:[88]

$$D_{obs} = D_{Df}\frac{CMC}{c} + D_{Dm}\frac{c - CMC}{c} \quad (2.13)$$

where c is the overall concentration of DTAB and CMC = 14 mM for DTAB based on PGSE-NMR. The shape and size of DTAB micelle should be approximately constant within the concentration range studied (when c = 36 mM, $D_{Df} = 4.8\times10^{-10}$ m^2s^{-1} and $D_{obs} = 2.25\times10^{-10}$ m^2s^{-1} $\Rightarrow$ Diffusion coefficient of micellar DTAB molecules, $D_{Dm} = 0.63\times10^{-10}$ m^2s^{-1}. When c = 32 mM, $D_{Df} = 4.8\times10^{-10}$ m^2s^{-1} and $D_{obs} = 2.38\times10^{-10}$ m^2s^{-1} $\Rightarrow$ Diffusion coefficient of micellar DTAB molecules, $D_{Dm} = 0.49\times10^{-10}$ m^2s^{-1}). Eq 2.13 can be converted to:

$$(D_{obs} - D_{Df}\frac{CMC}{c}) = D_{Dm}(\frac{c - CMC}{c}) \quad (2.14)$$

Plotting $(D_{obs} - D_{Df}\frac{CMC}{c})$ vs. $(\frac{c - CMC}{c})$ gives an average value (the slope of the line) of $D_{Dm} = 0.56\times10^{-10}$ m^2s^{-1}.

(4) A new solution of [DTAB] = [**2**] = 4 mM was prepared and the observed diffusion coefficients for DTAB and **2** are $D_D = 2.43\times10^{-10}$ m^2s^{-1} and $D_{\mathbf{2}} = 3.10\times10^{-10}$ m^2s^{-1}, respectively. There are two species: Aggregates of **2** with associated DTAB molecule and free **2** molecules. Notice that free DTAB molecules are ignored due to the overall ratio of DTAB/**2** = 1:1 and assuming that a single **2** trianion can associate with more than one DTAB molecule. Thereby, the diffusion coefficient of DTAB in the aggregates, $D_{Da} = D_D = 2.43\times10^{-10}$ m^2s^{-1}. It is assumed that the diffusion coefficient of **2** in the aggregates, $D_{\mathbf{2}a} = D_{Da} = 2.43\times10^{-10}$ m^2s^{-1}. Set x as the percentage of **2** molecules in the aggregates and (1-x) as the percentage of **2** as free molecules, then the observed diffusion coefficient of **2** can be written as:

$$D_2 = x \times D_{2a} + (1 - x) \times D_{2f} \quad (2.15)$$

where D_{2f} = 4.5×10^{-10} m^{2}s^{-1} is the diffusion coefficient of free **2** molecule. Substituting the above numbers into eq 2.5 gives x = 0.675, and so in the aggregates of DTAB and **2**, DTAB/2= 4 : (4 × 0.675) ≈ 1.5:1.

(5) For a solution of [DTAB] = 36 mM and [**2**] = 2.4 mM, the observeddiffusion coefficient of **2** and DTAB are $D_{\mathbf{2}}$ = 0.79×10^{-10} m^{2}s^{-1} and D_D = 1.92×10^{-10} m^{2}s^{-1}, respectively. There are three species in the solution (free **2** molecules are ignored due to the overall ratio of DTAB/**2** = 15:1). (I) Aggregates of **2** (*a*, mM) with associated DTAB (*b*, mM) (the diffusion coefficients are $D_{\mathbf{2}a}$ and D_{Da}, respectively). Ignore the size change of aggregates compared to the solution of [DTAB] = [2] = 4 mM, then D_{Da} = $D_{\mathbf{2}a}$ = 2.43×10^{-10} m^{2}s^{-1}. (II) Micellar DTAB ([DTAB] - CMC = 36 - 14 = 22 mM) with attached **2** (2.4 – *a*, mM). The diffusion coefficients of DTAB and **2** in/on micelles are D_{Dm} and $D_{\mathbf{2}m}$ respectively. If the size change of micelles with/without attached **2** is neglectable, then D_{Dm} = $D_{\mathbf{2}m}$ = 0.56×10^{-10} m^{2}s^{-1}. (III) Free DTAB molecules (14 – *b*, mM), D_{Df} = 4.8×10^{-10} m^{2}s^{-1}.

Based on the following equation:

$$D_D = \frac{b}{[\mathrm{DTAB}]} \times D_{Da} + \frac{\mathrm{CMC} - b}{[\mathrm{DTAB}]} \times D_{Df} + \frac{[\mathrm{DTAB}] - \mathrm{CMC}}{[\mathrm{DTAB}]} \times D_{Dm} \quad (2.16)$$

the concentration of DTAB as species I, *b*, is calculated (≈ 4.4 mM), and the concentration of free DTAB, 14 – *b*, equals to 9.6 mM. In a similar behavior, the concentration of **2** as species I, *a*, is also gained (0.3 mM) and the concentration of 2 as species II, 2.4 – *a*, equals to 2.1 mM. For species I, DTAB/**2** = 4.4 : 0.3 ≈ 15:1. For species II, DTAB/**2** = 22 : 2.1 ≈ 10:1, indicating that one micelle has only several **2** attached. The distributions of **2** in aggregates and DTAB micelles are 12 % (= 0.3/2.4)

and 88 % (= 2.1/2.4), respectively. These data, from one hand, show that in solutions of [DTAB] > CMC, trianion **2** prefers to bind with DTAB micelles rather than form small aggregates with DTAB monomers. This preference may due to the fact that micelles have multiple cationic sites and enhanced electrostatic attraction to **2**. From the other hand, the ratio of DTAB/**2** = 15:1 in aggregates reveals that the size change of aggregate with the overall ratio of DTAB/**2** can not be neglected. Actually, the aggregate size should increase with higher ratio of DTAB/**2**. According to Wanchisen et al.,[117] ion pair stability is enhanced by increasing cation/anion ratio in solutions of cationic surfactants. Therefore, the real $D_{Da} = D_{\mathbf{2}a}$ in a solution of [DTAB] = 36 mM and [**2**] = 2.4 mM is smaller than 2.43×10^{-10} m^2s^{-1} (nonetheless larger than $D_{Dm} = D_{\mathbf{2}m} = 0.56\times10^{-10}$ m^2s^{-1}). Replacing D_{Da} and D_{Ta} with a smaller value (2.0×10^{-10} m^2s^{-1}) gives 16 % of **2** in small aggregates and 84 % on DTAB micelles which is only slightly different from the previous result.

The above data analysis confirms that in solutions of [DTAB] > CMC, trianion **2** can exist in both forms of aggregates (species I and II) but seems to prefer to attach to DTAB micelles. The exact distribution of **2** in the two forms depends on the ratio of DTAB/**2** and the overall concentration of DTAB (the higher [DTAB], the higher [micelle]). Likewise, hexanion **1** preferentially binds to micelles when [DTAB] > CMC. It explains the cloudy phenomena in solution of DTAB/1 = 30:1 when [DTAB] < CMC. **1** has multiple negative charges which lead to a strong binding ability for cationic DTAB and **1** can only form complex with DTAB monomers (no micelles available below CMC). Unlike micelle, which is generally soluble in water owing to the partial-hydrated layer on the micelle surface, the large complex formed by **1** and DTAB molecules is more

electrically neutral and has a rather limited solubility. Actually, it was reported that the complex formation between ionic surfactant and oppositely charged dyes below CMC often causes precipitation.[118,119]

Conclusions

In conclusion, six organic additives, each bearing a different number of anionic charges, were added to solutions of a cationic surfactant (dodecyltrimethylammonium bromide, DTAB).[120] The surface tension study shows that saturation of surfactant at the air/water interface occurs at much lower concentrations than the CMC of the system as determined by two "bulk methods" (conductivity and NMR). The interfacial saturation is promoted by electrostatic attraction between cationic surfactants and anions. Geometric considerations may also play a role: multicharged planar anions are more powerful than the monocharged or flexible linear ones. PGSE-NMR reveals that the trianions do indeed bind to the micelles.

The above results, combined with the film balance study of hexadecanol monolayer call into question of the traditional theory that the abrupt surface tension decline in Region-B (Figure 2.13) is only caused by "increased activity of the surfactant in the bulk phase". As a matter of fact, the increasing packing density of surfactant at the surface in Region-B can contribute substantially to the reduction of surface tension as well. Consequently, the areas per molecule at saturation are overestimated by ignoring the increasing difference between surface excess concentration (Γ_2) and the real saturated surface concentration (C_{sat}). The point here is that saturation of the interface appears in Region-C rather than in Region-B as assumed in the Gibbs analysis. Therefore, the vast literature in this area should be reconsidered accordingly. It is hardly the first time that a time-honored notion falls victim to the malleability of science.

Experiments

Materials

Dodecyltrimethylammonium bromide (DTAB) was purchased from Aldrich and purified by recrystallization three times from a 50 : 50 (wt %) acetone/methanol mixture (yield: 20 %).[121] Sodium dodecyl sulfate (SDS) was purchased from EM Science and purified by recrystallization three times from ethanol (yield: 40 %).[122,123]

1,3,6-naphthalene-trisulfonic acid trisodium (**2**) was purified from 1,3,(6 or 7)-naphthalene-trisulfonic acid, trisodium salt hydrate (Aldrich) by following literature method[119] and its purity was proved by ^{1}H NMR.[124-127] 4,4'-Biphenyldisulfonic acid was purchased from TCI and neutralized by NaOH (pH = 7) to give 4,4'-biphenyldisulfonic acid disodium (**4**). 2,6-Naphthalene-disulfonic acid, disodium salt (**3**), sodium benzensulfonate (**5**), and sodium hexanesulfonate (**6**) were purchased from Aldrich and used without additional purification.

All solvents used were reagent or HPLC grade and dried over 4 Å molecular sieves. Deionized water with a resistivity of 18 MΩ cm was obtained using Milli-Q Water System from Millipore. Cellulose ester membrane tubes (Spectra/Por Float-A-Lyzer, MWCO: 100) were purchased from Spectra Laboratories.

Methods

^{1}H and ^{13}C NMR spectra were acquired on a Varian INOVA 400 MHz (100 MHz for ^{13}C) or INOVA 600 MHz (150 MHz for ^{13}C) Spectrometer. Melting points were measured on a Thomas Hoover Capillary Melting Point Apparatus. Mass spectra experiments were completed by the Emory University Mass Spectrometry Center.

Conductivity

All experiments were conducted at room temperature using a sample volume of 10 mL. A Fischer Scientific Traceable™ Conductivity Meter was used and calibrated with three standard solutions of 100, 1000, and 10,000 μS/cm from Fischer Scientific.

UV-Vis Spectroscopy

A JASCO V530 UV/VIS Spectrophotometer was used and calibrated with H_2SO_4 solution (5.0 mM) and $K_2Cr_2O_7$ solution (10.06 mg/L in 5.0 mM H_2SO_4 solution). All experiments were conducted at room temperature with a sample volume of 2 mL in a 10 mm cuvette. The cuvette was cleaned by acetone and deionized water and air dried. All spectra were recorded as an average of three cycles in the absorption mode. The spectrum of deionized water was subtracted as background from the spectrum of each sample.

Film Balance

Experiments were performed in an isolate and clean room using a Kibron Micro Trough X Langmuir film balance running Filmware software (V 3.57) for data analysis. Prior to use, all glassware was washed with base bath (KOH/isopropanol/water) and rinsed with copious amounts of deionized water and finally with 80% ethanol/20% ether solution. The probe was flame dried using a propane torch. After being cooled to room temperature, the probe was rubbed with ethanol soaked kimwipe (to ensure removal of burned solid residues), air dried and placed on the sensor head. The surface of the sub phase was aspirated with pipette to insure no contaminates were present on the surface. Exactly 20 μL of 1.0 mM hexadecanol in chloroform was spread onto the surface of the sub-phase using microsyringe. The hexadecanol was applied in very small amounts (at least 10 points), keeping away from the barriers as well as the sensor probe. After about

30 minutes (for the chloroform to evaporate), the barriers began to compress at a rate of 4.0 Å/molecule/min.

Dynamic Light Scattering

A Coulter N4 Plus Submicron Particle Size Analyzer was used and calibrated with four standard polystyrene latex solutions (bead size: 100, 200, 300, and 500 nm). The cuvette was washed by acetone and air dried, and then cleaned by deionized water without drying. Deionized water and all solutions were filtered through a sterile syringe filter (pore size: 200 nm) and results were recorded as an average of three cycles.

Tensiometry

Surface tension measurements were conducted at room temperature on a Fisher Surface Tensiomat following the Du Nouy ring procedure. All solutions were prepared using deionized water in a 25 mL volumetric flask. Each solution was measured 10 times in a 50 mL crystallizing dish and the obtained values were averaged. Between each solution, the platinum ring (mean circumference: 5.920 cm) was rinsed by 0.1 M HCl solution and deionized water and flame dried.

PGSE-NMR

All experiments were performed using INOVA 600 MHz NMR equipped with a pulsed field gradient (PFG) generator and a PFG amplifier. The solutions were all prepared by dilution of a stock solution. Each sample was placed into the NMR for at least 20 minutes prior to the experiments to allow thermal equilibration. Selected experiments were repeated for verification. The diffusion experiments were completed using a Hahn-echo pulse sequence with intervening pulse field gradient (PG). The pulse sequence was 90^{o}-PG-180^{o} -PG with the delays between the PG (Δ) fixed to 140ms. The

width (δ) of PG was set to 7 ms and the strength of the pulsed gradient (G) was increased linearly from 0.01 up to 0.4 T/m (with the maximum varying among experiments and samples) in 16 steps. The gradient strength and gradient amplifier linearity in the applied gradient strength interval were calibrated by measurements on a trace amount of H_2O in D_2O (D = 1.902×10^{-9} m^2s^{-1}). Traditional NMR tubes with a volume of 800 μL were employed for the solutions. The self-diffusion coefficients (D) of the amphiphiles were obtained from the attenuation of relevant echo peaks by linear least squares fits to the Stejskal-Tanner equation:

$$\ln(I / I_0) = -(\gamma G\delta)^2 D(\Delta - \delta / 3) \qquad (2.17)$$

where I is the measured signal intensity, I_0 is the signal intensity in the absence of gradient pulses, and γ is the magnetogyric ratio of protons and the rest of the parameters are defined above. In all experiments, the observed echo decays gave good fits to eq 1, which shows that they represent single self-diffusion coefficients.

Syntheses and Purifications

*Synthesis of hexaphenylbenzene hexasulfonyl acid hexasodium (**1**)*

A 50 mL round-bottom flask was charged with 2.0 g of hexaphenylbenzene (HPB) and 25 mL of CH_2Cl_2. The flask was placed in an ice bath. Chlorosulfonic acid (15 mL, 60 eq.) was added slowly to the stirred reaction mixture under Argon protection. The reaction was allowed to return to room temperature and continued for 24 hours. Then the mixture was carefully poured into ice/water. The precipitate was collected and dissolved in acetone. The acetone solution was dried over MgSO4, filtered, and evaporated to dryness. After vacuuming overnight, 4.0 g of hexaphenylbenzene hexasulfonyl chloride (HPB-SO_2Cl) was achieved as yellow solid (yield: 97 %). ^{1}H NMR (400 M Hz, acetone-

d6): δ 7.77 (d, 12H), 7.54 (d, 12H). 66 mL of 1.0 M NaOH (38 eq.) was added to a 100 mL round-bottom flask containing 2.0 g of HPB-SO_2Cl at room temperature. The mixture was stirred at 50 ℃ for 36 hours. Cooled to room temperature, the reaction mixture was neutralized to pH ≈ 11 with 1.0 M HCl solution. This solution was then transferred to cellulose ester membrane tubes (MWCO: 100). The tubes were washed three times with deionized water and soaked in deionized water under stirring for 30 min to remove the 0.1 % NaN_3 preservative prior to use). The tubes were stirred in a bucket containing 4 L of deionized water for 48 hours. Deionized water was replaced every 8 hours. The elimination of NaCl was confirmed by a concentrated $AgNO_3$ solution. Then the solution was recollected. Water was removed by evaporation and high vacuum under P_2O_5 dry at 75 ℃. Finally, 0.32 g of hexaphenylbenzene hexasulfonyl acid hexasodium was achieved as pale yellow crystal (Yield: 16 %). ^{1}H NMR (400 M Hz, D_2O): δ 7.33 (d, 12H), 7.10 (d, 12H). ^{13}C NMR (100 M Hz, D_2O): δ 142.7 (6 C-SO_3Na), 140.2 (6 C para to the sulfonyl group), 139.6 (6 C of the substituted phenyl group), 131.8 (12 C ortho to the sulfonyl group), 124.3 (12 C meta to the sulfonyl group). Melting Point: > 260 ℃. Mass spec. $(M-4Na)^{4-}$: theory 263.47761 amu, found 263.47740 amu (relative intensity: 100); $(M-3Na)^{3-}$: theory 358.96655 amu, found 358.96644 amu (relative intensity: 99); $(M-5Na)^{5-}$: theory 206.18424 amu, found 206.18398 amu (relative intensity: 31).

*Purification of 1,3,6-naphthalene-trisulfonic acid trisodium (**2**)*

12 g of 1,3,(6 or 7)-naphthalene-trisulfonic acid, trisodium salt hydrate was recrystallized four times from deionized water. After drying, 2.8 g of 1,3,6-naphthalene-trisulfonic acid trisodium was achieved as white powder (Yield: 23 %). ^{1}H NMR (400 M Hz, D_2O): δ 8.81 (d, 1H), 8.67 (d, 1H), 8.60 (d, 1H), 8.52 (d, 1H), 8.13 (dd, 1H). ^{13}C

NMR (100 M Hz, D_2O): δ 141.30 (1C), 139.75 (1C), 139.70 (1C), 132.77 (1C), 130.63 (1C), 130.03 (1C), 127.41 (1C), 126.62 (1C), 125.52 (1C), 123.98 (1C).

Synthesis of 4,4'-bis(bromomethyl)tolane

0.30 g (1.4 mmol) of 4,4'-Bis(methyl)tolane and 0.59 g (3.3 mmol) of N-bromo succimide were placed in a three neck flask. The flask was vacuumed and filled with argon. Then a drying tube ($CaCl_2$) was installed. 20 mL of dry CCl_4 was injected. The mixture was heated under reflux, and catalytic amount of AIBN was added after 2 and 5 hours. After 18 hours, the reaction was cooled to room temperature and filtered. The solid residue was washed with 35 mL of boiling CCl_4. The combined solution was evaporated to remove CCl_4. The product was purified by flash column chromatography followed by recrystallization from EtOAc and 0.078 g white crystal was obtained (yield: 15 %). ^{1}H NMR (400 M Hz, $CDCl_3$): δ 7.51 (d, 4H), 7.39 (d, 4H), 4.51 (s, 4H). ^{13}C NMR (100 M Hz, $CDCl_3$): δ 138.16 (2C), 132.22 (4C), 129.32 (4C), 123.43 (2C), 89.94 (2C), 33.19 (2C).

References

(1) Cooke, G.; Rotello Vincent, M. *Chem. Soc. Rev.* **2002,** *31*, 275-286.

(2) Oshovsky, G. V.; Reinhoudt, D. N.; Verboom, W. *Angew. Chem., Int. Ed.* **2007,** *46*, 2366-2393.

(3) Badjic, J. D.; Nelson, A.; Cantrill, S. J.; Turnbull, W. B.; Stoddart, J. F. *Acc. Chem. Res.* **2005,** *38*, 723-732.

(4) Voskuhl, J.; Ravoo Bart, J. *Chem. Soc. Rev.* **2009,** *38*, 495-505.

(5) Brunsveld, L.; Folmer, B. J. B.; Meijer, E. W.; Sijbesma, R. P. *Chem. Rev.* **2001,** *101*, 4071-4097.

(6) Burley, S. K.; Petsko, G. A. *Science* **1985,** *229*, 23-28.

(7) Miller, L. L.; Mann, K. R. *Acc. Chem. Res.* **1996,** *29*, 417-423.

(8) Sansone, F.; Baldini, L.; Casnati, A.; Lazzarotto, M.; Ugozzoli, F.; Ungaro, R. *Proc. Natl. Acad. Sci. U.S.A.* **2002,** *99*, 4842-4847.

(9) Yashima, E.; Maeda, K.; Furusho, Y. *Acc. Chem. Res.* **2008,** *41*, 1166-1180.

(10) Kool, E. T. *Chem. Rev.* **1997,** *97*, 1473-1487.

(11) Bhosale, S.; Sisson, A. L.; Talukdar, P.; Fuerstenberg, A.; Banerji, N.; Vauthey, E.; Bollot, G.; Mareda, J.; Roeger, C.; Wuerthner, F.; Sakai, N.; Matile, S. *Science* **2006,** *313*, 84-86.

(12) Yu, E. W.; McDermott, G.; Zgurskaya, H. I.; Nikaido, H.; Koshland, D. E., Jr. *Science* **2003,** *300*, 976-980.

(13) Lee, M.; Cho, B.-K.; Zin, W.-C. *Chem. Rev.* **2001,** *101*, 3869-3892.

(14) Sakai, N.; Mareda, J.; Matile, S. *Acc. Chem. Res.* **2005,** *38*, 79-87.

(15) Yang, W.-Y.; Ahn, J.-H.; Yoo, Y.-S.; Oh, N.-K.; Lee, M. *Nat. Mater.* **2005,** *4*, 399-402.

(16) Sisson, A. L.; Shah, M. R.; Bhosale, S.; Matile, S. *Chem. Soc. Rev.* **2006,** *35*, 1269-1286.

(17) Muller, M.; Kubel, C.; Mullen, K. *Chem. Eur. J.* **1998,** *4*, 2099-2109.

(18) Watson, M. D.; Fechtenkotter, A.; Mullen, K. *Chem. Rev.* **2001,** *101*, 1267-1300.

(19) Nguyen, T.-Q.; Martel, R.; Bushey, M.; Avouris, P.; Carlsen, A.; Nuckolls, C.; Brus, L. *Phys. Chem. Chem. Phys.* **2007,** *9*, 1515-1532.

(20) Zang, L.; Che, Y.; Moore Jeffrey, S. *Acc. Chem. Res.* **2008,** *41*, 1596-1608.

(21) Bunz, U. H. F. *Chem. Rev.* **2000,** *100*, 1605-1644.

(22) Bunz, U. H. F. *Adv. Polym. Sci.* **2005,** *177*, 1-52.

(23) Schwab, P. F. H.; Levin, M. D.; Michl, J. *Chem. Rev.* **1999,** *99*, 1863-1933.

(24) Schwab, P. F. H.; Smith, J. R.; Michl, J. *Chem. Rev.* **2005,** *105*, 1197-1279.

(25) Hoeben, F. J. M.; Jonkheijm, P.; Meijer, E. W.; Schenning, A. P. H. J. *Chem. Rev.* **2005,** *105*, 1491-1546.

(26) Kumar, S. *Chem. Soc. Rev.* **2006,** *35*, 83-109.

(27) Sergeyev, S.; Pisula, W.; Geerts, Y. H. *Chem. Soc. Rev.* **2007,** *36*, 1902-1929.

(28) Rehm, T.; Schmuck, C. *Chem. Commun.* **2008**, 801-813.

(29) Philp, D.; Stoddart, J. F. *Angew. Chem., Int. Ed. Engl.* **1996,** *35*, 1155-1196.

(30) Claessens, C. G.; Stoddart, J. F. *J. Phys. Org. Chem.* **1997,** *10*, 254-272.

(31) Zych, A. J.; Iverson, B. L. *J. Am. Chem. Soc.* **2000,** *122*, 8898-8909.

(32) Gabriel, G. J.; Iverson, B. L. *J. Am. Chem. Soc.* **2002,** *124*, 15174-15175.

(33) Ryu, J.-H.; Jang, C.-J.; Yoo, Y.-S.; Lim, S.-G.; Lee, M. *J. Org. Chem.* **2005,** *70*, 8956-8962.

(34) Lee, M.; Jang, C.-J.; Ryu, J.-H. *J. Am. Chem. Soc.* **2004,** *126*, 8082-8083.

(35) Lee, M.; Cho, B. K.; Zin, W. C. *Chem. Rev.* **2001,** *101*, 3869-3892.

(36) Ryu, J.-H.; Lee, M. *J. Am. Chem. Soc.* **2005,** *127*, 14170-14171.

(37) Lee, E.; Jeong, Y.-H.; Kim, J.-K.; Lee, M. *Macromolecules* **2007,** *40*, 8355-8360.

(38) Ryu, J.-H.; Oh, N.-K.; Lee, M. *Chem. Commun.* **2005**, 1770-1772.

(39) Ryu, J.-H.; Kim, H.-J.; Huang, Z.; Lee, E.; Lee, M. *Angew. Chem., Int. Ed.* **2006,** *45*, 5304-5307.

(40) Moon, K.-s.; Kim, H.-J.; Lee, E.; Lee, M. *Angew. Chem., Int. Ed.* **2007,** *46*, 6807-6810.

(41) Kim, J.-K.; Lee, E.; Jeong, Y.-H.; Lee, J.-K.; Zin, W.-C.; Lee, M. *J. Am. Chem. Soc.* **2007,** *129*, 6082-6083.

(42) Lee, M.; Kim, J.-W.; Peleshanko, S.; Larson, K.; Yoo, Y.-S.; Vaknin, D.; Markutsya, S.; Tsukruk, V. V. *J. Am. Chem. Soc.* **2002,** *124*, 9121-9128.

(43) Wu, J.; Li, J.; Kolb, U.; Mullen, K. *Chem. Commun.* **2006**, 48-50.

(44) Menger, F. M.; Sorrells, J. L. *J. Am. Chem. Soc.* **2006,** *128*, 4960-4961.

(45) Norgaard, K.; Bjornholm, T. *Chem. Commun.* **2005**, 1812-1823.

(46) Lv, J.; Liu, H.; Li, Y. *Pure Appl. Chem.* **2008,** *80*, 639-658.

(47) Bushey, M. L.; Nguyen, T.-Q.; Zhang, W.; Horoszewski, D.; Nuckolls, C. *Angew. Chem., Int. Ed.* **2004,** *43*, 5446-5453.

(48) Brown, S. P.; Schnell, I.; Brand, J. D.; Muellen, K.; Spiess, H. W. *J. Am. Chem. Soc.* **1999,** *121*, 6712-6718.

(49) Kobayashi, K.; Kobayashi, N.; Ikuta, M.; Therrien, B.; Sakamoto, S.; Yamaguchi, K. *J. Org. Chem.* **2005,** *70*, 749-752.

(50) Kastler, M.; Pisula, W.; Wasserfallen, D.; Pakula, T.; Muellen, K. *J. Am. Chem. Soc.* **2005,** *127*, 4286-4296.

(51) Herwig, P.; Kayser, C. W.; Muellen, K.; Spiess, H. W. *Adv. Mater.* **1996,** *8*, 510-513.

(52) Wu, J.; Fechtenkotter, A.; Gauss, J.; Watson Mark, D.; Kastler, M.; Fechtenkotter, C.; Wagner, M.; Mullen, K. *J. Am. Chem. Soc.* **2004,** *126*, 11311-11321.

(53) Stabel, A.; Herwig, P.; Muellen, K.; Rabe, J. P. *Angew. Chem., Int. Ed.* **1995,** *34*, 1609-1611.

(54) Iyer, V. S.; Wehmeier, M.; Brand, J. D.; Keegstra, M. A.; Mullen, K. *Angew. Chem., Int. Ed.* **1997,** *36*, 1604-1607.

(55) Wang, Z.; Dotz, F.; Enkelmann, V.; Mullen, K. *Angew. Chem., Int. Ed.* **2005,** *44*, 1247-1250.

(56) Ito, S.; Wehmeier, M.; Brand, J. D.; Kubel, C.; Epsch, R.; Rabe, J. P.; Mullen, K. *Chem. Eur. J.* **2000,** *6*, 4327-4342.

(57) Hill, J. P.; Jin, W.; Kosaka, A.; Fukushima, T.; Ichihara, H.; Shimomura, T.; Ito, K.; Hashizume, T.; Ishii, N.; Aida, T. *Science* **2004,** *304*, 1481-1483.

(58) Mynar, J. L.; Yamamoto, T.; Kosaka, A.; Fukushima, T.; Ishii, N.; Aida, T. *J. Am. Chem. Soc.* **2008,** *130*, 1530-1531.

(59) Yamamoto, T.; Fukushima, T.; Yamamoto, Y.; Kosaka, A.; Jin, W.; Ishii, N.; Aida, T. *J. Am. Chem. Soc.* **2006,** *128*, 14337-14340.

(60) Zhang, G.; Jin, W.; Fukushima, T.; Kosaka, A.; Ishii, N.; Aida, T. *J. Am. Chem. Soc.* **2007,** *129*, 719-722.

(61) Houk, K. N.; Menzer, S.; Newton, S. P.; Raymo, F. M.; Stoddart, J. F.; Williams, D. J. *J. Am. Chem. Soc.* **1999,** *121*, 1479-1487.

(62) Muller, A.; Wenz, G. *Chem. Eur. J.* **2007,** *13*, 2218-2223.

(63) Utley, J. H. P.; Gao, Y.; Gruber, J.; Lines, R. *J. Mater. Chem.* **1995,** *5*, 1297-1308.

(64) Grimsdale Andrew, C.; Wu, J.; Mullen, K. *Chem. Commun.* **2005**, 2197-2204.

(65) Wu, J.; Watson, M. D.; Muellen, K. *Angew. Chem., Int. Ed.* **2003,** *42*, 5329-5333.

(66) Wu, J.; Watson, M. D.; Zhang, L.; Wang, Z.; Muellen, K. *J. Am. Chem. Soc.* **2004,** *126*, 177-186.

(67) Wu, J.; Baumgarten, M.; Debije, M. G.; Warman, J. W.; Muellen, K. *Angew. Chem., Int. Ed.* **2004,** *43*, 5331-5335.

(68) Robello, D. R.; Andre, A.; McCovick, T. A.; Kraus, A.; Mourey, T. H. *Macromolecules* **2002,** *35*, 9334-9344.

(69) Robello, D. R.; Andre, A.; Davis, T. A.; Kraus, A.; Mourey, T. H. *Polym. Mater. Sci. Eng.* **2001,** *84*, 365-366.

(70) Kraus, A.; Robello, D. R. *Polym. Prepr.* **1999,** *40*, 413-414.

(71) Tugcu, N.; Park, S. K.; Moore, J. A.; Cramer, S. M. *Ind. Eng. Chem. Res.* **2002,** *41*, 6482-6492.

(72) Przybilla, L.; Brand, J.-D.; Yoshimura, K.; Raeder, H. J.; Muellen, K. *Anal. Chem.* **2000,** *72*, 4591-4597.

(73) Yoshimura, K.; Przybilla, L.; Ito, S.; Brand, J. D.; Wehmeir, M.; Rader, H. J.; Mullen, K. *Macromol. Chem. Phys.* **2001,** *202*, 215-222.

(74) Faustino, C. M. C.; Calado, A. R. T.; Garcia-Rio, L. *J. Phys. Chem. B* **2009,** *113*, 977-982.

(75) Holmberg, K.; Lindman, B.; Joensoon, B.; Kronberg, B. *Surfactants and Polymers in Aqueous Solution*, 2nd ed.; Wiley: Chichester, UK, 2002.

(76) Menger, F. M.; Azov, V. A. *J. Am. Chem. Soc.* **2002,** *124*, 11159-11166.

(77) Schulz, P. C.; Minardi, R. M.; Vuano, B. *Colloid Polym. Sci.* **1999,** *277*, 837-845.

(78) Svenson, S. *Curr. Opin. Colloid Interface Sci.* **2004,** *9*, 201-212.

(79) Lin, Y.; Han, X.; Cheng, X.; Huang, J.; Liang, D.; Yu, C. *Langmuir* **2008,** *24*, 13918-13924.

(80) Park, J.; Rader, L. H.; Thomas, G. B.; Danoff, E. J.; English, D. S.; DeShong, P. *Soft Matter* **2008,** *4*, 1916-1921.

(81) Li, H.; Hao, J.; Wu, Z. *J. Phys. Chem. B* **2008,** *112*, 3705-3710.

(82) Shioi, A.; Hatton, T. A. *Langmuir* **2002,** *18*, 7341-7348.

(83) Patist, A.; Chhabra, V.; Pagidipati, R.; Shah, R.; Shah, D. O. *Langmuir* **1997,** *13*, 432-434.

(84) Lucassen-Reynders, E. H.; Lucassen, J.; Giles, D. *J. Colloid Interface Sci.* **1981,** *81*, 150-157.

(85) Acosta, E. J.; Mesbah, A.; Tsui, T. *J. Surfactants Deterg.* **2006,** *9*, 367-376.

(86) Penfold, J.; Tucker, I.; Thomas, R. K.; Zhang, J. *Langmuir* **2005,** *21*, 10061-10073.

(87) Muzzalupo, R.; Gente, G.; La Mesa, C.; Caponetti, E.; Chillura-Martino, D.; Pedone, L.; Saladino, M. L. *Langmuir* **2006,** *22*, 6001-6009.

(88) Holmberg, K.; Shah, D. O.; Schwuger, M. J., Eds. *Handbook of Applied Surface and Colloid Chemistry*; Wiley: Chichester, UK, 2002; Vol. 2.

(89) Taylor, D. J. F.; Thomas, R. K.; Li, P. X.; Penfold, J. *Langmuir* **2003,** *19*, 3712-3719.

(90) Zhang, J.; Thomas, R. K.; Penfold, J. *Soft Matter* **2005,** *1*, 310-318.

(91) Monteux, C.; Llauro, M.-F.; Baigl, D.; Williams, C. E.; Anthony, O.; Bergeron, V. *Langmuir* **2004,** *20*, 5358-5366.

(92) Myers, D. *Surfaces, Interfaces, and Colloids: Principles and Applications*, 2nd ed.; Wiley: New York, 1999.

(93) Perez, L.; Pinazo, A.; Rosen, M. J.; Infante, M. R. *Langmuir* **1998,** *14*, 2307-2315.

(94) Tsujii, K. *Surfactant Activity: Principles, Phenomena, and Applications*; Academic Press: San Diego, CA, 1998.

(95) Clint, J. H. *Surfactant Aggregation*; Chapman and Hall: New York, 1992.

(96) Rosen, M. J. *Surfactants and Interfacial Phenomena*, 3rd ed.; Wiley: Chichester, UK, 2004.

(97) Dreja, M.; Pyckhout-Hintzen, W.; Mays, H.; Tieke, B. *Langmuir* **1999,** *15*, 391-399.

(98) Pilakowska-Pietras, D.; Lunkenheimer, K.; Piasecki, A. *Langmuir* **2004,** *20*, 1572-1578.

(99) Alami, E.; Beinert, G.; Marie, P.; Zana, R. *Langmuir* **1993,** *9*, 1465-1467.

(100) Wettig, S. D.; Li, X.; Verrall, R. E. *Langmuir* **2003,** *19*, 3666-3670.

(101) Rosen, M. J.; Mathias, J. H.; Davenport, L. *Langmuir* **1999,** *15*, 7340-7346.

(102) Eastoe, J.; Dalton, J. S.; Rogueda, P. G. A.; Crooks, E. R.; Pitt, A. R.; Simister, E. A. *J. Colloid Interface Sci.* **1997,** *188*, 423-430.

(103) Burczyk, B.; Wilk, K. A.; Sokolowski, A.; Syper, L. *J. Colloid Interface Sci.* **2001,** *240*, 552-558.

(104) Chevalier, Y.; Storet, Y.; Pourchet, S.; Le Perchec, P. *Langmuir* **1991,** *7*, 848-853.

(105) Menger, F. M.; Lu, H.; Lundberg, D. *J. Am. Chem. Soc.* **2007,** *129*, 272-273.

(106) Menger, F. M.; Galloway, A. L. *J. Am. Chem. Soc.* **2004,** *126*, 15883-15889.

(107) Mitropoulos, A. C. *J. Eng. Sci. Technol. Rev.* **2008,** *1*, 1-3.

(108) Li, Z. X.; Dong, C. C.; Thomas, R. K. *Langmuir* **1999,** *15*, 4392-4396.

(109) Vasilescu, M.; Caragheorgheopol, A.; Caldararu, H. *Adv. Colloid Interface Sci.* **2001,** *89-90*, 169-194.

(110) Cazes, J., Ed. *Ewing's Analytic Instrumentation Handbook*, 3rd ed.; Marcel Dekker: New York, 2005.

(111) Degiorgio, V.; Piazza, R. *Curr. Opin. Colloid Interface Sci.* **1996,** *1*, 11-16.

(112) Dorshow, R.; Briggs, J.; Bunton, C. A.; Nicoli, D. F. *J. Phys. Chem.* **1982,** *86*, 2388-2395.

(113) Imae, T.; Ikeda, S. *J. Phys. Chem.* **1986,** *90*, 5216-5223.

(114) Claridge, T. *High-Resolution NMR Techniques in Organic Chemistry*, 2nd ed.; Elsevier: Oxford, UK, 2008.

(115) Stilbs, P. *Prog. Nucl. Magn. Reson. Spectrosc.* **1987,** *19*, 1-45.

(116) Soederman, O.; Stilbs, P.; Price, W. S. *Concepts Magn. Reson., Part A* **2004,** *23A*, 121-135.

(117) Totten, G. E.; Goddard, E. D.; Matteson, G. H.; Wanchisen, M. L. *J. Am. Oil Chem. Soc.* **1986,** *63*, 1586-1589.

(118) Mukerjee, P.; Mysels, K. J. *J. Am. Chem. Soc.* **1955,** *77*, 2937-2943.

(119) Murakami, K. *Langmuir* **2004,** *20*, 8183-8191.

(120) Menger, F. M.; Shi, L. *J. Am. Chem. Soc.* **2009,** *131*, 6672-6673.

(121) Roscigno, P.; D'Auria, G.; Falcigno, L.; D'Errico, G.; Paduano, L. *Langmuir* **2005,** *21*, 8123-8130.

(122) Hines, J. D. *J. Colloid Interface Sci.* **1996,** *180*, 488-492.

(123) Wang, T.-Z.; Mao, S.-Z.; Miao, X.-J.; Zhao, S.; Yu, J.-Y.; Du, Y.-R. *J. Colloid Interface Sci.* **2001,** *241,* 465-468.

(124) Zou, Y.-S.; Lin, J. *Youji Huaxue* **1995,** *15,* 433-440.

(125) Wang, Y.; Song, D.; Zhang, Y. *Ranliao Gongye* **2001,** *38,* 37-39.

(126) Snobl, D.; Lycka, A.; Horyna, J. *Collect. Czech. Chem. Commun.* **1985,** *50,* 1852-1861.

(127) Cerfontain, H.; Zou, Y.; Bakker, B. H. *Recl. Trav. Chim. Pays-Bas* **1994,** *113,* 403-410.